WIND-FORCED DYNAMICS IN BONNE BAY, NEWFOUNDLAND

CLARK RICHARDS

Wind-Forced Dynamics in Bonne Bay, Newfoundland

by

© Clark Richards
B.Sc. Honours (2002) University of New Brunswick

A thesis submitted to the
School of Graduate Studies
in partial fulfillment of the
requirements for the degree of
Master of Science.

Department of Physics and Physical Oceanography
Memorial University of Newfoundland

November 30, 2005

ST. JOHN'S NEWFOUNDLAND

Your file Votre référence
ISBN: 978-0-494-19391-4
Our file Notre référence
ISBN: 978-0-494-19391-4

Contents

Abstract

Ten Acoustic Doppler Current Profilers were deployed between September 2002 and September 2004 on the sill of the East Arm in Bonne Bay, a glacial fjord in Gros Morne National Park on the west coast of Newfoundland. The moorings were deployed to measure the velocity of water flowing over the sill, in order to better understand the exchange dynamics of the system. In addition to the current meter data, several cruises were conducted in June 2004 to collect hydrographic data in the Bay, specifically temperature, salinity and density profiles. Meteorological data from the area are also presented. Tidal flow over the sill is dominated by the M_2 tide, with a vertical asymmetry between ebb and flood tides due to the superposition of the estuarine flow. Internal tides were detected during times of the year when the stratification supports internal motions. Similarly, tidal currents were seen to give rise to higher frequency flow (periods less than 5 hours) attributed to high frequency internal waves. Subtidal flow over the sill is two layer, and is primarily forced by the local wind stress. The development of a simple two layer numerical model supports this analysis, and with it some of the effects of spatially varying wind stress were examined. Topographic steering of the wind in the region was determined to be significant in accounting for discrepancies between data and model results.

Acknowledgements

I would like to thank my supervisor, Dr. Brad de Young, for his guidance and support throughout the writing of this thesis and during my Masters program. I also would not have been able to complete this work without the help of Dr. Daniel Bourgault, who constantly entertained my questions and discussions (especially with regard to the numerical model), and for this I am very grateful.

Thanks also go to Jack Foley for providing the data and all technical support regarding the instruments, and to Len Zedel and James Helbig for their comments and criticisms as reviewers.

Finally I would like to thank my fiancée Tara Simmonds, for her patience and support throughout this degree program and always.

Funding for this degree was graciously provided by the Natural Science and Engineering Research Council of Canada (NSERC).

List of Tables

List of Figures

List of Abbreviations

ADCP - acoustic Doppler current profiler

cpd - cycles per day

CIL - cold intermediate layer

GSL - Gulf of St. Lawrence

SLE - St. Lawrence Estuary

CTD - conductivity temperature depth

"Fascinating trade," said the old man, and a wistful look came into his eyes, "doing the coastlines was always my favourite. Used to have endless fun doing the little bits in fjords... "

Douglas Adams, *The Hitchhiker's Guide to the Galaxy* (1979)

Chapter 1

Introduction

The study of the physical oceanography of fjords began slightly more than 100 years ago, along the glacier carved coastline of Scandanavia. These pioneer studies determined the fundamental characteristics of fjord circulation, in which a surface layer of brackish water flows toward the ocean, with a compensating inflow of seawater underneath (Pickard and Emery, 1990). Interest in the physical oceanography of fjords was renewed in the latter half of the 20th century, with studies of fjord systems along the west coast of North America, particularly in British Columbia (Farmer and Freeland, 1983). The motivation for this renewed interest had much to do with the impacts of human activity on coastal systems, and as such has led to many comprehensive studies of fjords in North America, Scandinavia, and elsewhere.

1.1 Fjord Structure

Fjords are glacially carved embayments, typically characterized by steep sides, interior depths that are large compared to the coastal shelf, and a submarine sill which

separates them from the coastal sea. They are often quite long relative to their width, and typically have freshwater input at their head (Farmer and Freeland, 1983). Due to their glacial origin, most fjords occur at high latitudes and in areas of mountainous coast. They are most common in Scandanavia and western North America, but can also be found along the coasts of Newfoundland and Labrador, western South America, New Zealand and Scotland.

1.2 Fjord Circulation

The different terms that contribute to the circulation in fjords are many, and can vary significantly between different systems. In general, there are three primary forcing terms that are common to most fjords, and influence the special case of estuarine flow known as fjord circulation: freshwater forcing, tidal forcing, and wind forcing.

1.2.1 Freshwater Forcing

The underlying forcing for circulation within a fjord is a pressure gradient caused by sourced freshwater at the head of the bay. This forcing is common to all estuarine systems, and results in a layer of brackish outflow overlying a compensating inflow at depth due to the entrainment of salt and water into the upper layer. The entrainment causes a gradient of surface salinity which increases from freshwater at the head, to that of the coastal sea outside of the mouth, and results in an increase in volume outflow in the upper layer. The two layers are separated by an interface of zero flow. A simple model for this transport was demonstrated by Knudsen (see Pond and Pickard, 1983), and can be used to estimate volume flows in fjords based on the salinities at

the mouth. Using the principles of conservation of volume and conservation of salt, the volume outflow of the upper and lower layers can be expressed by:

$$V_U = \frac{S_L}{S_L - S_U} V_R \tag{1.1}$$

$$V_L = \frac{S_U}{S_L - S_U} V_R \tag{1.2}$$

where $V_{U,L}$ are the upper and lower layer transports, V_R is the freshwater input from rivers, and $S_{U,L}$ are the upper and lower layer salinities.

Velocities in the lower layer are typically much smaller than those of the upper layer, and due to the sill, residence times for the deep water of the fjord can be very long. Exchange of the bottom water in a deep fjord can occur on time scales of months to years, depending on the hydrographic conditions outside the bay, the rate of entrainment, and wind and tidal forcing. If water of sufficient density is raised above the level of the sill, it can propagate as a density current into the lower layer of the fjord displacing deep water upward. This in turn displaces surface water out of the fjord, and causes an exchange event. These events are characterized by sharp changes in temperature and salinity of the water within the fjord (de Young and Pond, 1988) and are often referred to as gravitational circulation.

1.2.2 Tidal Forcing

Barotropic tides typically make a significant contribution to the flow and exchange of fjords, especially for timescales on the order of tidal periods. Acceleration of tidal flow over the sill can create critical conditions, and in some locations energy can be extracted from the tide and used for mixing. In this way tidal flow can have

a significant effect on the gravitational circulation of fjords, and tidally generated turbulence can influence the frequency of deep water renewal (Farmer and Freeland, 1983).

In addition to the barotropic tide, observations of the motion of isopycnal surfaces in a fjord will often indicate the presence of internal oscillations at tidal frequencies (Farmer and Freeland, 1983). These internal tides result from the interaction of the barotropic flow of the stratified fluid with the sill at the mouth of the fjord. It has also been proposed that breaking of the internal tide supplies energy for turbulent mixing (Stigebrandt, 1980).

1.2.3 Wind Forcing

Local wind can affect the circulation in a fjord in several different ways. The frictional stress on the surface will cause an acceleration of the flow, while turbulence generated near the surface will produce mixing. This mixing increases the potential energy of the water column, and can potentially drive gravitational circulation within the fjord.

Momentum is transferred from the atmosphere to the ocean through viscous stress at their interface. As such, surface velocities are typically much less than wind speeds, due to the large difference in density. Specifically, the stress at the surface of the ocean is related to the wind speed by the relation

$$\vec{\tau} = c_D \rho_a |\vec{u}| \vec{u} \tag{1.3}$$

where u is the wind speed, ρ_a is the density of air and c_D is a drag coefficient (Gill, 1982). The value of c_D, a dimensionless scaling term, depends on wind speed, air

stability, and the roughness of the surface. Values for different surfaces are typically determined from measurement. It has been found that for low wind speeds the value of c_D is approximately 1.2×10^{-3}, but for speeds above 11 m/s, c_D varies linearly with u and is given by (Large and Pond, 1981):

$$10^3 c_D = 0.49 + 0.065u \qquad \text{for } 11m/s < u < 25m/s \tag{1.4}$$

c_D is also generally not a constant for a given wind speed, but can have a significant amount of variability due to the fact that the momentum transfer is a turbulent process (Pond and Pickard, 1983). The standard deviation is typically about 20% of the mean. For wind speeds above 25 m/s the same linear relation for c_D is assumed, and thus strong winds blowing for a short period of time can have a significant effect on ocean currents.

Wind direction is usually along-inlet because of topographic steering by the steep sides present along the coastline. Wind speed in the fjord will vary along the channel due to changes in width and to the feeding of air into tributary valleys. Mid-latitude cyclones are the primary source of wind forcing at synoptic timescales at mid-latitudes, but at short timescales the modulation is often dominated by a sea-breeze effect (Farmer and Freeland, 1983). Katabatic winds can be important in high latitude fjords bounded by high coastal plateaus, which are often ice covered.

The effect of wind on the current in a fjord differs from that of the deep ocean due to the narrowness of the channel and the underlying bottom topography. In the deep ocean, wind driven flows tend to result in inertial motions, while in fjords rotation effects are generally quite limited. A typical fjord width ($\sim$5 km) is generally

of the order of, or much smaller than, the internal Rossby width (1-10 km). In the absence of rotation, wind driven currents in the surface layer can result in changes in the depth of the pycnocline, which manifest themselves in the form of seiches or progressive waves (Farmer and Freeland, 1983).

1.3 Hydrography

There are many different classification schemes for estuaries (including fjords), based on different properties of the system such as: vertical profiles, circulation, and hydraulic control (see Pickard 1961, Hansen and Rattray 1966, and Stigebrandt 1981 for details).

Within the estuarine classification scheme of Cameron and Pritchard (1963), which categorizes estuaries based on stratification and salinity distributions, most fjords are categorized as *Highly Stratified Estuaries.* These systems are distinguished by a surface layer thickness that is roughly constant along the length of the estuary, and by bottom layer velocities that are much smaller than the upper layer velocities (except at the sill). Salinity and density profiles show a marked two layer system, with mostly constant values in the bottom layer, and an increase toward the mouth in the upper layer due to entrainment of salt from below. Temperature generally decreases with depth, though there can often be instances of seasonal maxima and minima, especially in fjords that are subject to the inflow of melt water from glaciers (Dyer, 1997).

The fjord classification scheme of Pickard (1961) is a descriptive scheme which places fjords in different categories based on the shape of the profiles. It must be

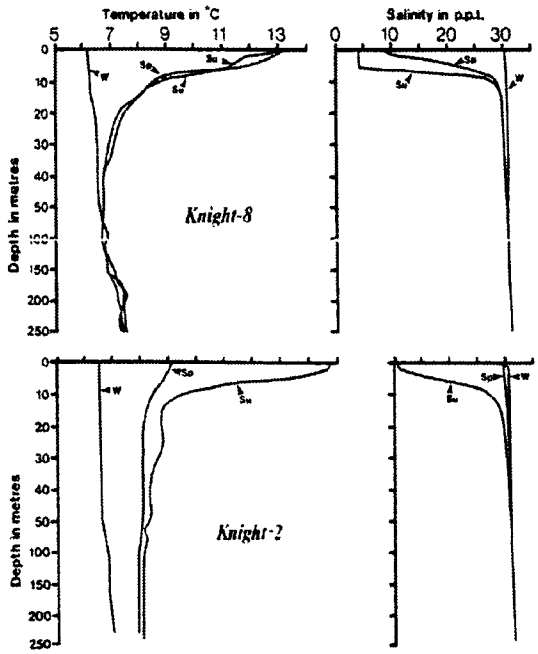

Figure 1.1: Typical spring, summer and winter fjord profiles from Knight Inlet B.C. Knight-8 and Knight-2 are two hydrographic stations located near the head and the mouth respectively (Farmer and Freeland, 1983).

realized however that the shape of a profile within a fjord can be quite different not only from one fjord to another, but also at different times of the year. In this way fjords will often migrate between classifications due especially to variations in freshwater input. Reduced inflow during winter months can have a large effect on vertical profiles, and thus on the particular classification. Figure 1.1 shows typical S and T profiles for a fjord (Knight Inlet, British Columbia) in spring, summer, and winter, emphasizing both the temporal and spatial variability to the observed profiles.

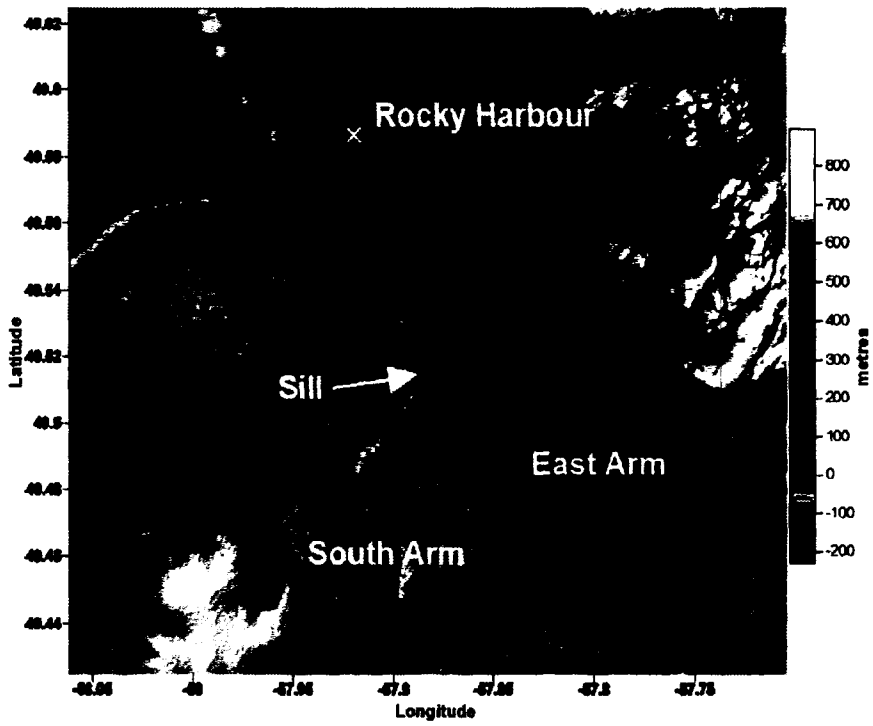

Figure 1.2: Bathymetry and topography of the Bonne Bay region.

While the actual values in Figure 1.1 differ from Bonne Bay, the general shape of the profiles should be consistent.

1.4 Geography and Significance of Bonne Bay

Bonne Bay is a fjord located within Gros Morne National Park on the west coast of the island of Newfoundland (Figure 1.2). It has two arms, the South arm and the

East arm, the latter being separated from the northeastern Gulf of St. Lawrence by a sill. Depths within the East arm are around 230 metres, in the bay proper and the South arm are around 100 metres, and they are separated by the sill which is about 14 metres deep. Depths in the Gulf of St. Lawrence just outside of Bonne Bay are about 60 metres.

Much of the research conducted at Bonne Bay to date has focused on biological oceanography, and this is one of the primary goals of the Bonne Bay Marine Station in Norris Point, operated by Memorial University of Newfoundland. The bay is an important habitat for many marine organisms, including whales, crab, fish, and plankton.

As an accessible fjord, Bonne Bay offers the opportunity to study the interaction of forcing, stratification, and topography in relation to the exchange dynamics of a coastal embayment. The details of this exchange are of interest for many reasons, the most important being the basis of an ongoing physical oceanographic study of the area. Flow of water in the bay and over the sill can also strongly influence biological organisms and productivity of Bonne Bay. Finally, as an area influenced by human habitation, the exchange processes can also be important in the flushing of anthropogenic pollutants such as waste and oil. Bonne Bay is unique in this aspect however, because as a part of Gros Morne National Park (a UNESCO world heritage site), many of the anthropogenic factors that influence other accessible coastal bays in Newfoundland are limited.

Of course, as a coastal embayment, the circulation and hydrography can be largely determined by the oceanographic system to which it is connected, the Gulf of St. Lawrence. The next section presents an overview of the physical oceanography of the

Gulf of St. Lawrence, paying special attention to the northeastern Gulf, and to the influence of the Straight of Belle Isle which connects the Gulf to the Labrador Sea.

1.5 Oceanography of the Gulf of St. Lawrence and the Strait of Belle Isle

The Gulf of St. Lawrence (GSL) is a highly stratified semi-enclosed sea, connected to the Atlantic Ocean through the Cabot, and Belle Isle Straits. It exchanges water through both straits, receives fresh water input from surrounding rivers, and thus responds like a large estuary in which Coriolis effects are important (Koutitonsky and Bugden, 1991) because of the large spatial scale (O(1000 km)). Because of its proximity, the Strait of Belle Isle has a significant effect on the water properties and synoptic variability along the west coast of Newfoundland, and therefore on Bonne Bay. The Strait of Belle Isle has an average depth of about 60 metres, average width of 15 km, and a cross section of approximately 1 km^2.

Deep channels within the GSL occupy about one half of the area and are the main paths through which Atlantic waters flush the system. Forcing of the GSL system can be divided into 4 main categories: buoyancy, meteorological, tidal, and oceanic.

1.5.1 Buoyancy Forcing

Much of the freshwater input to the system is derived from the St. Lawrence Estuary (SLE) watershed and the northern shore rivers, which contribute about 84% and 14% respectively (Koutitonsky and Bugden, 1991). Freshwater input to the GSL typically reaches a maximum of 32,000 m^3/s in May, and a minimum of 14,000 m^3/s

in February. Surface heat fluxes can also contribute to buoyancy forcing, with the formation of a seasonal thermocline in summer, vertical mixing in autumn, and ice formation in winter. Isotherms are typically zonal in summer, and temperatures reach a maximum in the Strait of Belle Isle of about 12°C. In the winter, subzero surface temperatures appear in the northern Gulf by November. Sea ice generally forms in the northern Gulf by the middle of January, and melts in mid to late April.

1.5.2 Wind Forcing

Wind stress over the Gulf is a major source of kinetic energy, while also driving much of the the circulation variability. From December to April, strong winds blow from the north over the Gulf, while from June to October weaker winds blow from the northeast over the SLE region, but from the southwest over the Newfoundland region. The results of a seasonal study performed by Saunders (1977) using winds reported from ships over a 32 year period indicate a predominantly westerly direction for all seasons, with northerly components in spring and southerly components in summer. Aside from the mean seasonal forcing, the wind stress over the GSL can exert significant forcing for time scales on the order of several days, particularly due to the passage of storms. Storms over the Gulf can be divided into two main categories: *northern storms*, which propagate from west to northeast with the centre lying to the north of the Gulf; and *southern storms*, which move from south to northeast, with the centre lying near the eastern boundary of the GSL. Southern storms produce meridional fluctuations, while northern storms tend to produce zonal wind fluctuations over the Gulf, and are generally of longer duration. The result is that northern storms tend to influence the wind driven motion much more effectively

than southern storms, as they are of longer duration relative to the spin-up time of the Gulf.

1.5.3 Tidal Forcing

Tidal forcing in the GSL is a result of non-local forcing from the Cabot and Belle Isle Straits, and local tide-generating forces. M_2 tides propagate in an anticlockwise direction around an amphidromic point near the Magdelen Islands, with phases at the Strait of Belle Isle and Cabot Strait of about 0°(Godin, 1980). The amplitude of the M_2 constituent increases along the west coast of Newfoundland toward the Strait of Belle Isle. The K_1 constituent has large phase differences across the Cabot Strait due to the proximity of its amphidromic point on the Scotian Shelf. The K_1 amplitudes are roughly constant along the west coast of Newfoundland, so the mixed tide becomes more and more of M_2 character toward the Strait of Belle Isle (Koutitonsky and Bugden, 1991).

1.5.4 Oceanic Forcing

The deep waters in the GSL are a mixture of Labrador and North Atlantic water in proportions that vary on timescales of several years. In particular, the characteristics of the deep waters of the GSL are determined by changes in properties of oceanic waters on the continental shelf. Exchange with deep ocean water is primarily through the Cabot Strait, although there is shelf-water exchange that takes place through the Strait of Belle Isle (Garrett and Petrie, 1981).

1.5.5 Response of the Gulf of St. Lawrence to Forcing

The basic state of the GSL is estuarine-like, stratified motion, with the upper layer (10 to 30 m) of low salinity (27 to 32 psu) water moving towards the Atlantic. A sharp seasonal thermocline in summer separates the upper layer from a cold intermediate layer (CIL) which extends to a depth of about 125 m. In winter, the cold layer extends to the surface. The CIL is formed partially from in situ winter cooling, though it has been estimated that as much as 35% of its volume comes from Labrador waters entering through the Strait of Belle Isle (Koutitonsky and Bugden, 1991).

The Gulf's response to tides is dominated by the M_2 tide in the semidiurnal band, and the K_1 tide in the diurnal band. In particular, the M_2 tide dominates in the SLE, as well as the northwest and northeast sections of the Gulf. There is also a marked neap-spring modulation of the semidiurnal tides, especially in shallow coastal areas where tidal waves experience a significant amount of friction. The Strait of Belle Isle has been identified as an area of intense vertical mixing, implied by the detection of CIL water at the surface.

The mean surface circulation in the Gulf has been observed to be cyclonic, with estuarine-like exchanges at the Cabot and Belle Isle Straits. Notable features are the Gaspé current (a strong coastal current that develops in the SLE) and a northeastward flow along the west coast of Newfoundland (Koutitonsky and Bugden, 1991; Garrett and Petrie, 1981).

Ice in the Gulf can play an important role in the variability of current and water properties, particularly due to its year-to-year variability in formation, cover, drift, and melting. This is due to the high variability inherent in air temperature, wind stress, surface layer convection and surface currents, which all have a direct effect

on sea ice in the Gulf. The mean dates of ice formation and melting for the Bonne Bay area of the Gulf are February 5th and April 9th respectively, but it must be remembered that it is difficult to speak of average ice conditions in the GSL because wide climatic variations in winter months can have significant effects on ice formation (Black, 1972).

1.5.6 Strait of Belle Isle

Due to its proximity to the western and northwestern coasts of Newfoundland, and its influence on the GSL via exchange of Labrador water, a brief discussion of the characteristics of the Strait of Belle Isle will be presented. Flow through the strait is controlled by sea level differences at opposite ends produced by large scale meteorological forcing, and spins down in about 1.1 days. The flow is coherent with geostrophic wind for periods of 2 to 30 days, for directions parallel to the Newfoundland coast (Garrett and Toulany 1981). Variability of the flow through the strait for periods longer than 30 days is most likely caused by the estuarine circulation. Net transport through the strait is towards the GSL, with summer rates of about 0.13×10^6 m^3/s and higher winter rates of 0.3×10^6 m^3/s. As mentioned previously, during the winter cold water transported through the Strait of Belle Isle can account for about 35% of the CIL in the Gulf.

All of the characteristics of the GSL system can have an effect on the circulation in and around Bonne Bay, and thus contribute to the flow in the area of study. While the scope of the experiment undertaken does not directly consider measurements from the Gulf, one must be aware of the potential for outside influence on the exchange within the fjord.

1.6 Outline of Thesis

The goal of this thesis is to obtain a clear picture of the circulation and physical oceanography of Bonne Bay, with a particular focus on the dynamics of exchange over the sill as it relates to different forcing methods. This will be done by interpreting current measurements obtained at the sill. The layout of this thesis is as follows: Chapter 2 presents the instruments and data used, with some preliminary analysis; Chapter 3 discusses the tidal and high frequency flow in Bonne Bay, while Chapter 4 deals with the subtidal flow and the results of a two layer numerical model. Conclusions will be presented in Chapter 5.

Chapter 2

Experimental

2.1 Data

2.1.1 Current Data

The bulk of the data used in this study were current data from various locations on the sill, collected using acoustic Doppler current profilers (ADCPs) placed on the bottom looking upwards. The instruments were deployed on the sill to determine the character, structure, and dynamics of the along-channel flow.

An ADCP is an acoustic instrument that measures water velocity using the Doppler effect. Sound pulses of a specific frequency emitted from a transducer travel through the water column at the speed of sound. A small amount of sound energy will be reflected by scatterers in the water - usually small particles or plankton, including both phytoplankton such as diatoms, and zooplankton such as copepods (RD Instruments, 1996) - and will return toward the transducer. By measuring the Doppler shift of the reflected pulses, the velocity of the water can be determined, provided

that the scatterers are moving passively with the currents. As a single transducer can only measure velocity radial to it, many ADCPs consist of 4 transducers oriented in 4 different directions in what is known as a Janus configuration (RD Instruments, 1996). This configuration allows the ADCP to measure the u, v, and w components of the water velocity, as well as obtain an estimate of the uncertainty in the velocity measurement (known as the error velocity). Large error velocities can be caused either by malfunctioning equipment, spatial inhomogeneities of the current in the water column, low backscatter, or biological bias. One of the big advantages of ADCPs over traditional current meters, is that they can measure velocity profiles throughout an entire water column, depending on depth. By dividing the total profile into segments (known as depth cells or bins), the instrument can differentiate between velocities at different distances from the transducer. Bins are of equal length, but differing volume, and the measured velocity represents an average over the entire bin.

The 2002 and 2003 moorings were deployed directly on the bottom, while the 2004 moorings were about 1 metre above the bottom. The mooring positions did change somewhat from year to year (see Figures 2.1, 2.2 and 2.3) because they were diver deployed. The moorings were arranged to provide good coverage of the channel in the centre of the sill, as well as the shallower areas to the north and south. Each ADCP was equipped with a temperature sensor that measured the temperature of the water at the location of the instrument. The instruments were all RDI 4 beam Workhorse Broadband ADCPs at a frequency of 300 kHz, except for M1-2003 and M2-2003 which were 1200 kHz and 600 kHz respectively. A summary of mooring instruments and parameters is given in Tables 2.1 and 2.2.

Mooring	Lat (°N)	Long (°W)	Depth (m)	Averaging period	Bin Size
M1-2002	49 30.640	57 52.999	12	20 min	1m
M2-2002	49 30.769	57 53.002	27.4	20 min	1m
M3-2002	49 30.757	57 53.002	27.4	20 min	1m
M4-2002	49 30.816	57 52.954	15	20 min	1m
M1-2003	49 30.630	57 53.000	12.5	30 min	0.5m
M2-2003	49 30.827	57 53.077	21	30 min	0.5m
M3-2003	49 30.750	57 52.992	27.4	30 min	1m
M4-2003	49 30.695	57 52.996	17.4	20 min	1m
M1-2004	49 30.604	57 53.070	12	30 min	1m
M2-2004	49 30.804	57 53.139	17	20 min	1m

Table 2.1: Location and details of Bonne Bay 2002-2004 ADCP moorings.

Mooring	Start day (mm/dd/yyyy)	End day (mm/dd/yyyy)	Serial Number	Freq (kHz)
M1-2002	09/07/2002	11/21/2002	2460	300
M2-2002	11/22/2002	07/17/2003	2477	300
M3-2002	09/07/2002	06/06/2003	2459	300
M4-2002	09/07/2002	11/21/2002	0879	300
M1-2003	10/11/2003	05/30/2004	1336	1200
M2-2003	10/28/2003	06/14/2004	2069	600
M3-2003	11/10/2003	06/19/2004	2459	300
M4-2003	07/19/2003	04/30/2004	2477	300
M1-2004	06/16/2004	09/16/2004	2460	300
M2-2004	06/16/2004	09/17/2004	2477	300

Table 2.2: Dates and instrument parameters of Bonne Bay 2002-2004 ADCP moorings.

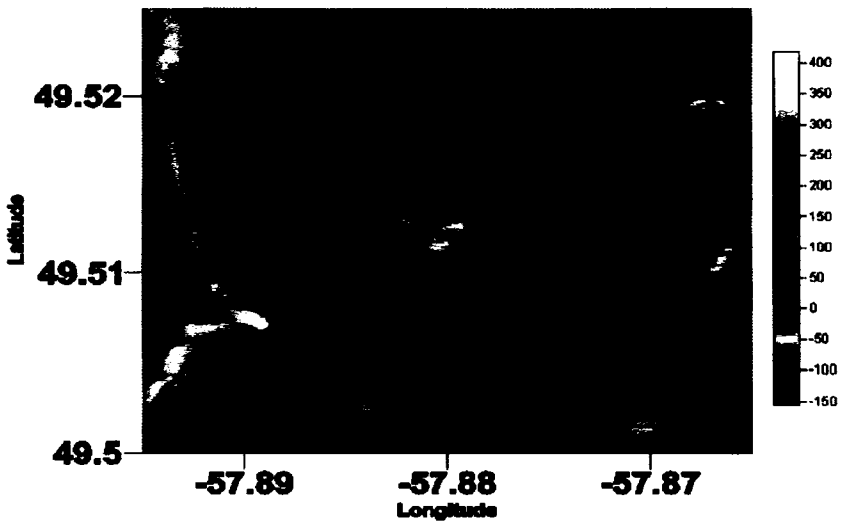

Figure 2.1: 2002 mooring positions.

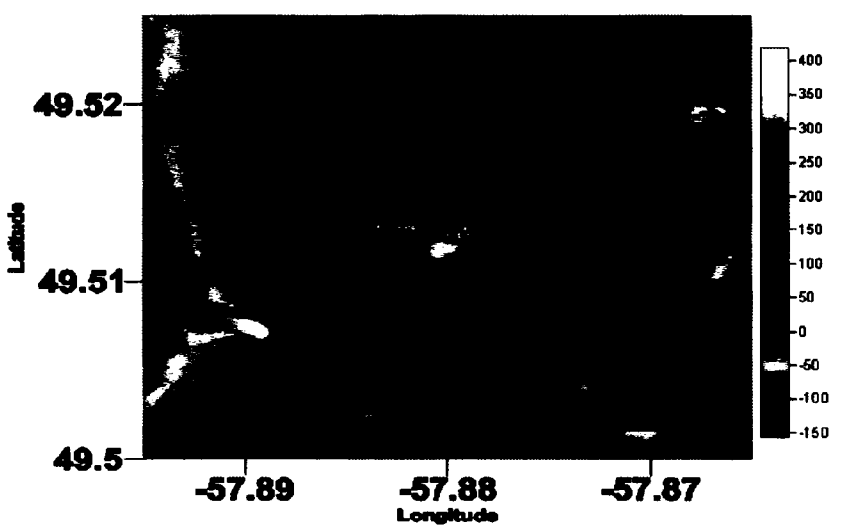

Figure 2.2: 2003 mooring positions.

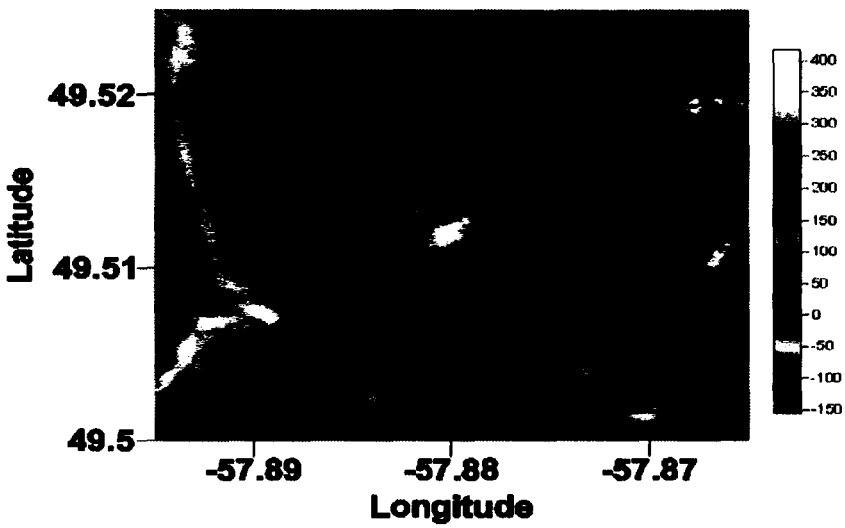

Figure 2.3: 2004 mooring positions.

2.1.2 Atmospheric Data

In addition to the current data, atmospheric data were obtained from Environment Canada for the period from January 2002 to December 2004 for the nearby weather monitoring station at Rocky Harbour. Atmospheric data for the summer of 2004 were also obtained from a weather monitoring station installed on the roof of the Bonne Bay Marine Station in Norris Point (Figure 2.4).

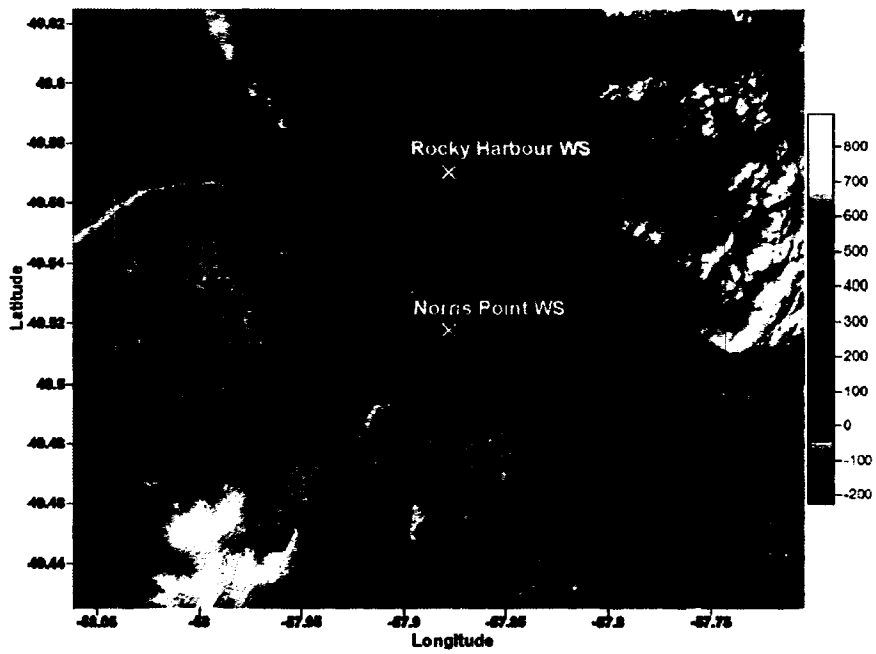

Figure 2.4: Rocky Harbour and Norris Point weather station locations. Note that both are located near very steep coastal topography.

2.1.3 Hydrographic Data

In addition to the ADCP and atmospheric data, several cruises were conducted during June 2004 to gather temperature, salinity, and density data in the area surrounding the sill, in the arms of the bay, and out into the Gulf of St. Lawrence. Cast locations for the East Arm and South Arm transects are shown in Figures 2.5 and 2.6.

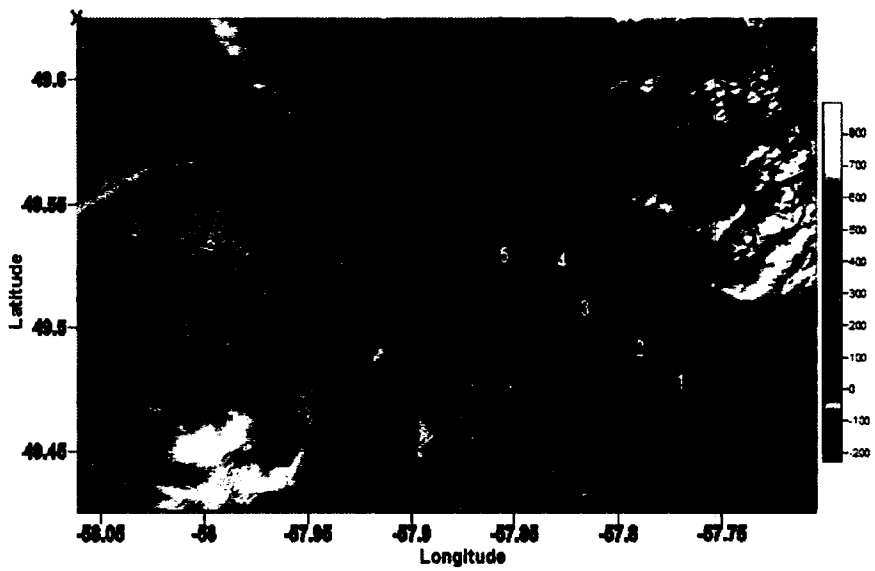

Figure 2.5: Cast locations for the East Arm, June 2004. Stations 1-6 were collected June 8, while stations 7-10 were collected June 13.

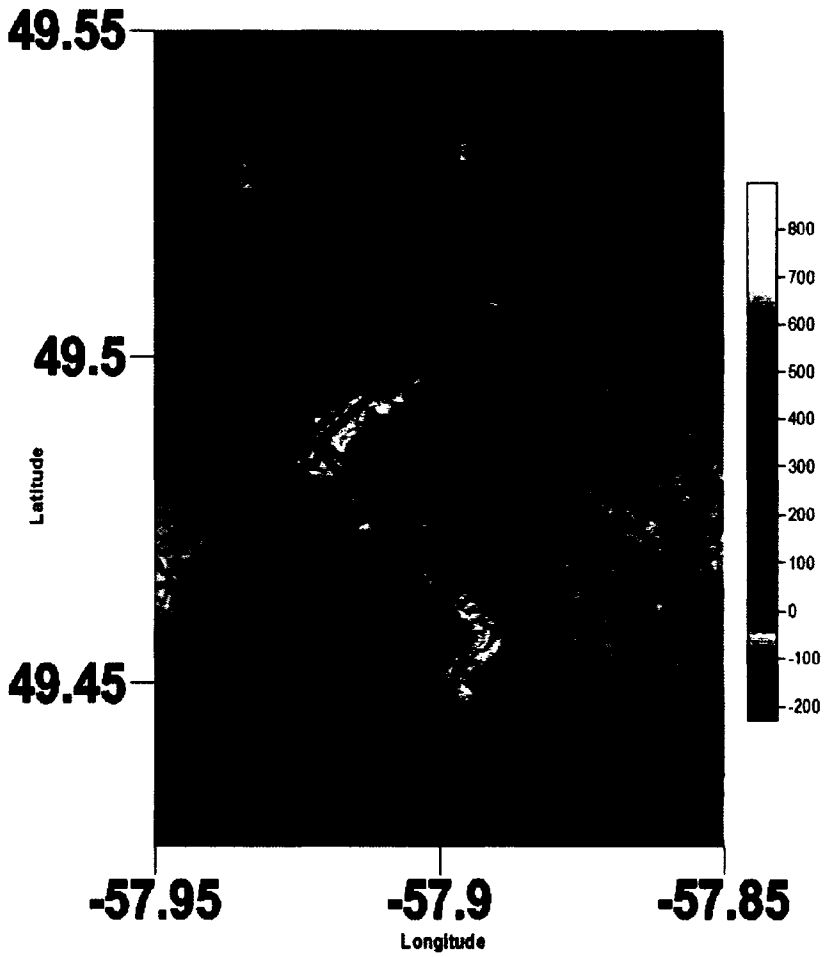

Figure 2.6: Cast locations for the South Arm, June 2004. Stations 2 and 4 were collected June 9, while stations 1, 3 and 5 were collected June 13.

2.2 Data Processing

The ADCP data were processed in a manner similar to that followed by Tittensor *et al.* (2002). First the data were extracted from the instrument output files and missing data were interpolated linearly. The data were collected in 1 metre depth bins for most instruments, although M1-2003 and M2-2003 were sampling with 0.5 metre bins. Instruments averaged the data in either 20 or 30 minute ensembles (Table 2.1) with 80 and 90 pings per ensemble respectively. The theoretical error velocity for the moorings is about 1 cm/s. The backscatter was calibrated following standard techniques (Deines, 1999) utilizing instrument characteristics as well as environmental factors such as the sound absorption coefficient and the speed of sound at each depth cell. These parameters, together with the slant range to each depth cell, were then used in the sonar equation to estimate the volume backscattering strength. For subtidal analysis, the raw velocity data were then decomposed into u (eastern) and v (northern) components, subsampled to hourly data, de-tided, and filtered using a 5th order forward and reverse Butterworth low pass digital filter with a cut-off of 30 hours. A similar filter was applied to the backscatter. The data were also corrected for the changing surface elevation due to tides by adjusting the data from each time step according to the level of maximum backscatter intensity (assumed to be the surface). This allowed the data to be referenced in terms of depth below the surface rather than distance above the bottom. The uppermost two metres of data for each mooring were discarded, due to suspicious readings caused by side lobes and surface effects.

The hourly wind and air temperature data for Rocky Harbour were obtained from Environment Canada as a series of text files. The data were examined for large peaks

and errors which were manually removed, and any short gaps were linearly interpolated. The data were extracted from these files, decomposed into u and v components, converted to wind stress (Large and Pond, 1981) and saved in a MATLAB format. Wind data for the period from June 19th to September 19th 2004 were also obtained from the weather station installed at the Bonne Bay Marine Station in Norris Point. The data were extracted from text files and missing points were interpolated.

Vertical CTD profiles were collected using an SBE-25 probe. Only the temperature, salinity and density data are presented here. The CTD data were extracted from the instrument output text files and saved in a MATLAB format. The up-cast portion was removed, as was the part of the data from when the instrument was sitting at the surface. The data were then plotted as two-dimensional vertical contour maps (Figure 2.17).

2.3 Data Discussion and Preliminary Analysis

2.3.1 Acoustic Doppler Current Profiler Data

Average profiles for the ADCP data were calculated by averaging the data from each depth bin over their respective time periods. The variance in velocity typically shows a minimum at around 5-8 metres depth (Figure 2.7) associated with the interface. Mooring M2-2003 is one of the deeper moorings, and the shape of the profile in Figure 2.7 is representative of that from the other moorings. The estuarine circulation is clearly shown, with outflowing water in the upper 6 metres, and the compensating inflow below. Also apparent in the profile is a decrease in amplitude as the bottom is approached, likely due to frictional drag. Though it would appear that the velocity

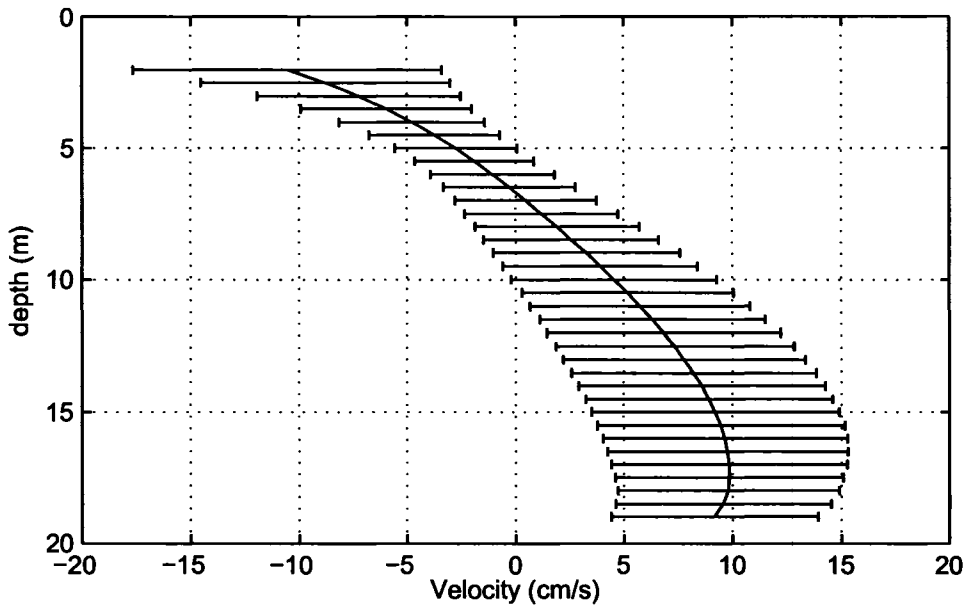

Figure 2.7: Average u velocity for M2-2003. Prior to averaging the data was de-tided and low pass filtered with a 30 hour cutoff to remove tidal fluctuations. Error bars show the standard deviation for each depth. Data is from 10/28/2003 to 06/14/2004.

profile shown in Figure 2.7 is not volume conserving, it must be kept in mind that this is the velocity at one point on the sill. Also not yet accounted for are the two metres of contaminated data near the surface.

To get a sense of how this average estuarine circulation varied over time periods on the order of several months, seasonal averages for the moorings were compared. Figure 2.8 shows the change in vertical structure for 2 moorings, M3-2002 and M2-2003 over 3 seasons: fall, winter and spring. The results from these two moorings are displayed because they cover the same seasons in both 2002 and 2003, and also because they were from approximately the same position in the deep part of the channel. Clearly the highest velocities occur during the fall season in both cases. It

also appears as though the interface is slightly shallower in 2003. Due to the timing

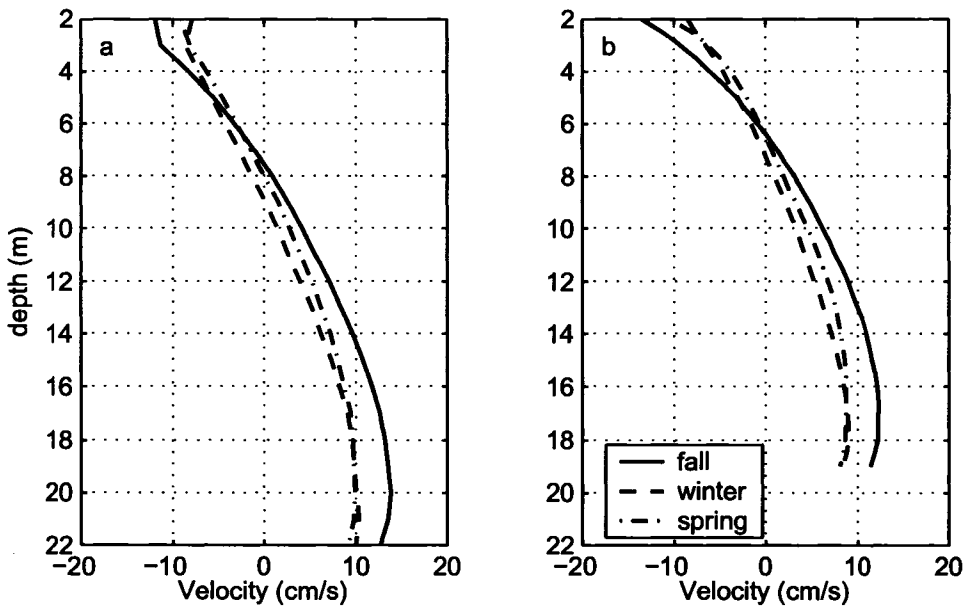

Figure 2.8: Change in average u velocity profile for a) M3-2002, and b) M2-2003 through fall, winter and spring.

of instrument deployment, there is no coverage of the deepest part of the channel during the summer months. In fact, the only summer mooring permitting a similar comparison to Figure 2.8 is M4-2003, which was located north of the channel in a shallower area (Figure 2.1). As such, it does not provide as much insight into the vertical structure below the interface. Results for the seasonal average for summer, fall and winter are shown in Figure 2.9. In this case the velocities during the fall season are greater than both summer and winter velocities, with surface velocities during the summer being only slightly larger than during the winter.

To examine the spatial variability of the data from each mooring, average profiles were compared with a transport averaged velocity (Figure 2.10), calculated using

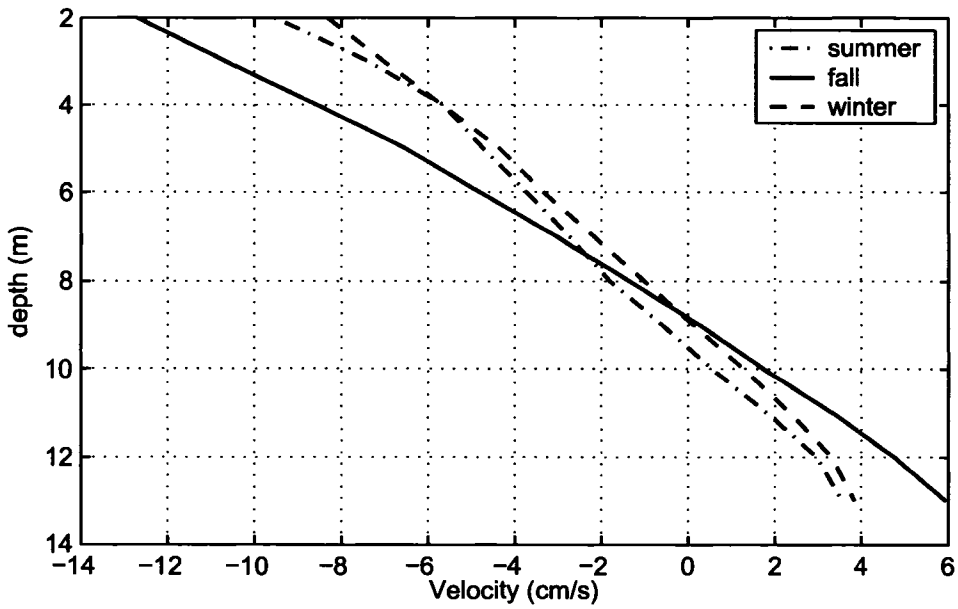

Figure 2.9: Change in average u velocity profile for M4-2003 through summer, fall and winter.

the across channel interpolation script discussed later in this section. Comparison of average profiles from each of the four 2003 moorings shows that there is 2-3 metres of variability in the depth of the zero-crossing, and about 1-2 cm/s variability in the currents at a particular depth.

Horizontal coherence of the moorings was considered, because of the desire to study the cross-channel structure of the flow. Figure 2.11 shows the coherence between moorings pairs from 2003 (M2-2003 and M3-2003), using currents at depths of 2, 6 and 15 metres from the surface. The time period considered is from day 301 to 530 2003 (where January 1st 2003 is day zero). Coherence between the data at the surface and at depth (Figure 2.11a and 2.11c) is very high for tidal (especially diurnal and semidiurnal), and for subtidal frequencies. Cross correlation analysis indicated a zero

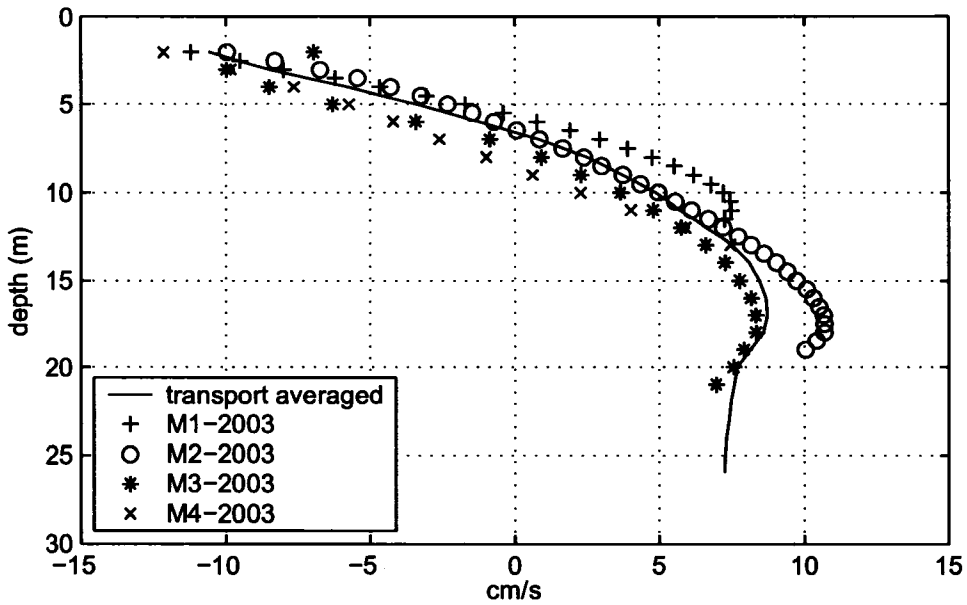

Figure 2.10: Average through channel velocity profiles from 2003 data, compared with the transport averaged velocity profile. The latter is calculated by dividing the total velocity across the channel by the area at each depth. Data are from day 301 to 485 2003, where January 1st 2003 is day zero.

lag between the time series. Coherence at depths of around 6 metres (corresponding to the interface) showed high coherence for tidal frequencies, but little to no significant coherence for frequencies below the diurnal tide (Figure 2.11b).

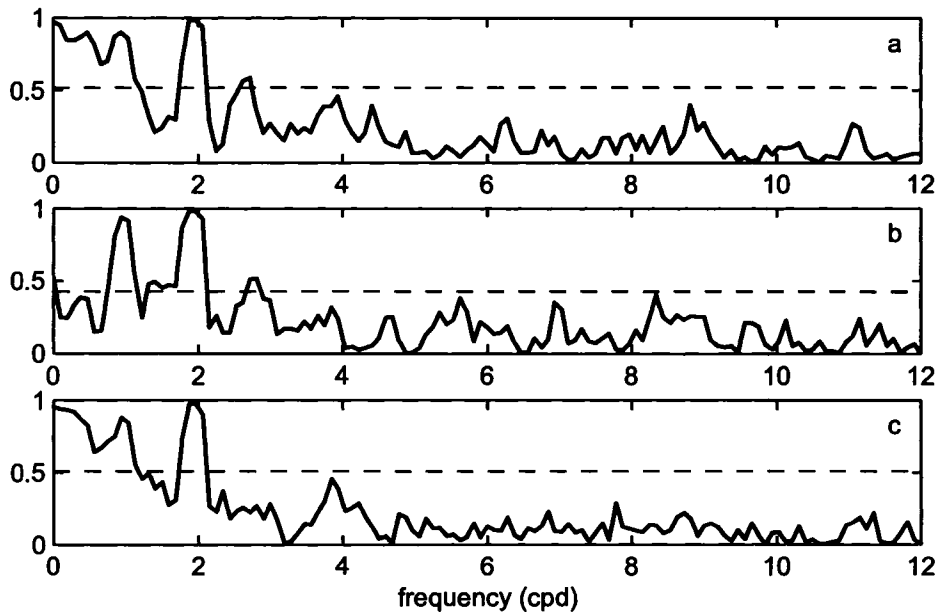

Figure 2.11: Horizontal coherence squared between M2-2003 and M3-2003 at a) 2 metres, b) 6 metres, and c) 15 metres. Data is from day 301 to 530 2003. The 95% confidence limit is indicated by the dashed horizontal line.

An analysis of the major axis direction for each mooring was performed (Emery and Thomson, 1998) and the results are shown in the Bonne Bay data report (Richards and de Young, 2004). By solving for the eigenvalues of the covariance matrix for the u and v velocities, the angle of the principle axis θ_p can be found using:

$$\tan(2\theta_p) = \frac{\overline{2u'v'}}{\overline{u'^2} - \overline{v'^2}} \tag{2.1}$$

where $u' = u - \overline{u}$ and $v' = v - \overline{v}$. The depth dependant angles calculated through this process were then used to rotate the u and v axes for each depth at each mooring to visualize the through and cross channel velocities.

In addition, a MATLAB script was setup to process the data so that an across sill interpolation could be performed. The position of the transect is shown in Figure 2.12. This was necessary for visualizing the two-dimensional structure of the flow through the channel. Using this across channel interpolation, various parameters could be calculated and displayed, such as averages, transport, and the results of an Empirical Orthogonal Function analysis. The across channel interpolation was also used to create a series of movies for direct visualization of the flow time series. The average along channel flow for the 2003 data (Figure 2.13) shows a two layer system with outflow in the upper layer, and inflow below. The letters above indicate the positions of the moorings, and it is clear that in order to calculate transport for the entire channel, the values must be extrapolated to the sides. Values between the moorings were linearly interpolated, while values outside the area were extended horizontally from the edges.

By using the across channel interpolation to calculate average flow, the average

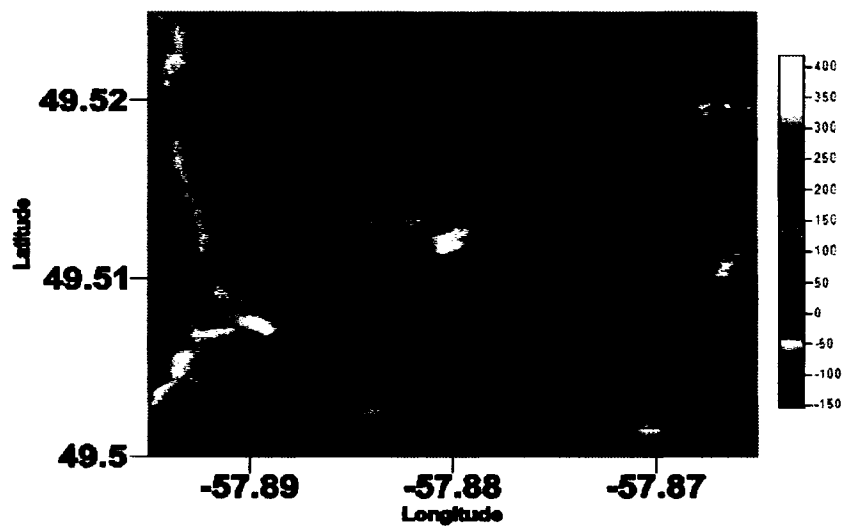

Figure 2.12: Transect across the sill on which the across channel interpolation is performed.

transport of the two layers can be determined. Combined with salinity data from the sill, these transports can then be used in Knudsen's relation (see Chapter 1) to estimate parameters such as the freshwater input. Estimation of the freshwater input to Bonne Bay was determined using this method, however it must be kept in mind that the accuracy of this analysis is limited by the salinity data, the uncertainty in the measured velocity, and the validity of the extrapolation to estimate the through channel transport. By considering an error velocity in the ADCP measurements of about 1 cm/s, the uncertainty in the across channel transport was estimated to be about 5×10^1 m^3/s.

Salinities obtained in June 2004 give upper and lower layer values of 27 and 32

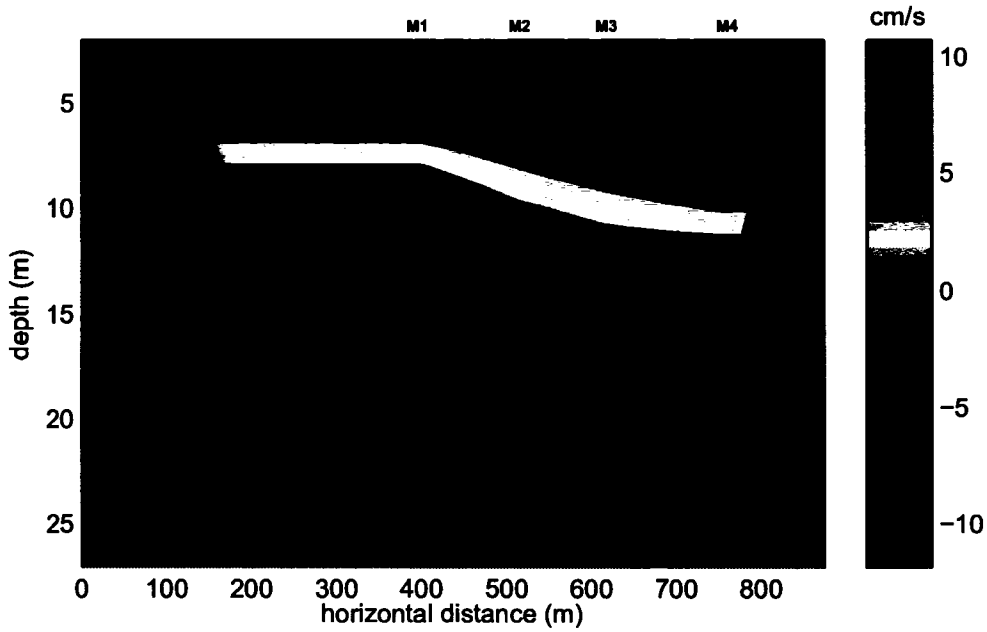

Figure 2.13: Average cross channel structure of the along channel flow for 2003 data, from day 301 to 485 2003. The letters above the plot indicate the positions of the moorings. Values in between moorings are linearly interpolated, while those outside the covered area are extended from the edges. The solid black line shows the zero contour.

psu respectively. The lower layer transport calculated from the average flow in Figure 2.13 is $(3.6 \pm 0.5) \times 10^2$ m^3/s. Using the June 2004 salinities gives a freshwater input of $(0.7 \pm 0.1) \times 10^2$ m^3/s. By comparison, estimation of the upper layer transport from Figure 2.13 gives a value of $(2.4 \pm 0.5) \times 10^2$ m^3/s, much less than expected considering that Knudsen's relation $V_U = V_L + V_R$, indicates that V_U should be about $(4.3 \pm 0.6) \times 10^2$ m^3/s. This difference could result from the discarding of ADCP data from the upper two metres where surface effects contaminate the velocity estimate. To obtain an estimate of the transport of the entire upper layer, the transport of the topmost depth bin in Figure 2.13 was added in twice. The result of this approximation gives a value for the upper layer transport of $(4.2 \pm 0.5) \times 10^2$ m^3/s. The agreement

of this calculation with the value of $(4.3 \pm 0.6) \times 10^2$ m^3/s determined using the salinities indicates that this is a reasonably good approximation for calculating upper layer transport, and is used in latter parts of the analysis when comparing model calculated transports over the sill with data (Chapter 4).

As was mentioned above, the accuracy of the Knudsen analysis for Bonne Bay depends largely on the salinities used. Salinity profiles were collected during June 2004, and unfortunately hydrographic data for the area does not exist for any other times during the deployment period. As the 2003 data set allowed for transport calculations to be performed between the 29th of October 2003 and the 1st of May 2004 (day 301 to 485 2003) the use of hydrographic data from that spring would have represented the salinity structure near the sill for at least the latter parts of the time period. At the very least the Knudsen analysis provides some indication of the scale of the estuarine circulation in the Bay. Clearly the June 2004 salinity data are not well suited for use with the 2002 data set (day 251 to 321 2002).

2.3.2 Wind Data

Due to the mountainous terrain and the strong winds that are common to the area, it was necessary to consider the validity of the Rocky Harbour wind data (approximately 4 km away from the sill, see Figure 2.4) for determining wind forcing in Bonne Bay.

Because there was overlapping data for the period from June 19th to September 19th 2004 for both the Rocky Harbour and Norris Point weather stations, these data sets could be compared directly (Figure 2.14). It was apparent that the Rocky Harbour weather station was receiving much less northerly wind than Norris Point, which was attributed to the hilly terrain directly to the north of the station, as well

as tree cover in that direction (Brian Hulan, personal communication). There were also several strong wind events that were visible at both stations, but in different directions. For example, on day 193, a strong wind event was seen to blow from the north at Norris Point, while the Rocky Harbour station registered it as a westerly of approximately the same magnitude. This is likely due to a northwesterly wind separating to flow over the land and the water. In the bay, the wind is directed along channel to the south, while on land the wind follows the topography and is directed eastward.

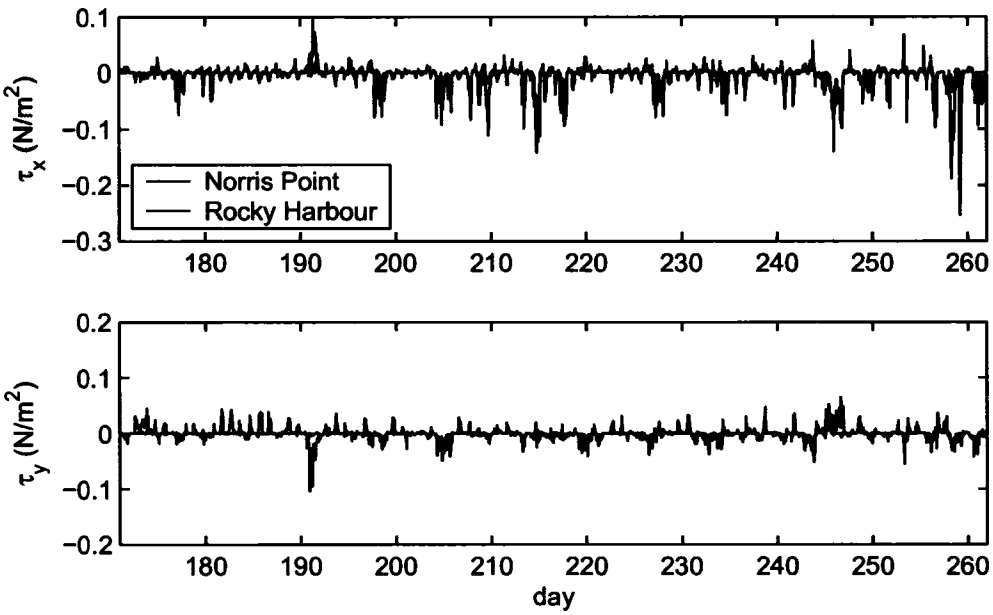

Figure 2.14: Comparison of Rocky Harbour and Norris Point wind stress during summer 2004. Wind stress is reported in the oceanographic convention.

Another way to compare the dynamics of wind in the two locations is to construct a polar histogram (rose plot in MATLAB) (Figure 2.15). From these plots, it can be seen that the northwest and southwest components are approximately of the same

magnitude, while the northeast component at Rocky Harbour appears to have been rotated further to the north at Norris Point. Also, Norris Point shows very strong easterlies, which do not occur at all at the Rocky Harbour station, a fact which can be attributed to along-channel winds being funnelled out of the east arm of Bonne Bay. At the Rocky Harbour station, these easterlies are blocked by topography.

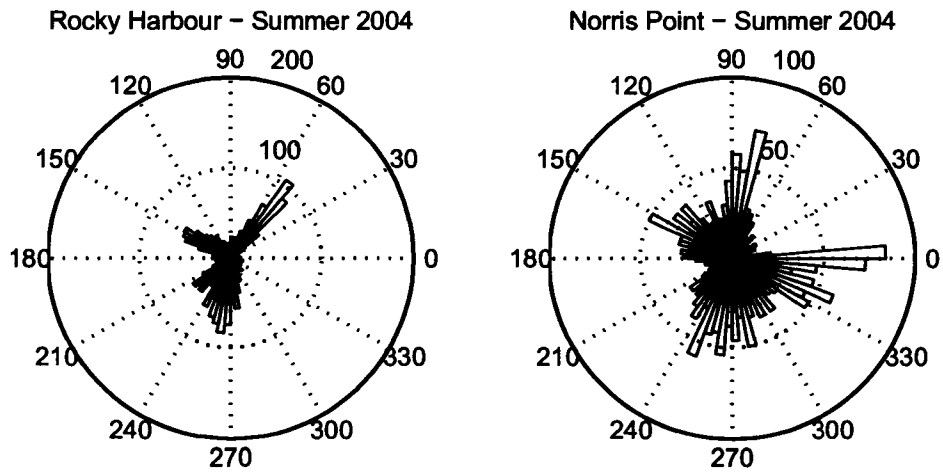

Figure 2.15: Rocky Harbour and Norris Point rose plot comparison for days 170-265 2004. Winds are shown in the meteorological convention, reported as the direction from which the wind is blowing.

Although the data recorded at Norris Point are likely a better representation of the local wind over the sill, they can only be used to accompany moorings M1-2004 and M2-2004, and therefore the Rocky Harbour data must be used for most of the analysis. The fact that spatial inhomogeneities exist in the wind field however, should be kept in mind for any analysis using these data.

2.3.3 Hydrographic Data

The hydrographic data collected during cruises in June 2004 are presented here in Figures 2.16 and 2.17. The transect in the South arm (Figure 2.16) shows iso-lines for temperature, salinity and σ_t which are all relatively horizontal. The data also reveal a pycnocline at a depth of 6 to 8 m. The rapid contour changes that occur near the mooring locations are due to the fact that stations 2 and 4 were collected on June 9 2004, while stations 1, 3 and 5 were collected on June 13 2004, and were therefore collected at different tidal cycles. The transect from the East arm over the sill and out into the Gulf of St. Lawrence (Figure 2.17) shows typical distributions of temperature, salinity and σ_t for a fjord. The surface salinity increases from 25.4 psu at the head to 31.8 psu in the Gulf. Note the effect of the sill, in that deeper water on the Gulf side is denser than that within the bay by approximately 0.2 kg/m^3, also typical for a shallow-silled fjord.

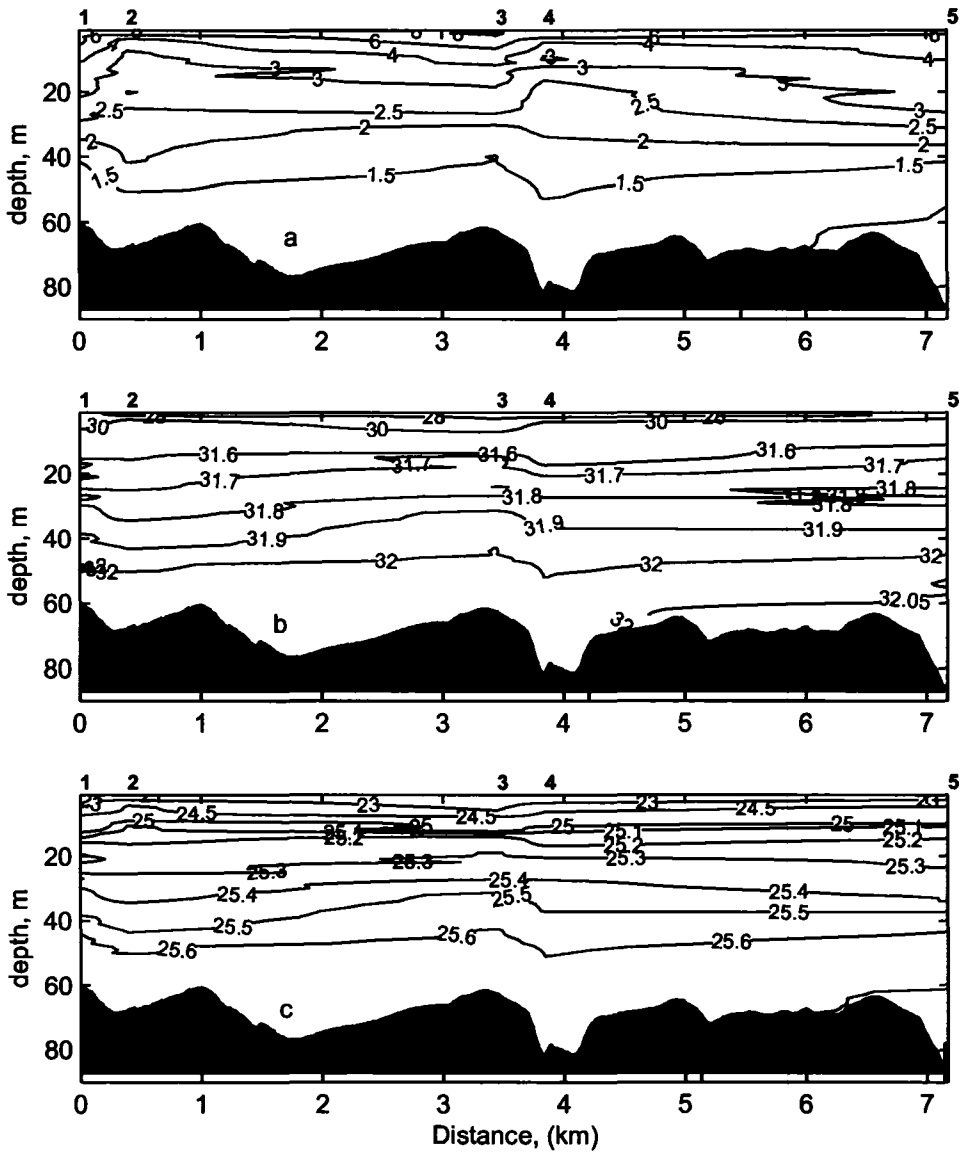

Figure 2.16: a) T, b) S, and c) σ_t along the South arm of Bonne Bay, June 2004. Numbers indicate CTD station locations in Figure 2.6. Stations 2 and 4 were collected June 9 2004, while stations 1, 3 and 5 were collected June 13 2004. This is the cause of the rapid contour changes near the stations.

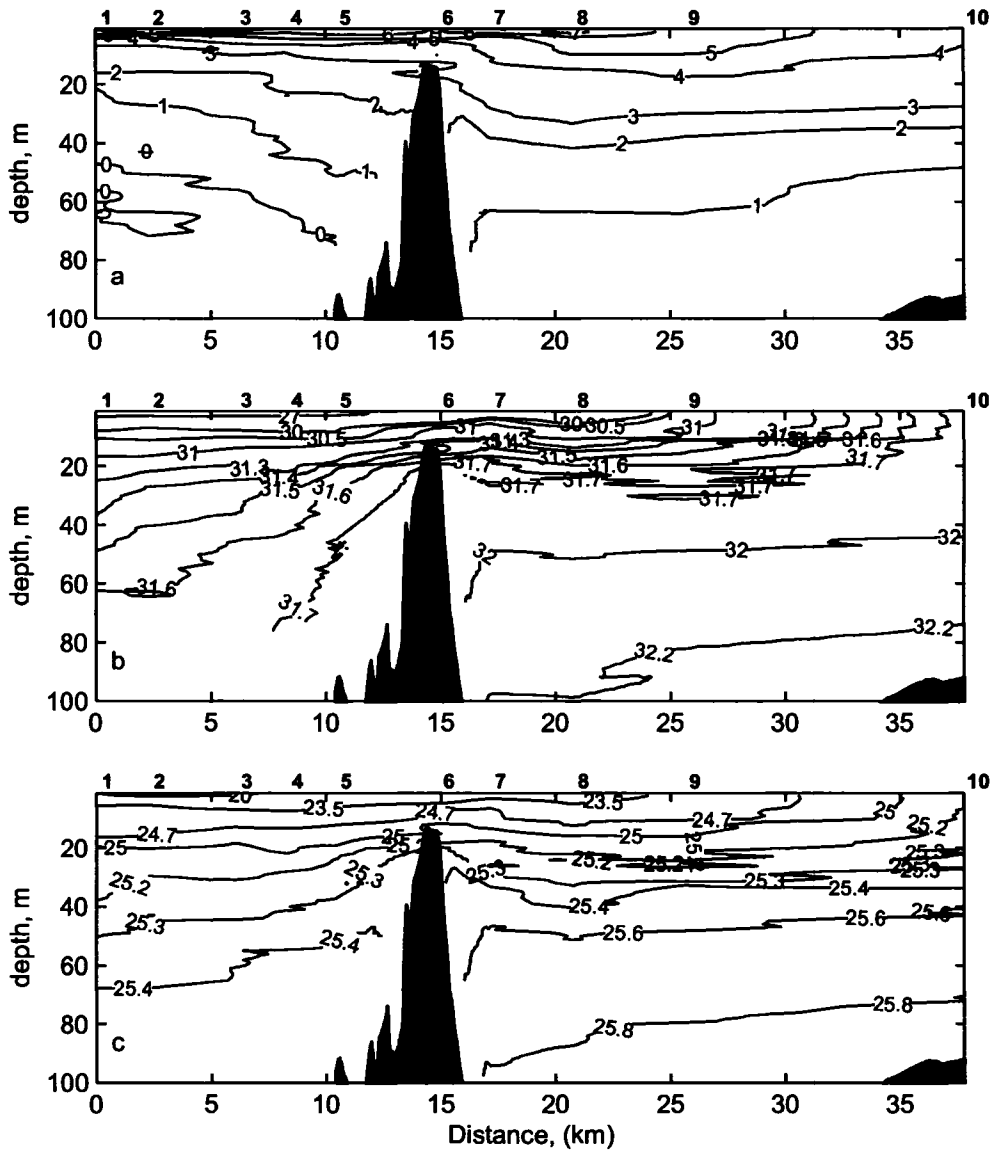

Figure 2.17: a) T, b) S, and c) σ_t over the sill of Bonne Bay, June 2004. Numbers indicate CTD station locations in Figure 2.5. Stations 1-6 were collected June 8 2004, while stations 7-10 were collected June 13 2004.

Chapter 3

Tidal and High-Frequency Flow

In this and the following chapter, I present analysis of the flow at several different timescales, and therefore the sections are divided accordingly. Section 3.1 deals with the tidal nature of the flow over the sill while section 3.2 examines the very high frequency flow in Bonne Bay, specifically for periods of 5 hours or less. The subtidal flow over the sill, in particular at periods from days to months, will be discussed in Chapter 4.

The analysis in this and the following chapter focuses on data from two different time periods during the two years corresponding to when there was the best coverage of the sill. During the time period from the 9th of September to the 18th of November (day 251 to 321) 2002, there were 3 ADCPs collecting data: M1-2002, M3-2002, and M4-2002. Similarly from the 29th of October 2003 to the 1st of May 2004 (day 301 to 485 2003) all four moorings were collecting data.

3.1 Tidal Characteristics of the Flow

Due to the shallowness of the sill (~14 metres), and the lateral constriction at the mouth of the East arm, tidal currents are very important for time periods ranging from hours to days. Tidal velocities over the sill can be in excess of 1.5 m/s, and the area is known for tide rips. High tidal velocities can also lead to mixing in the vicinity of the sill, due to the interaction of the stratified flow with the topography to produce internal waves, which can then break locally under critical flow conditions.

3.1.1 Tidal Analysis

Tidal harmonic analysis of the current data was performed for each mooring at all depths using T_TIDE, the Foreman tidal analysis scripts for MATLAB (Pawlowicz *et al.*, 2002). Before analysis the data from each depth were rotated along the major axis angle determined from equation 2.1. The results for selected tidal constituents are summarized in Tables 3.1 and 3.2. In addition a plot of the amplitude of each tidal constituent with depth is shown in Figure 3.1 for M2-2003.

The shape of the tidal amplitude plot in Figure 3.1 is consistent with that from the other moorings. It shows the tidal current velocities for all major constituents decreasing with depth, and a general pattern in the deeper moorings (like that shown in Figure 3.1) of the tidal currents near the bottom being about 30 to 50 percent of those near the surface. This decrease is attributed to frictional drag at the bottom.

Figure 3.2 shows a power spectral density plot (PSD) of east-west current velocity from M2-2003 at all depths. It is clear that the energy spectrum is dominated by tidal frequencies, with clear bands occurring at 1 and 2 cycles per day (diurnal and

	M1-02	M2-02	M3-02	M4-02	M1-03
O1	3.3847	2.9619	3.1007	1.8643	4.5025
K1	3.6587	4.4669	4.1717	3.8913	3.8338
N2	7.672	4.7343	5.1694	5.7751	4.8655
M2	28.714	20.049	22.212	23.196	25.156
S2	11.136	6.9914	7.3674	8.6211	8.1085
K2	2.5186	1.4606	1.8695	3.1464	2.1382
M4	2.2628	1.0955	1.7726	1.4877	0.7206
	M2-03	M3-03	M4-03	M1-04	M2-04
O1	4.1137	3.4378	3.9749	3.1373	2.7033
K1	4.4869	3.3808	3.7726	4.4124	4.4504
N2	4.4686	3.7121	5.3796	6.2531	4.5796
M2	23.322	20.012	27.706	24.675	19.527
S2	8.219	7.0213	9.5977	8.1202	7.398
K2	2.2603	1.8595	2.6063	2.545	2.0411
M4	0.2713	1.2957	0.8433	3.8177	1.7458

Table 3.1: Amplitudes (cm/s) of selected tidal constituents at a depth of 2 metres for the dates given in Table 2.2.

semidiurnal), as well as a weaker band at 4 cycles per day (the M_4 tide - a shallow water overtide of M_2 caused by non-linear interactions). There is also clearly energy in subtidal bands (below 1 cpd), which will be further discussed in Chapter 4.

The tidal currents over the sill are dominated by the semi-diurnal M_2 tide (Figures 3.1 and 3.2), which is about three times larger than the next largest constituent - S_2. In addition, the semidiurnal tide is clearly dominant over the diurnal. This is consistent with results for the northeast GSL as seen in Godin (1980). M_2 tidal current phases of 350°at the surface in Bonne Bay are approximately 90°out of phase with surface height along the west coast of Newfoundland.

3.1.2 Across Channel Structure of the Tidal Flow

The results from the tidal harmonic analysis were plotted on a two dimensional plane using the interpolation script discussed in Section 2.3.1 so that they could be viewed in terms of their across channel values. The results for days 301 to 485 2003 show the across channel structure of the amplitudes of the M_2 and K_1 components, each

	M1-02	M2-02	M3-02	M4-02	M1-03
O1	158.32	183.96	176	169.33	190.88
K1	170.13	169.36	163.82	188.6	167
N2	348.24	351.88	341.4	354.16	9.5444
M2	355.07	358.54	352	11.386	10.751
S2	356.5	1.3513	350.28	18.35	11.561
K2	301.21	350.88	352.17	335.46	21.653
M4	218.65	230.94	203.87	221.76	293.35
	M2-03	M3-03	M4-03	M1-04	M2-04
O1	190.09	185.59	185.37	217.61	170.17
K1	171.29	164.69	187.57	222.32	201.57
N2	13.704	354.22	359.2	353.76	336.37
M2	6.4811	357.24	3.7712	0.0193	350.98
S2	17.517	4.4448	6.2859	0.1107	345.14
K2	5.7477	1.9013	0.8078	2.7214	358.05
M4	58.918	330.04	256.93	199.52	136.55

Table 3.2: Phase (degrees relative to Greenwich) of selected tidal constituents at a depth of 2 metres for the dates given in Table 2.2.

rotated according to the inclination determined from the harmonic analysis of the tidal ellipse (Figure 3.3). There is some across channel structure to the tidal response with stronger tidal currents on the northern side of the channel in deeper water.

In addition to the tidal amplitude plots, empirical orthogonal function (EOF) analysis was performed on the tidal data for both the 2002 and 2003 data, following Björnsson and Venegas (1997). The results of the analysis showed that approximately 76% and 84% of the respective variance was explained by the first mode (Figures 3.4 and 3.5). Mode 2 of the analysis, accounting for 16% and 8% of the respective variance, showed a two layer exchange and is attributed to the subtidal flow over the sill, to be discussed in Chapter 4. Comparison of Figures 3.3 and 3.5 reinforce the observation that tidal flow through the channel is dominated by the M_2 tide, which is consistent with the tidal analysis of the principle component of the EOF shown in Figures 3.4c and 3.5c.

In addition to the EOF analysis of the tidal data, average flows were determined for ebb and flood tidal periods for both the 2002 and 2003 data. The results for 2002

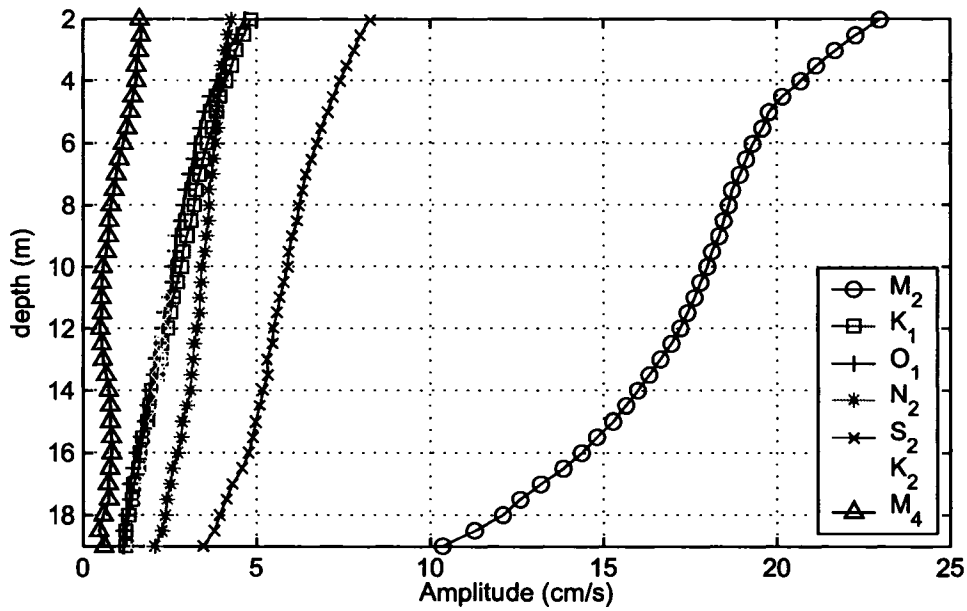

Figure 3.1: Amplitude of selected tidal constituents for mooring M2-2003 at all depths, between days 301 and 530 2003, from tidal analysis.

are quite similar and so only the results for 2003 are shown in Figure 3.6. These calculations were performed by first separating the tidal flow into ebb and flood periods and then calculating averages.

The structure of the tidal transport differs on ebb and flood tide (Figure 3.6). During an ebb tidal phase, the average flow is out of the bay and the strongest currents occur at the surface. The magnitude decreases with depth, to the point where at the bottom of the channel, the current actually reverses and there is a net inflow. For the flood phase, the flow is everywhere into the bay, and the strongest currents occur around the deepest part of the channel, between 15 to 20 metres depth. This asymmetry between ebb and flood tides is attributed to a combination of the fjord estuarine circulation, the decrease of tidal amplitude with depth, and

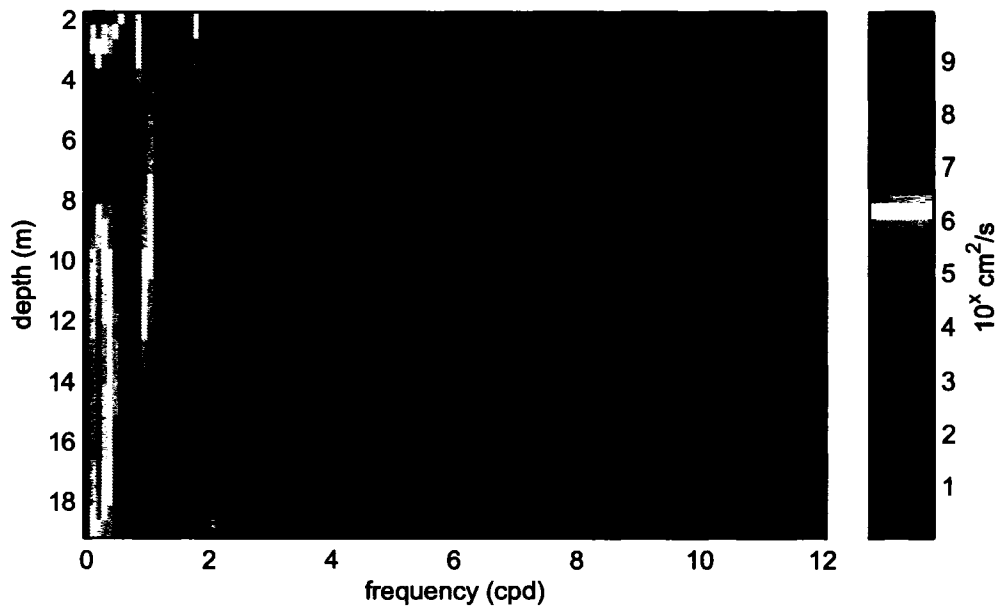

Figure 3.2: Power Spectral Density of through channel velocity from mooring M2-2003 at all depths, between days 301 and 530 2003. The colour scale on the right is logarithmic. Number of degrees of freedom is 21.

possibly the across channel topography of the sill. During the ebb phase, the weaker tidal amplitudes near the bottom are not enough to overcome the inflow due to the estuarine circulation. During the flood phase, the larger tidal amplitudes near the surface are enough to overcome the estuarine surface outflow, while the estuarine inflow at depth is enhanced by the incoming tidal flow. This hypothesis is reinforced by Figure 3.7, which shows the average estuarine flow (Figure 2.13) added to the across channel M_2 amplitudes determined with tidal analysis (Figure 3.3a).

Band pass filtering the ebb and flood flow to isolate the diurnal and semidiurnal before average produces a different result. The across channel structure of the flow looks more like what would be expected based on the tidal analysis plot shown in

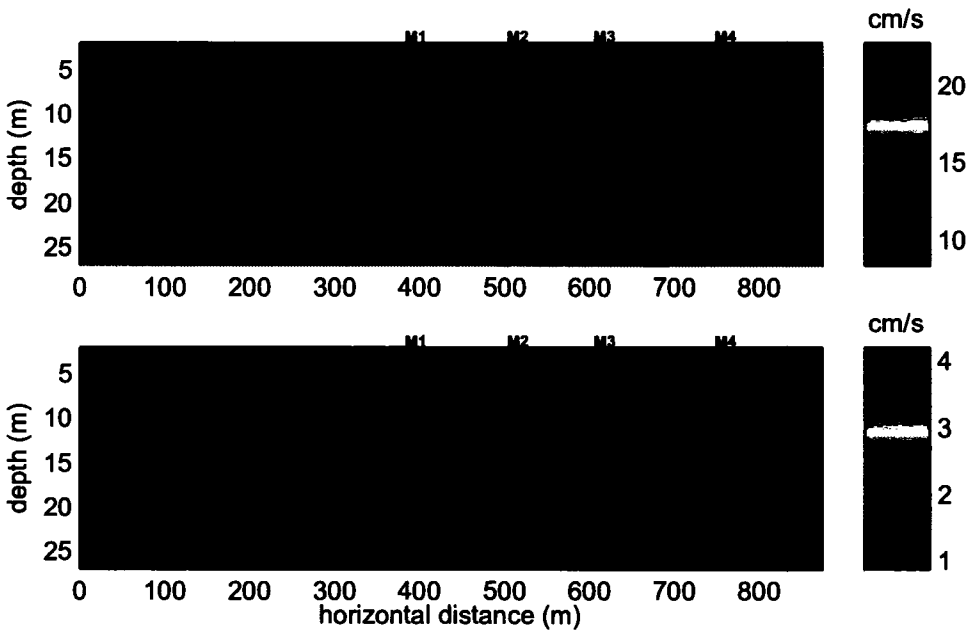

Figure 3.3: Across channel structure of the amplitudes of the a) M_2 and b) K_1 tidal constituents, days 301 to 485 2003, as determined from the tidal analysis. Interpolation between moorings is linear, and values outside are extrapolated from the edge.

Figure 3.1. The tidal currents are either in or out of the bay at all depths, and the amplitude decreases toward the bottom.

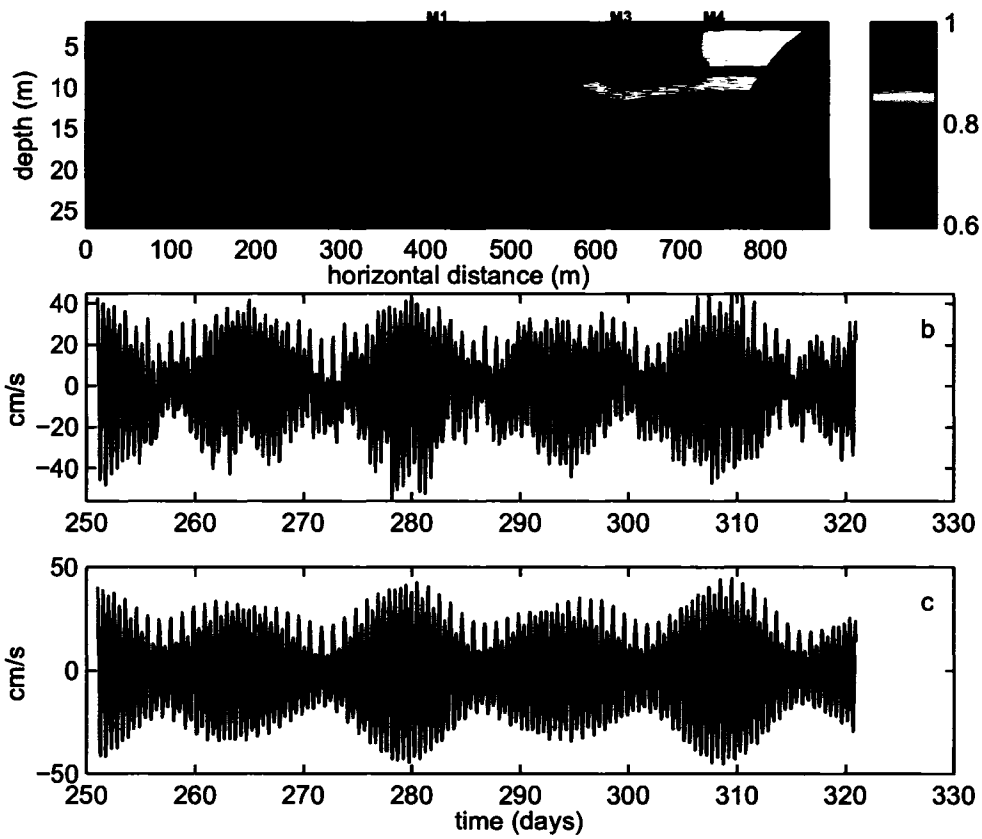

Figure 3.4: Mode 1 of the EOF analysis of the raw data from day 251 to 321 2002, containing 76% of the variance. Interpolation between moorings is linear, and values outside are extrapolated from the edge. Units in cross channel amplitude plot (a) have been normalized, so that units for the principle component time series in b) are in cm/s. Plot c) is the result of a tidal analysis of b) showing the dominant M_2 tide with a fortnightly modulation. The correlation coefficient between the two time series is 0.98.

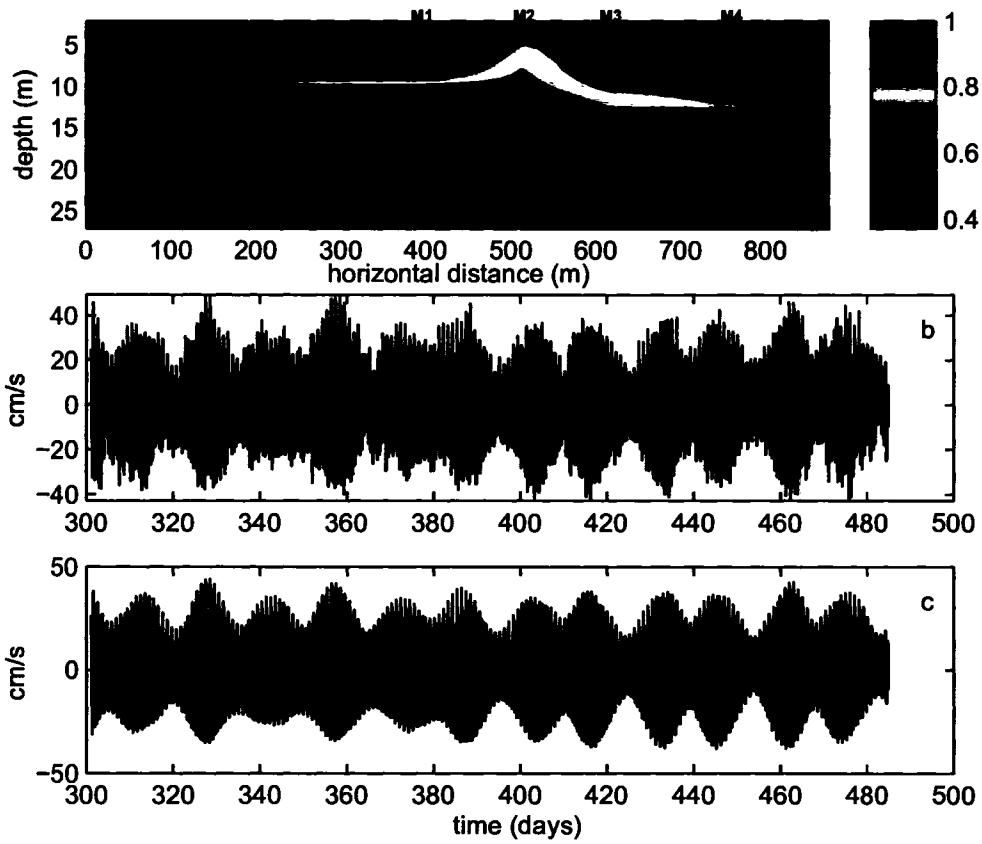

Figure 3.5: Mode 1 of the EOF analysis of the raw data from day 301 to 485 2003, containing 84% of the variance. Interpolation between moorings is linear, and values outside are extrapolated from the edge. Units in cross channel amplitude plot (a) have been normalized, so that units for the principle component time series in b) are in cm/s. Plot c) is the result of a tidal analysis of b) showing the dominant M_2 tide with a fortnightly modulation. The correlation coefficient between the two time series is 0.98.

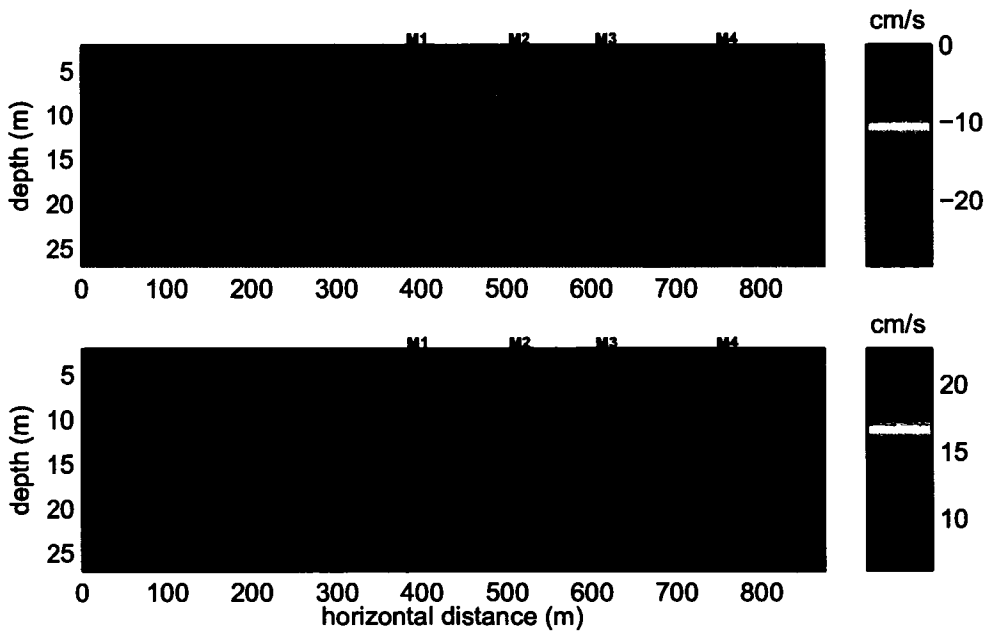

Figure 3.6: Average a) ebb and b) flood flow for 2003 data, from day 301 to 484 2003. Interpolation between moorings is linear, and values outside are extrapolated from the edge. The solid black line shows the zero contour.

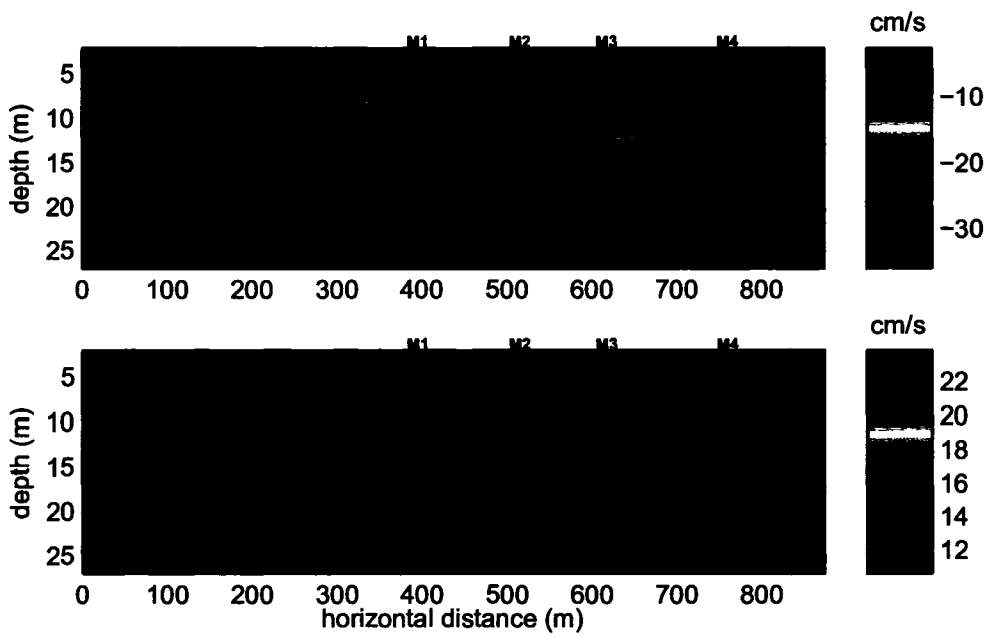

Figure 3.7: Average flow (Figure 2.13) added to the results of the tidal analysis for a) ebb tide, and b) flood tide for the same time period as in Figure 3.6.

3.1.3 Internal Tides

Internal tides are defined as internal waves at tidal frequencies, and they are generated in the ocean by the movement of stratified water over bottom topography by the barotropic tide (Baines, 1986). Internal tides occur frequently in areas such as continental shelf breaks, where a large change in water depth over a small horizontal scale can produce movement of isotherms in response to the surface tide. They can also occur in coastal regions due to variations in bottom topography, and high stratification. Internal tides have been observed in many coastal basins and estuaries, in particular fjords in western North America and Scandinavia, and are considered to be an important factor in vertical mixing (Farmer and Freeland, 1983).

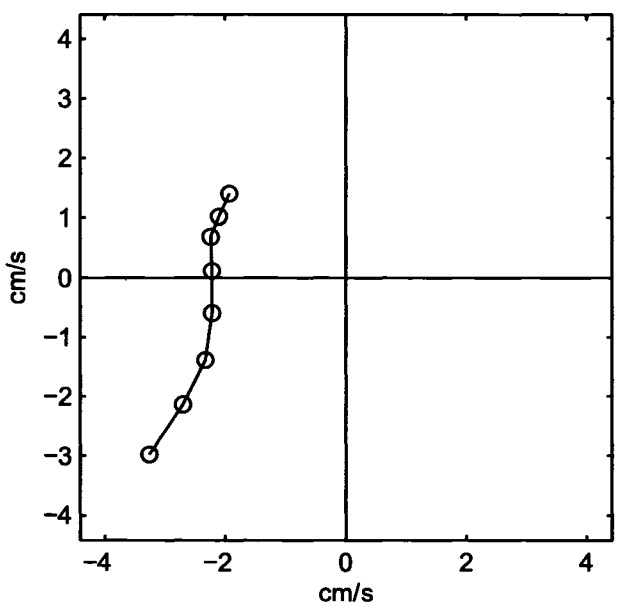

Figure 3.8: Plot of amplitude and phase on the complex plane for K_1 at M1-2004. The change in phase as a function of depth indicates the presence of internal tides.

As each ADCP instrument contained a temperature sensor, it is possible to reconstruct the presence of internal tides over the sill in conjunction with information on how the phase and amplitude of the constituents changes with depth. It is impossible to distinguish however whether these internal tides were generated locally at the sill, propagated onshore from a generation site outside the bay, or consist of some combination of the two. By plotting the amplitude and phase of a particular constituent on the complex plane for various depths, the presence of internal tides can be deduced by a change in phase throughout the water column. Figure 3.8 shows such a plot for the K_1 constituent at mooring M1-2004. Similar plots for other moorings show that changes in phase with depth are dependant on the season, with no phase change in the winter, and maximum in the summer.

Temperature data from the sill (Figure 3.9) reveal a clear annual cycle associated with seasonal warming and cooling, as well as higher frequency components which should consist mainly of tidal and subtidal frequencies.

Tidal analysis of the time series shows that there is a tidal signal to the variability but only at certain times of the year. Tidal analysis of the period from about day 300 to day 485 (late fall 2003 to early spring 2004) shows no significant tidal variation, while the early fall and late spring periods show a marked tidal signal, dominated by the M_2 constituent. This is shown for the summer and early fall period (day 200 to 300) in Figure 3.10. Note that spring tides correspond to stronger internal tidal signals, while during neap tides there is almost no internal tidal signal present. It is worth noting the step-like pattern to the tidal variations, which indicate a sharp thermocline in the region of the sill.

The absence of an internal tidal signal during the winter months is attributed to a

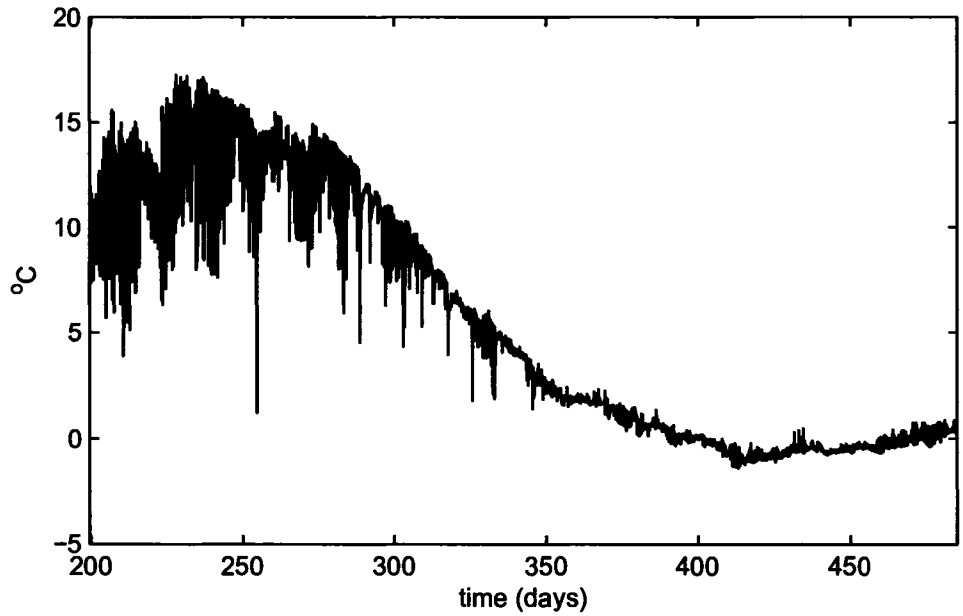

Figure 3.9: Temperature time series from M4-2003 (day 200 to 485 2003) showing the seasonal variation of temperature at the instrument, as well as the tidal fluctuations in the temperature record. Note the decrease in amplitude of tidal fluctuations after day 300.

decrease in stratification in the bay due to decreased river runoff, ice formation at the surface, and colder air temperatures. Decreased stratification reduces the capacity of the water column to support internal waves, and also potentially decreases the depth of the thermocline beyond that of the ADCP moorings. The effect of varying stratification on internal tidal motion has been observed many times while trying to study internal tides, making them much more difficult to study than their barotropic counterpart (Baines, 1986).

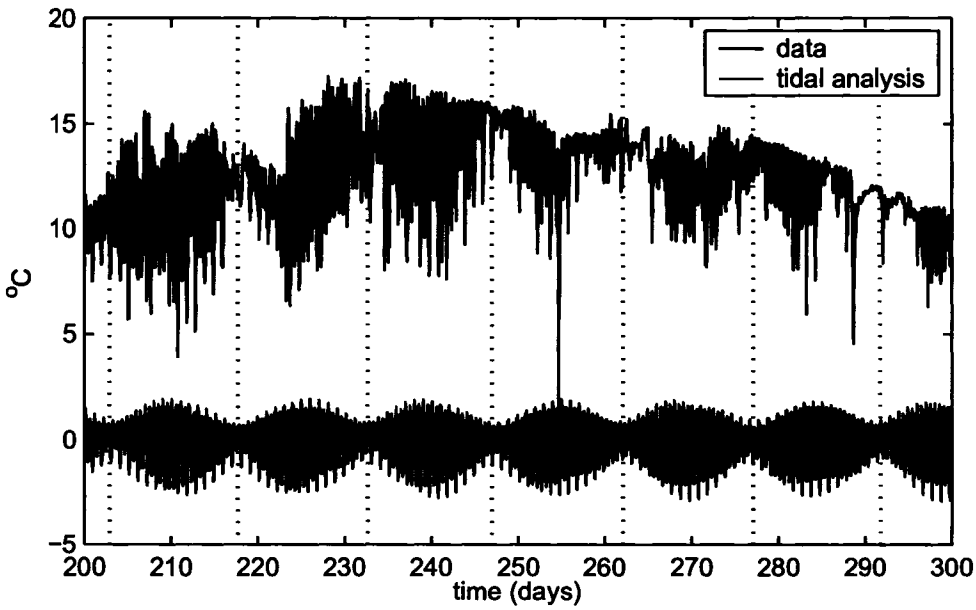

Figure 3.10: Superposition of raw temperature time series with tidal harmonic analysis of the temperature record from M4-2003 (day 200 to 300 2003). The tidal analysis time series has been detrended and so no longer contains seasonal variations. Vertical dotted lines indicate the positions of neap tides.

3.2 High Frequency Characteristics of the Flow

It was apparent from a visual inspection of the raw data that there was significant variability at frequencies greater than the semidiurnal tide. An expanded time series plot, focusing on just a few days of data, shows that there was current variability at periods of a few hours or less (Figure 3.11). Though it is possible that oscillations with frequencies greater than the Nyquist frequency are being aliased to produce the jagged features seen in Figure 3.11, examination of more recent data from the area (not shown here) with a sample rate of about 1 minute shows similar characteristics. To study the high frequency component of the flow over the sill, the ADCP data

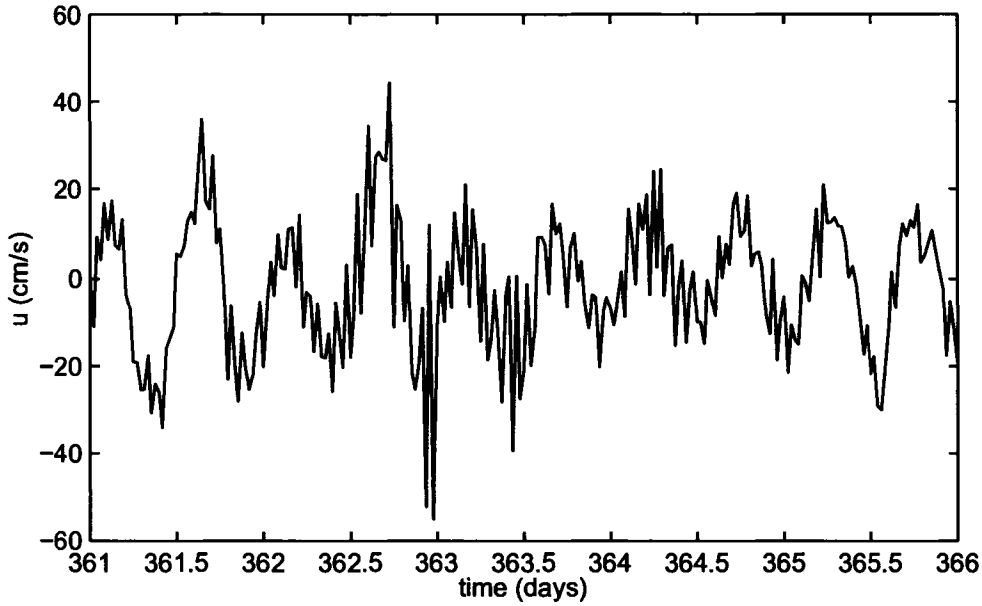

Figure 3.11: Closeup of unprocessed time series from M2-2003 spanning several days showing the high frequency variability at a depth of 6 metres. The averaging period is 30 minutes.

were filtered with a 5th order 5 hour cutoff forward and reverse highpass Butterworth filter. This removed all semidiurnal and lower frequencies from the record.

It was suspected that the high frequency nature of the flow was related to the presence of internal waves generated at the sill, and therefore should be related in some way to the currents in that location. In particular, tidal currents from diurnal and semidiurnal tides should cause high frequency internal waves and thus high frequency components in the flow over the sill. In addition, the fortnightly modulation of the M_2 tide should also affect the amplitude of the generated internal waves, and thus the energy of high frequency flow.

To examine the relationship between the high frequency flow and the tidal currents over the sill, the tidal and high frequency time series were converted from velocity

to a normalized kinetic energy. This procedure allowed for low pass filtering, so that the amplitude envelope of the signals could be directly compared. Filtering was done using a forward and reverse 5th order Butterworth filter (similar to that described in section 2.2) with a cutoff period of 10 days. Coherence analysis between the low pass filtered tidal kinetic energy and low pass filtered high frequency kinetic energy was then performed for every depth in the record, and examined specifically for coherence at a frequency of 0.07 cpd (ie. the beat frequency for the fortnightly modulations of the M_2 tide).

Results from the comparison show that there is indeed a relationship between the low pass filtered kinetic energy time series, but that the magnitude of the coherence at 0.07 cpd varies both with depth and time of year. Figures 3.12 through 3.15 show the results of this analysis from fall 2002 to summer 2003. Different moorings (and therefore depths) are examined as a result of the spatial and temporal coverage. Where possible, the analysis is carried out using moorings in the deepest part of the channel. As with internal tides, the ability of the water column to support internal waves depends on the stratification. Analysis from fall 2002 (Figure 3.12) shows the highest squared coherence of 0.6 at a depth of about 8 metres, implying the position of the pycnocline. There is little coherence above this depth. During winter 2003 (Figure 3.13), squared coherence is everywhere low, though there does seem to be a small peak of about 0.3 around 20 metres. This is consistent with the discussion of seasonal variation in stratification in Section 3.1.3 where the water column is less able to support internal motions due to reduced stratification in the winter months. Spring 2003 results (Figure 3.14) show low squared coherence at all depths except for 15 metres, where there is a very strong peak of 0.9. This peak is consistent between

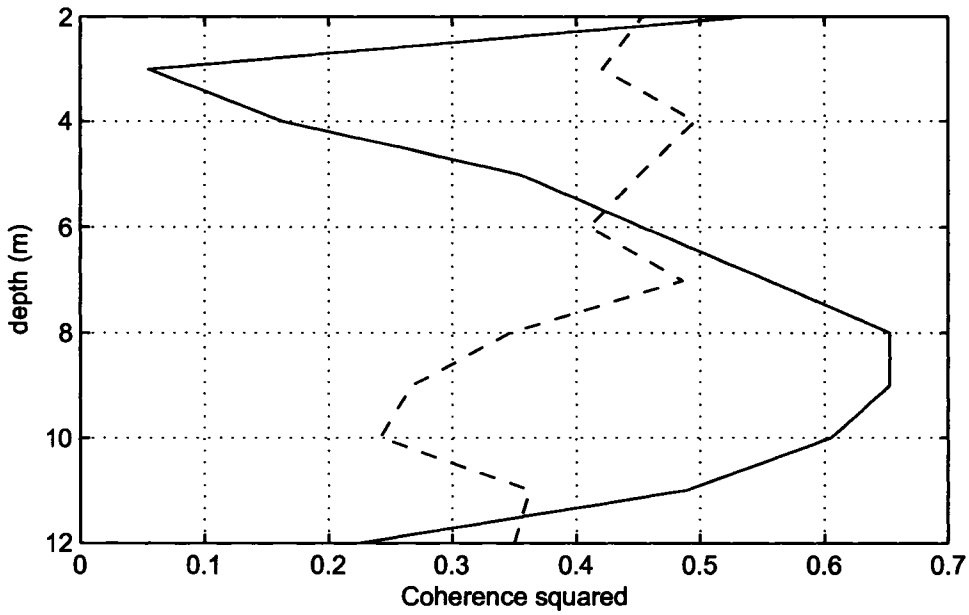

Figure 3.12: Coherence at 0.07 cpd between low pass filtered tidal kinetic energy and high frequency kinetic energy for fall 2002. The 95% confidence limit is indicated by the dashed line.

several moorings, and implies a well defined pycnocline at that depth. The results for summer 2003 indicate a return toward the conditions observed in fall, with a strong peak in the squared coherence of about 0.9 between 9 and 10 metres, implying that the spring pycnocline has gotten shallower, likely due to decreased river runoff after the spring melt was finished. Though this analysis reveals some aspects of the vertical structure the pycnocline depths given above should be treated only as approximate positions, due to the averaging time period (~3 months) and the lack of hydrographic time series.

The same analysis was performed on the data from fall 2003 to summer 2004, with similar results, except for some variations in the depth of maximum coherence and hence the implied position of the pycnocline. In particular, the analysis for winter

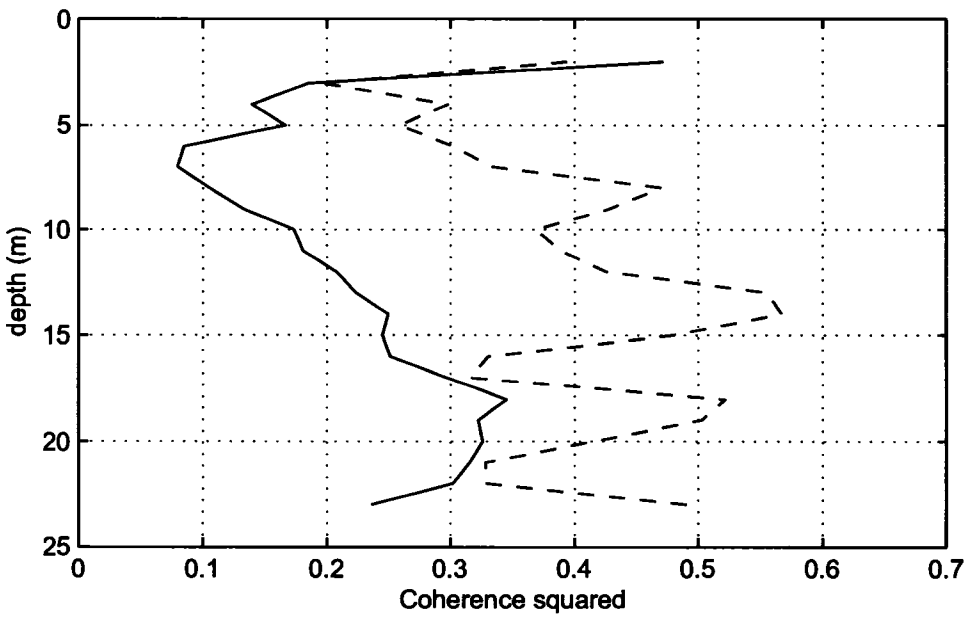

Figure 3.13: Coherence at 0.07 cpd between low pass filtered tidal kinetic energy and high frequency kinetic energy for winter 2003. The 95% confidence limit is indicated by the dashed line.

2004 (Figure 3.16) showed a strong peak in the squared coherence (greater than 0.9) at a depth of 20 metres. This may indicate that the depth of the mixed layer during that season was less than the previous year.

A plot of the low pass filtered tidal and high frequency kinetic energy time series (Figure 3.17) for summer 2004 from the depth of maximum coherence, illustrates the fortnightly modulation of the high frequency kinetic energy. Although peaks in the high frequency amplitude are clearly associated with spring tides, there is not complete agreement and at times there is substantial kinetic energy even during periods of weak, averaged tidal forcing.

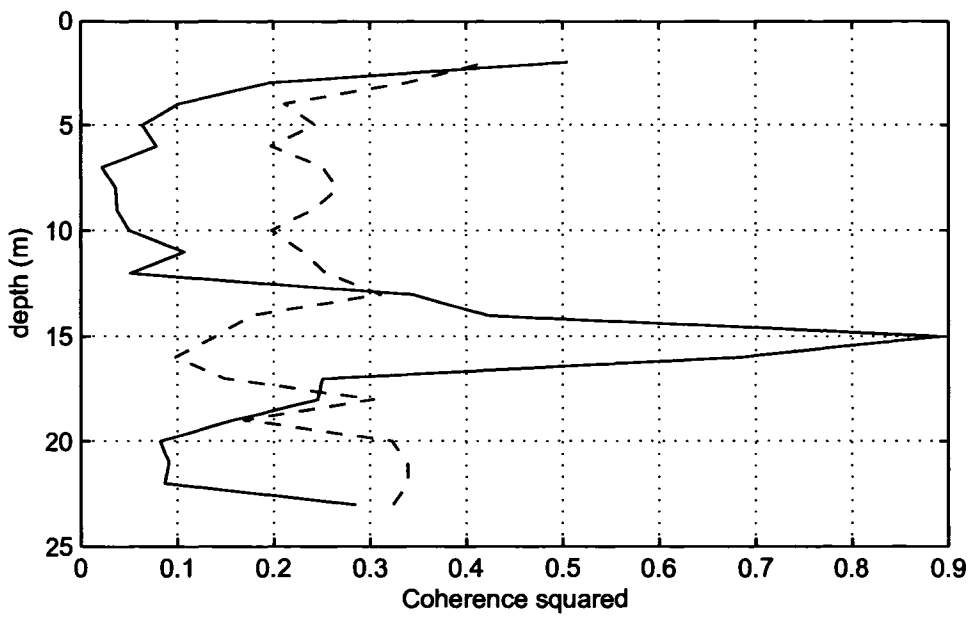

Figure 3.14: Coherence at 0.07 cpd between low pass filtered tidal kinetic energy and high frequency kinetic energy for spring 2003. The 95% confidence limit is indicated by the dashed line.

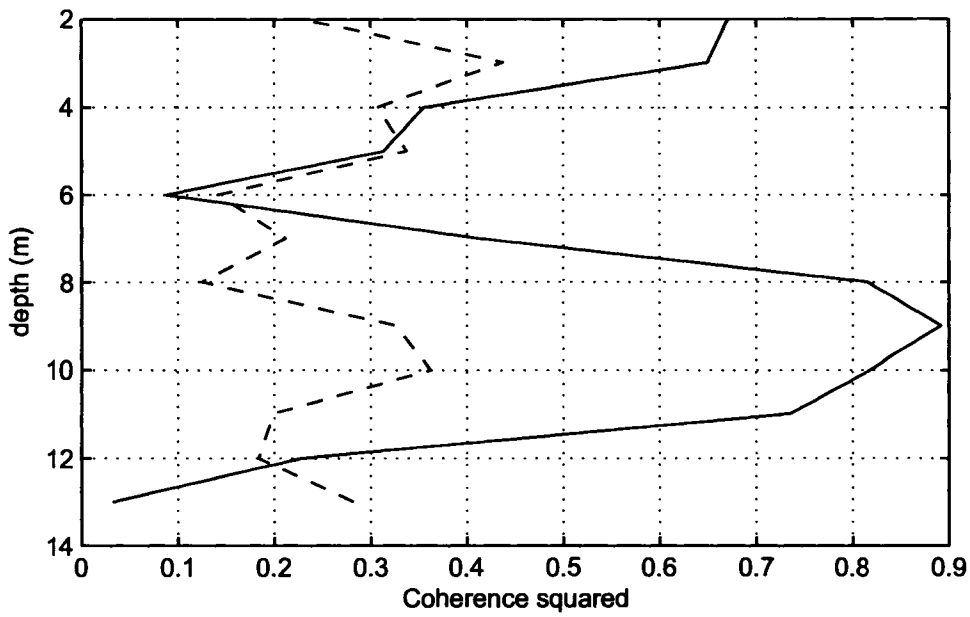

Figure 3.15: Coherence at 0.07 cpd between low pass filtered tidal kinetic energy and high frequency kinetic energy for summer 2003. The 95% confidence limit is indicated by the dashed line.

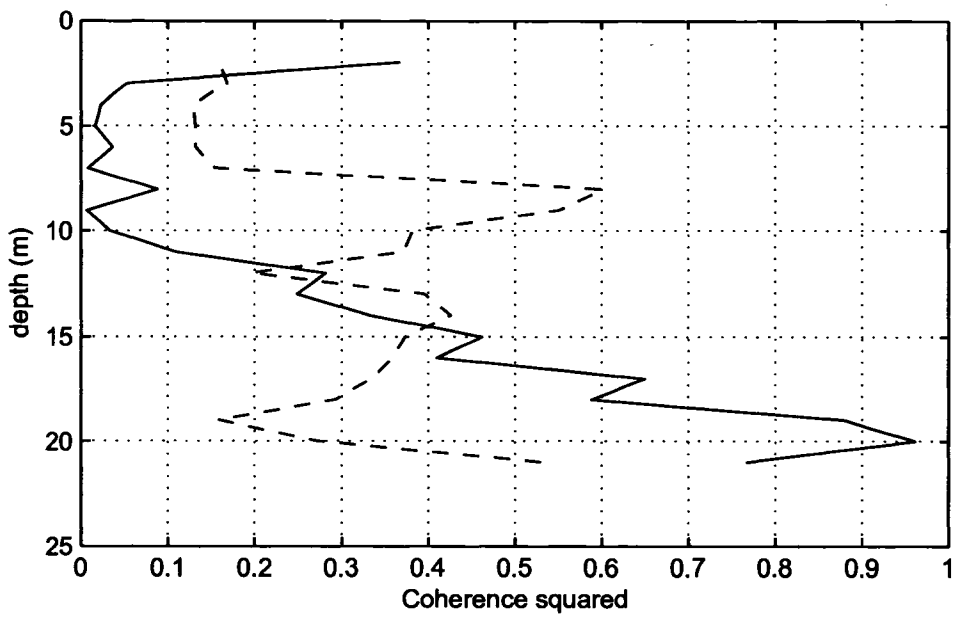

Figure 3.16: Coherence at 0.07 cpd between low pass filtered tidal KE and high frequency KE for winter 2004. The 95% confidence limit is indicated by the dashed line.

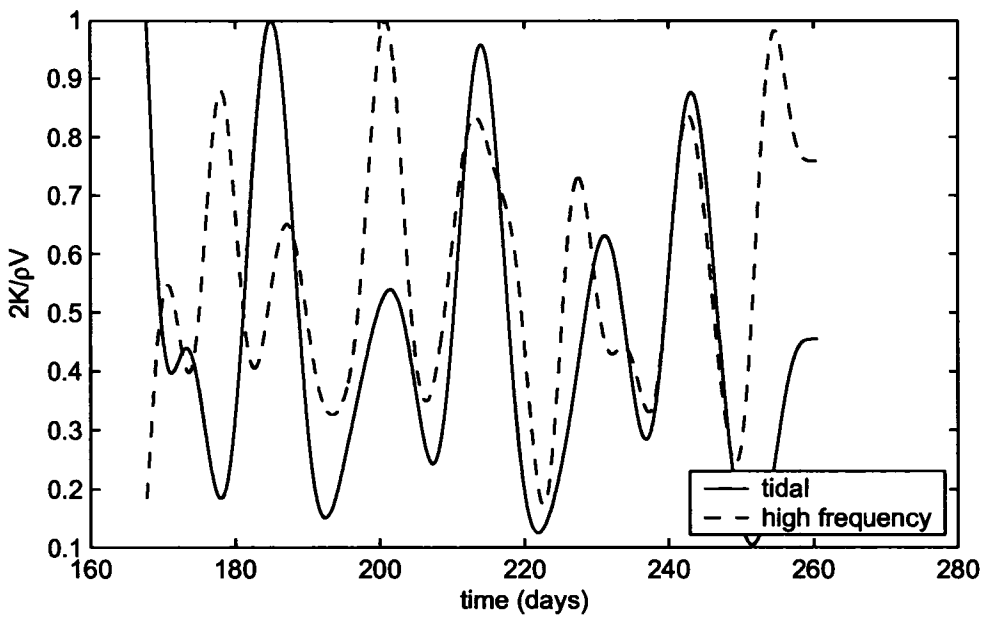

Figure 3.17: Comparison of tidal and high frequency kinetic energy for M1-2004 at a depth of 9 metres. Amplitudes of the two series have been normalized for easier comparison.

Chapter 4

Subtidal Flow

In addition to the tidal and high frequency components of the flow examined in Chapter 3, there is a significant amount of energy at frequencies less than one cycle per day (see Figures 3.2 and 4.1). This flow is referred to as subtidal, as it occurs at frequencies much lower than the dominant tidal frequencies, at periods from several days to months.

The subtidal flow in fjords and estuaries has been studied for many different systems with a variety of motivations. Subtidal flows in fjords have been attributed to many different causes. The most common of these include: wind forcing (Bretschneider et al., 1985; Matsuura and Cannon, 1997), deepwater renewal (de Young and Pond, 1988; Gillibrand et al., 1995), shelf processes occurring outside the fjord (Farmer and Freeland, 1983), and changes in freshwater discharge. It can be difficult at times to distinguish a subtidal exchange event as being related to one particular cause, as many exchanges will involve two or more of the different types of forcings.

4.1 Subtidal Characteristics of the Flow

In order to examine the subtidal characteristics of the flow over the sill, the velocity data from each mooring were filtered with a 30 hour cutoff filter as described in Section 2.2. A spectral density plot of the filtered data (Figure 4.1) shows that there is lower spectral energy 6 metres below the surface.

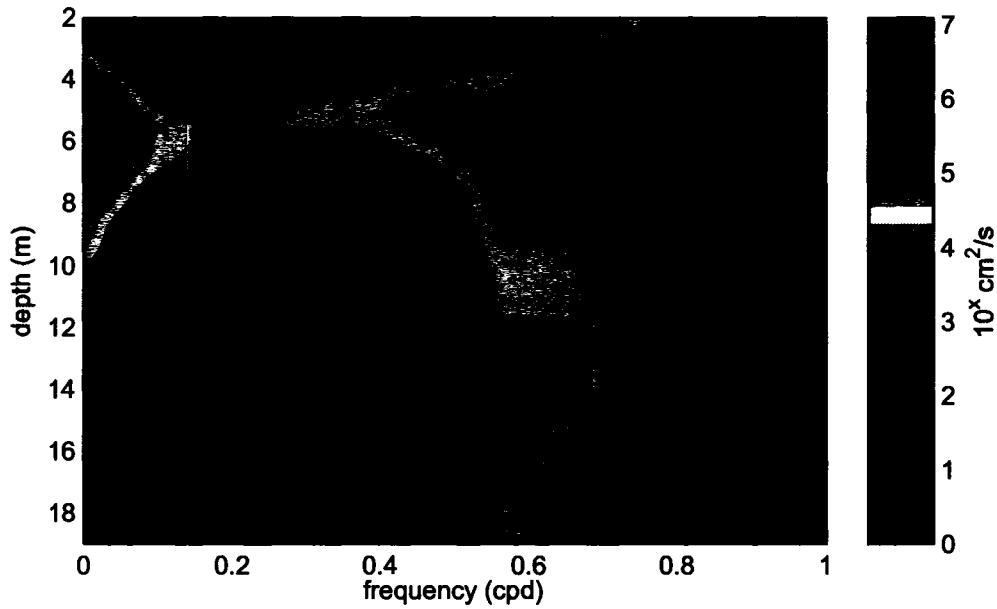

Figure 4.1: Power Spectral Density plot of u velocity from M2-2003 at all depths, filtered with a 30 hour cutoff. Data is from 11/10/2003 to 06/19/2004 (day 284 to 535 2003). Number of degrees of freedom is 21.

As with the tidal data, EOF analysis was performed on the filtered data from 2002 and 2003. Mode 1 of the analysis shows a distinctly two layer system with flow in the bottom layer in the opposite direction to the upper layer (see Figures 4.2 and 4.3). This mode is also the most significant, containing 84% and 74% of the variance for each data set respectively. Note that prior to the EOF analysis the data were

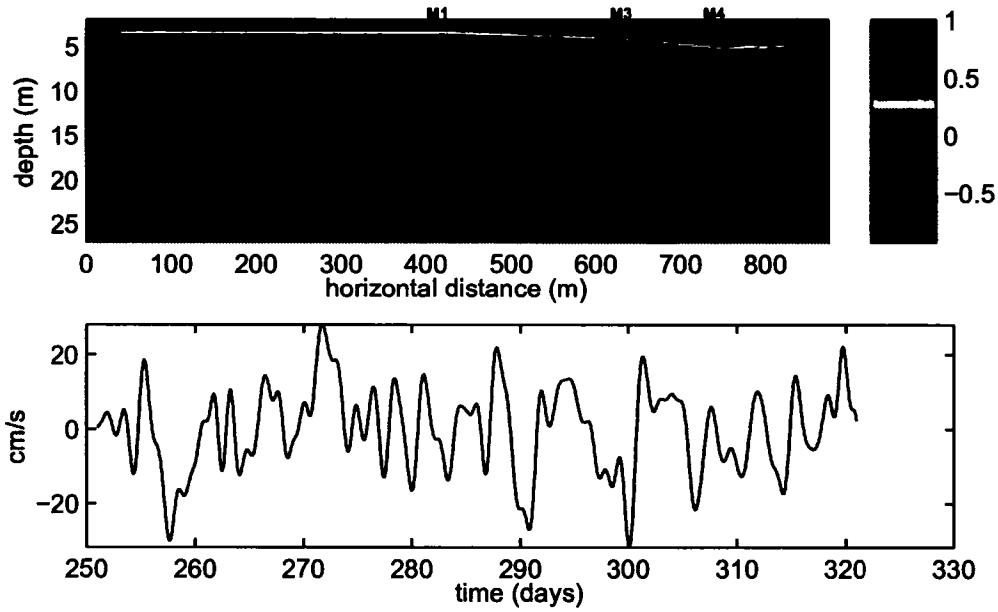

Figure 4.2: Mode 1 of the EOF analysis of the filtered data from day 251 to 321 2002, containing 84% of the variance. Interpolation between moorings is linear, and values outside are extrapolated from the edge. Units in the across channel amplitude plot have been normalized, so that units for the principle component time series are in cm/s. The black line indicates the zero contour.

rotated according to the direction of maximum variance as determined in section 2.3.1. Although the EOF analysis produced higher order modes, none of them were found to be significantly correlated with any physical variables, and contained comparatively low amounts of the total variance (less than 6%).

4.1.1 Causes of Subtidal Exchange

Local Wind

In a study of Alberni Inlet British Columbia, Farmer and Osborn (1976) noted the effect of local up-down fjord winds on the circulation and surface layer thickness.

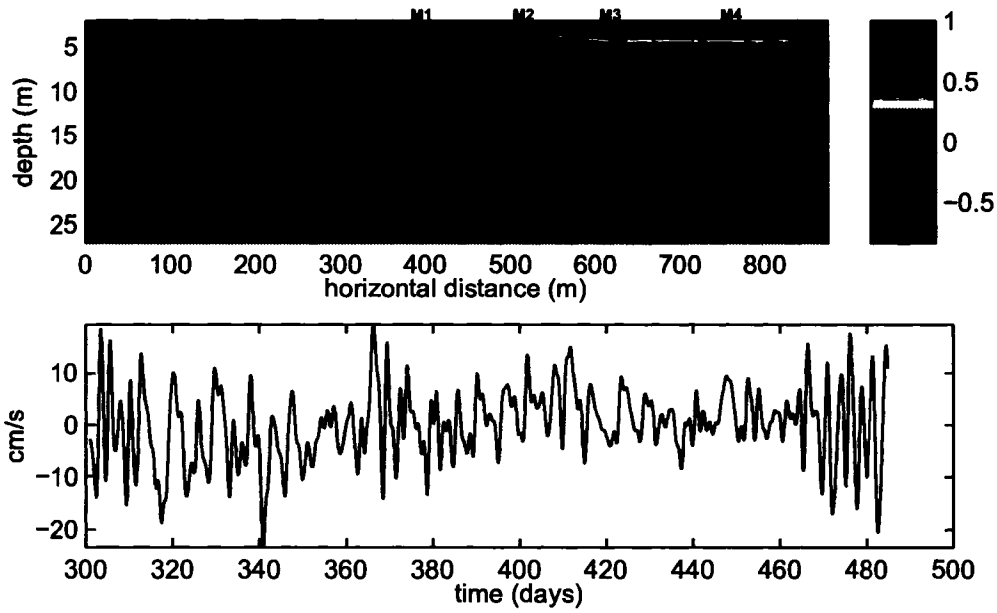

Figure 4.3: Mode 1 of the EOF analysis of the filtered data from day 301 to 485 2003, containing 74% of the variance. Interpolation between moorings is linear, and values outside are extrapolated from the edge. Units in the across channel amplitude plot have been normalized, so that units for the principle component time series are in cm/s. The black line indicates the zero contour.

They discovered that an up-inlet wind produced a rapid thickening of the freshwater layer at the inlet head, which persisted for several days, and propagated along the channel decreasing in amplitude as it went. Current observations indicated that surface currents (at two metres depth) were closely coupled with the local wind field.

Studies in Puget Sound Washington (Bretschneider *et al.*, 1985; Matsuura and Cannon 1997) and Jøsenfjord in Norway (Svendsen and Thomson, 1978) showed that the dominant subtidal flows were in fact caused by local wind stress. In these cases the effect of the wind was noted both in the surface freshwater layer, and in a compensating flow at depths below the pycnocline.

In order to investigate the effects of local wind on the subtidal exchange over

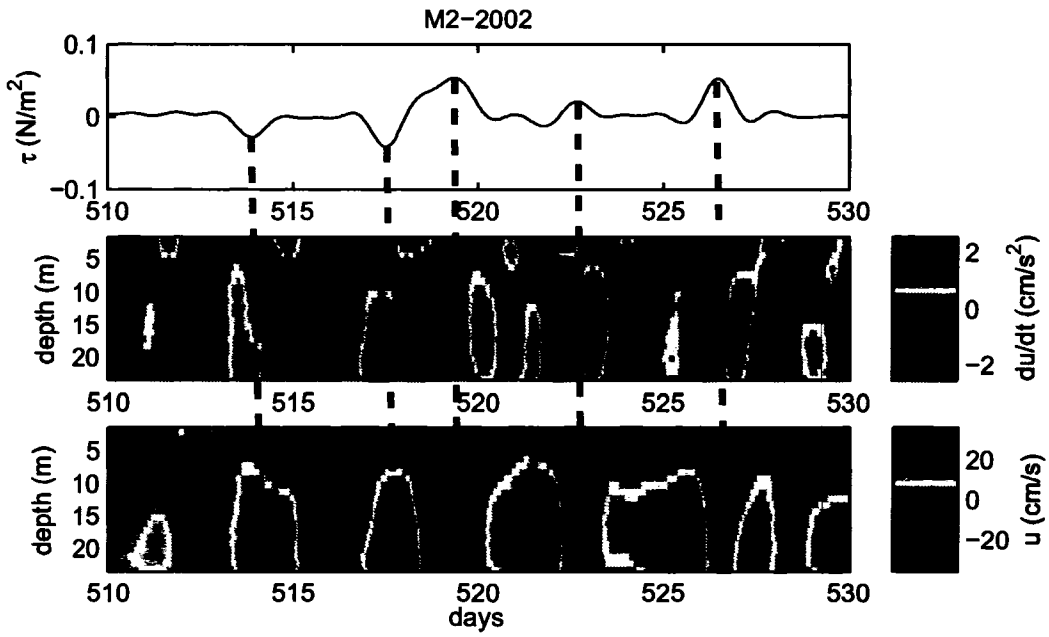

Figure 4.4: a) Through channel wind stress, b) acceleration and c) velocity of mooring M2-2002 for days 510 to 530. The black line indicates the zero-contour, and hence in c) the boundary between upper and lower layers. The arrows show the apparent relation between wind stress and exchange events.

the sill, the wind data were filtered with the same 30 hour cutoff filter used for the ADCP data. Figures 4.4 and 4.5 show plots of through channel wind stress, combined with acceleration and velocity timeseries for the entire water column for M2-2002 and M2-2003 respectively. The forcing throughout the entire water column is indeed correlated with the surface wind stress, as up-inlet and down-inlet winds clearly have an effect on the magnitude and direction of flow. The up-inlet winds (positive τ) cause a deceleration of the flow along with a deepening of the surface layer, while down-inlet winds (negative τ) result in an acceleration of the flow in both layers, with little change in the layer depth (Figures 4.4 and 4.5).

The first test performed to examine the relationship between local wind stress

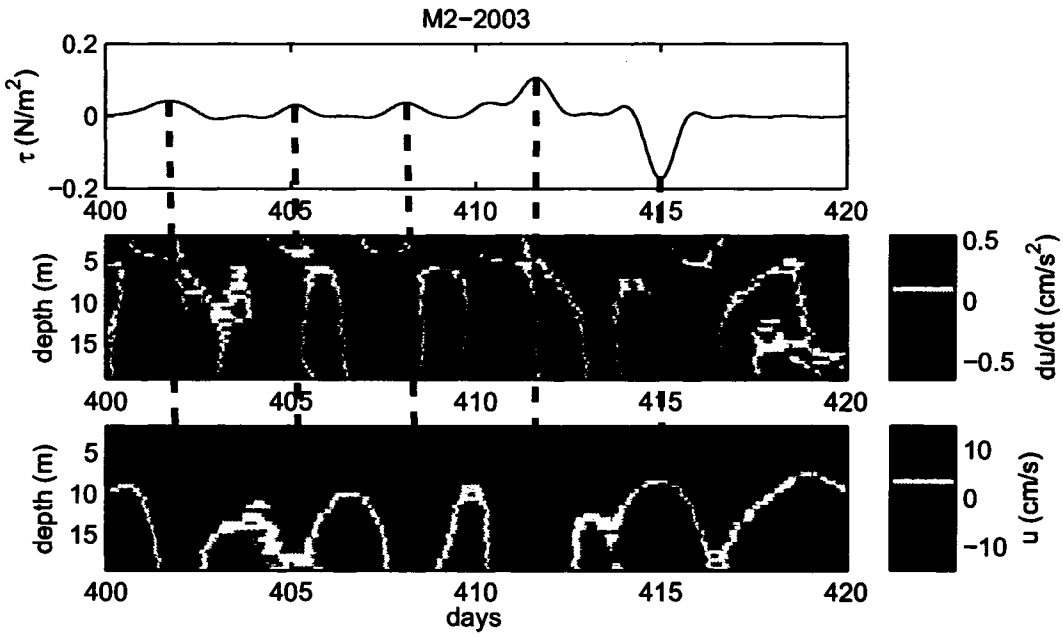

Figure 4.5: a) Through channel wind stress, b) acceleration and c) velocity of mooring M2-2003 for days 400 to 420. The black line indicates the zero-contour, and hence in c) the boundary between upper and lower layers. The arrows show the apparent relation between wind stress and exchange events.

and exchange over the sill was to calculate the squared coherence between the along channel wind (at an angle of approximately 20°north of east) with the principle component from mode 1 of the EOF analysis for both the 2002 and the 2003 data (see Figure 4.6). The principle component of mode 1 of the EOF analysis is coherent with wind stress for frequencies between approximately 0.2 and 0.8 cpd. There is much higher coherence between the wind stress and the principle component of the 2002 data than the 2003 data. This is likely because during the time period which the 2003 data covers, much of the bay would have been covered by ice, thus reducing its response to the local wind. Approximate dates for ice cover during winter 2004 are from January 8th to May 3rd (corresponding to days 372 to 488 2003), obtained

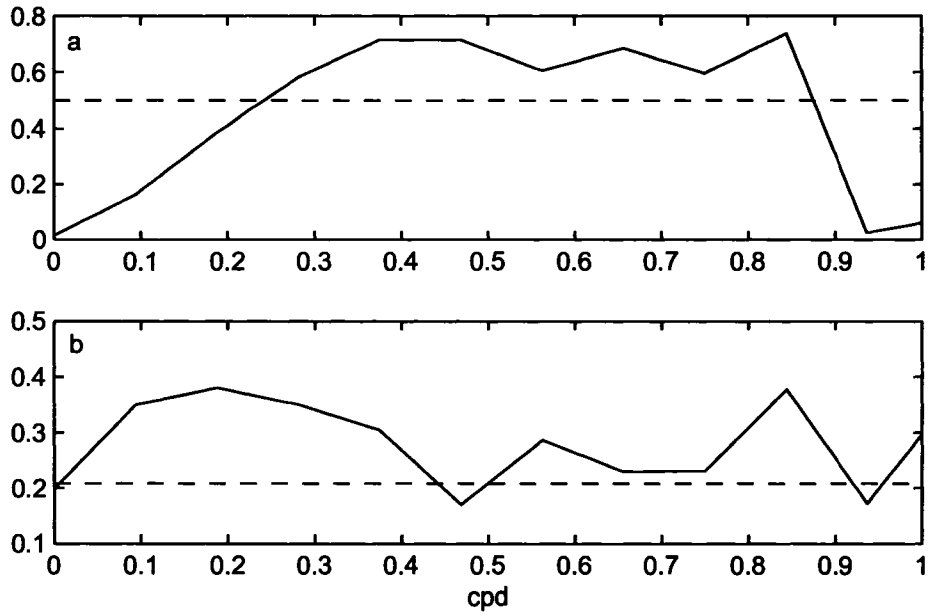

Figure 4.6: Squared coherence between EOF Mode 1 and wind stress for a) 2002 and b) 2003 data. The 95% confidence limit is indicated by the horizontal line.

from Canadian Ice Service ice archive charts on the web[1].

As a further indication of the relation between local wind and subtidal exchange over the sill, Figure 4.7 shows the squared coherence between wind stress and through channel current velocity with depth for the mooring M2-2003. It can clearly be seen that there is high coherence for frequencies between about 0.2 and 0.5 cpd. Also note the area of low coherence associated with the interface. It also appears that there is significant coherence between 7 and 16 metres, for a frequency of about 1 cpd. Coherence with wind at this frequency suggests that there is some response in the water column to a sea-breeze effect, however any energy that may exist at this

[1]http://ice-glaces.ec.gc.ca/App/WsvPageDsp.cfm?ID=11700&Lang=eng

frequency is small compared to the energy in subtidal bands.

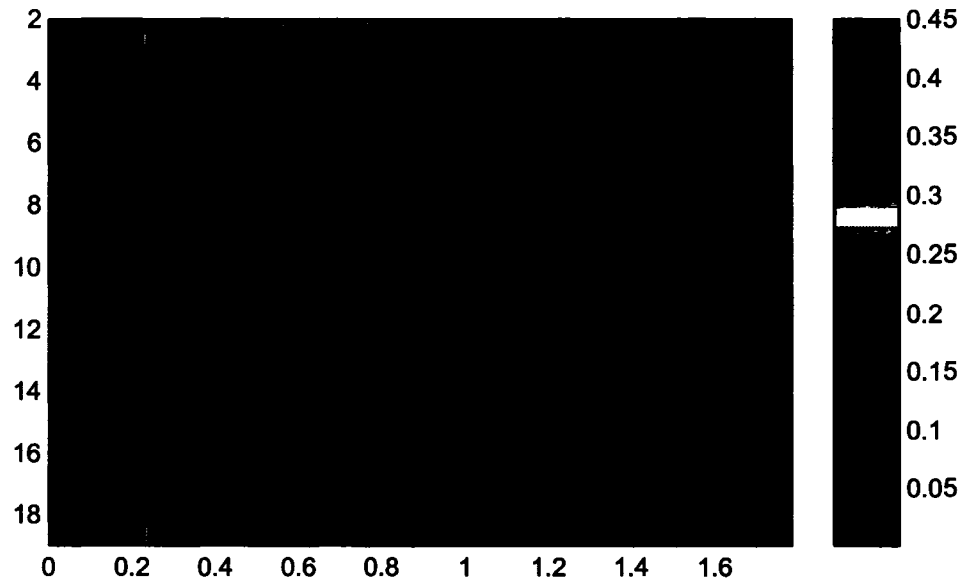

Figure 4.7: Squared Coherence between wind stress and through channel current for M2-2003. The average 95% confidence limit is indicated by solid black line.

Cross-correlation analysis of the through channel wind and the principle components of the EOF analyses was also performed, to determine the lag between the two data sets. Results indicate a lag of about 3 hours for the 2002 data, and about 6 hours for the 2003 data.

Non-local Wind

The effects of non-local wind on estuarine systems has long been considered an important factor leading to exchange, and has been investigated for many different systems. In particular, Holbrook *et al.* (1980) found that the subtidal currents in the Strait of Juan de Fuca were only weakly coherent with local along-strait winds, but were

strongly coherent with alongshore winds on the coastal shelf. A detailed investigation of Byfjord (Helle, 1978) showed that prolonged periods of upwelling favourable coastal wind produced deepwater exchange and hence subtidal flow. Several attempts to model the effect of remote coastal wind forcing in fjords and estuaries have confirmed this hypothesis for many different systems (Klinck et al., 1981; Garvine, 1985).

Because Bonne Bay is connected to the Gulf of St. Lawrence, it is likely that wind events occurring remotely could affect the exchange over the sill in the bay. In particular, the direction of the prevailing wind in the area tends to be towards the NNE, following the coastline and the coastal topography. A reversal of this wind would generate Ekman transport away from the coast, causing upwelling outside of the Bay, which could influence exchange over the sill.

Coherence analysis of the EOF results and through channel current with coastal wind did not reveal any significant correlation. Previous data collection in Bonne Bay (Gilbert and Pettigrew, 1993) showed that coastal wind reversals do indeed cause upwelling, and can even cause an inflow of denser upwelled water to the interior of the bay, though it would seem that in general it does not penetrate far enough to affect circulation over the sill, at least on a regular basis.

Other Factors

There are several other factors that could affect the exchange of water over the sill in Bonne Bay, although many of them were outside the scope of this analysis as data were not available. In particular, the exchange due to changing hydrographic conditions outside the bay, causing a bottom water renewal event cannot be studied without hydrographic time series. Many such studies have been performed on fjords

in the past, and the frequency of exchange events varies greatly from one location to another. In Indiam Arm B.C., the exchange was found to occur every few years, because of isolation from the Strait of Georgia by several sills (de Young and Pond, 1988). However in Puget Sound, a nearby fjord located in Washington State, bottom water intrusions were observed to occur with a fortnightly frequency (Bretschneider et al. 1985). Strong tidal currents during spring tides generate significant mixing near the sill, and thus inhibit the gravitational circulation. Weaker currents during neap tides allow stratification to occur, and denser water from the Strait of Juan de Fuca passes over the sill and propagates up estuary as a bottom current.

Another factor that can influence the circulation in Bonne Bay is the amount of freshwater runoff to the system. Though discharge measurements were not conducted at the mouths of the various rivers that flow into the East arm of Bonne Bay, an estimate of the freshwater input to the bay can be obtained from precipitation records from the Rocky Harbour weather station. To investigate the relationship between rainfall and flow over the sill, coherence tests were performed in a manner similar to the wind data. The results (Figure 4.8) show that there does appear to be significant coherence for frequencies of about 0.4 and less than 0.1 cpd for both the 2002 and 2004 data. There is no significant coherence for any frequencies for the 2003 data. This is somewhat expected, as much of the 2003 data were collected in the winter, when there is little correlation between the amount of freshwater input to the system and precipitation levels due to the accumulation of snow.

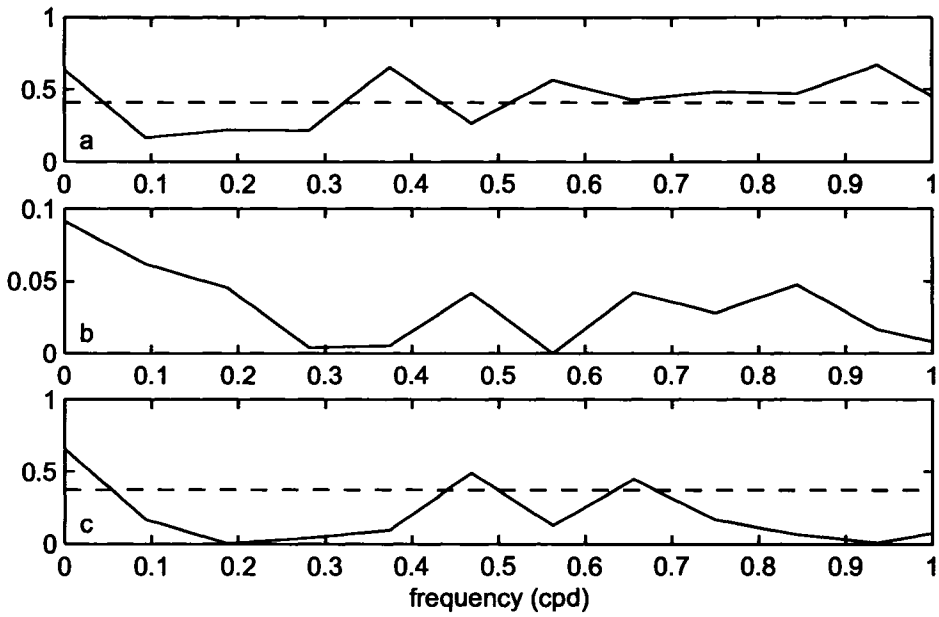

Figure 4.8: Squared Coherence between subtidal current and precipitation time series for a) M1-2002, b) M1-2003 (note the change of scale) and c) M1-2004, at a depth of two metres. The 95% confidence limit is indicated by the dashed horizontal line, except in b) where there was no significant coherence.

4.2 Two Layer Numerical Model

In an attempt to explore the underlying dynamics of the low-frequency exchange, I developed a two layer numerical model for application in Bonne Bay. The goal is to examine different forcing regimes, and to increase the understanding of the response of the system to forcing using the model as an exploration tool. Results of the subtidal EOF analysis, along with density profiles collected in the area, showed that the response of the system was largely two layer, and therefore suitable for use with the idealized two layer model. In addition, the EOF analysis indicated that there was subtidal flow in response to the local wind stress, which a simple model could help to

substantiate.

There have been many numerical models developed to examine the relationship between winds and coastal ocean currents (O'Brien and Hurlburt, 1972), and in particular the wind induced currents in estuaries and fjords (Klinck et al., 1981; Garvine 1985). More recently, Matsuura (1995) used a simple two layer model to reproduce wind-forced subtidal fluctuations in Puget Sound, Washington. The success of this simple model is profound, as stratification in Puget Sound is much lower than many other fjords, and thus the two layer approximation should not hold as well. Further justification for the use of a discrete layer model is provided by Farmer (1976), who found that in Alberni Inlet the wind forced subtidal flow was largely uncoupled from the estuarine flow.

4.2.1 Description of Model

The model used was a modified version of that developed by O'Brien and Hurlburt (1972) in a numerical study of wind forced coastal upwelling. Modifications mostly entailed adapting it for a two dimensional domain, but otherwise many of the details are similar. The equations describe a stably stratified, rotating, incompressible flow divided into two layers of density $\rho_1 < \rho_2$. Atmospheric pressure is assumed to be uniform at the ocean surface, and Coriolis effects are taken into account by using an f-plane approximation. The coordinate system is right-handed with x and y increasing eastward and northward respectively, while z increases upward. All thermodynamic effects are neglected, and there is no transport of heat or salt between the layers. In the model geometry (Figure 4.9), h_1 and h_2 are perturbations to the thickness of the respective layers.

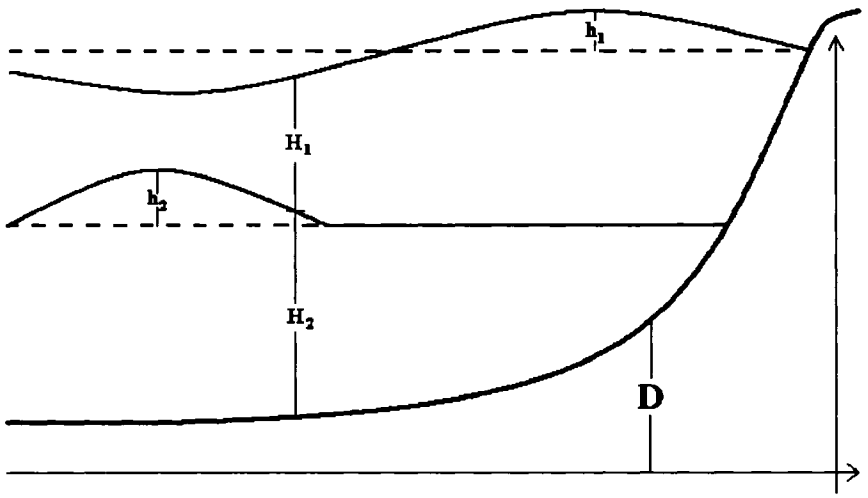

Figure 4.9: Model geometry for the Bonne Bay two layer model. $D(x,y)$ is the bottom topography, and H_1 and H_2 are the total thicknesses of each layer. Velocities are depth averaged.

Model Equations and Discretization Scheme

The equations of motion and continuity for each layer are:

$$\frac{\partial u_1}{\partial t} = fv_1 - g\frac{\partial}{\partial x}(h_1 + h_2) + \frac{1}{\rho H_1}(\tau^x - \tau^{Ix}) \tag{4.1}$$

$$\frac{\partial v_1}{\partial t} = -fu_1 - g\frac{\partial}{\partial y}(h_1 + h_2) + \frac{1}{\rho H_1}(\tau^y - \tau^{Iy}) \tag{4.2}$$

$$\frac{\partial h_1}{\partial t} + \frac{\partial H_1 u_1}{\partial x} + \frac{\partial H_1 v_1}{\partial y} = 0 \tag{4.3}$$

$$\frac{\partial u_2}{\partial t} = fv_2 - g\frac{\partial}{\partial x}(h_1 + h_2) - g'\frac{\partial h_1}{\partial x} + \frac{1}{\rho H_2}(\tau^{Ix} - \tau^{Bx}) \tag{4.4}$$

$$\frac{\partial v_2}{\partial t} = -fu_2 - g\frac{\partial}{\partial y}(h_1 + h_2) - g'\frac{\partial h_1}{\partial y} + \frac{1}{\rho H_2}(\tau^{Iy} - \tau^{By}) \tag{4.5}$$

$$\frac{\partial h_2}{\partial t} + \frac{\partial H_2 u_2}{\partial x} + \frac{\partial H_2 v_2}{\partial y} = 0 \tag{4.6}$$

In equations 4.1 through 4.6: u_i, v_i $(i = 1, 2)$ are the east-west and north-south velocities in the two layers respectively; H_i is the mean thickness of the two layers; h_i is the perturbation to the mean thickness of each layer; ρ is the mean density of seawater, g is the acceleration due to gravity, g' is the reduced gravity given by:

$$g' = g\frac{\Delta\rho}{\rho} \tag{4.7}$$

The stress terms are given by:

$$\begin{aligned} \tau^{Ix} &= \rho c_D \bar{q}(u_1 - u_2) \\ \tau^{Iy} &= \rho c_D \bar{q}(v_1 - v_2) \\ \tau^{Bx} &= \rho c_D \bar{q} u_2 \\ \tau^{By} &= \rho c_D \bar{q} v_2 \\ q_i &= \left(u_i^2 + v_i^2\right)^{\frac{1}{2}} \\ \bar{q} &= (q_1 + q_2)^{\frac{1}{2}} \end{aligned} \tag{4.8}$$

where $\tau^{Ix,y}$ and $\tau^{Bx,y}$ are the horizontal stresses on the interface and at the bottom respectively, and c_D is a drag coefficient. The values of parameters used in the model are given in Table 4.1.

The value of c_D was chosen to be 1×10^{-2}, by running the model with real wind stress and matching the magnitude of predicted currents to the data. This value

Values of parameters used in the model
$H_1 = 8$ m
$H_2 = 100 - H_1 - D$
$g = 9.8$ m/s^2
$g' = 0.04$ m/s^2
$\rho = 1028$ kg/m^3
$f = 10^{-4}$ s^{-1}
$c_D = 10^{-2}$
$\Delta t = 3$ s
$\Delta x = 200$ m
$\Delta y = 200$ m

Table 4.1: Parameters and values used in the two layer model

is larger than that used by O'Brien and Hurlburt (1972) for their model of coastal upwelling, though they mention specifically that they intended to keep interface and bottom stresses small (O'Brien and Hurlburt, page 23). It is not surprising therefore that the value of c_D must be increased for an environment such as Bonne Bay, where high velocities (especially in the vicinity of the sill) which lead to strong shear between the layers, and the friction caused by shallow topography will both serve to modify the wind forced flow. Also, it is likely that there is a large amount of turbulent mixing going on in the vicinity of the sill which is not accounted for in the simple two layer model. Flows in the vicinity of the sill in fjords generate significant amounts of mixing energy through turbulence (Farmer and Freeland, 1983). Winters and Seim (2000) found that entrainment and mixing between layers in two layer flow through a constriction, along with bottom friction, significantly altered the flow by carrying away a large fraction of the horizontal transport. As the model described above cannot handle mixing between the layers, the value of c_D was chosen to compensate by creating increased interfacial and bottom drag. Also, due to the relatively thin upper freshwater layer, the large value of c_D also served to keep the pycnocline from hitting the surface at the head of the bay during strong offshore wind events.

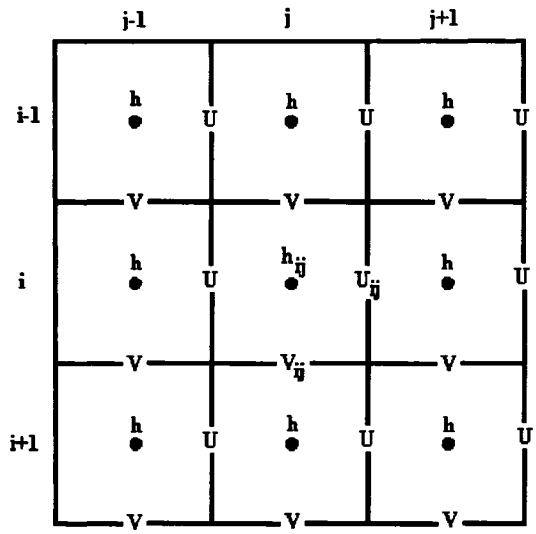

Figure 4.10: Arakawa C-grid.

Equations 4.1 to 4.6 were discretized on an Arakawa C grid (Figure 4.10), and stepped forward in time using a Leapfrog Trapezoidal scheme (Kowalik and Murty, 1993). An initial guess of the value to be determined is made using a leapfrog time step, which is then used in a trapezoidal step to determine the value at one time level after the current one. For the function

$$\frac{\partial \phi}{\partial t} = F(t) \tag{4.9}$$

an initial guess for ϕ_{n+1} (where n is the current time step) would be calculated with a leapfrog scheme using

$$\phi^*_{n+1} = \phi_{n-1} + 2\Delta t F_n \tag{4.10}$$

An initial guess for F^* would then be calculated from ϕ^*, and used in a trapezoidal step to give ϕ_{n+1}

$$\phi_{n+1} = \phi_n + \frac{\Delta t}{2}[F_n + F^*] \tag{4.11}$$

This scheme proved to be quite stable, and was not subject to the instabilities often observed in a simple leapfrog scheme of $O(2\Delta x)$.

Model Domain and Boundary Conditions

The domain used in the model runs is shown in Figure 4.11, with the bottom topography indicated by the colour scale. The depth of most of the bay, including the South and East Arms was assumed to be a maximum of 100 metres. This was chosen so that the time step would not be limited by the large depths of the East arm (230 metres), and justified by the fact that very little flow would even occur in that part of the bay. The horizontal grid size was 200 x 200 m, the minimum required to resolve the bathymetry and coastline in the area of the sill, while still allowing a reasonable time step. The time step required to ensure numerical stability was three seconds, determined both by the horizontal grid size, and the maximum depth using:

$$\Delta t \leq \frac{1}{2}\frac{(\Delta x^2 + \Delta y^2)^{\frac{1}{2}}}{\sqrt{gH}} \tag{4.12}$$

Coastal boundary conditions were chosen as closed and slip, where the velocity perpendicular to the boundary is set to zero using a coastline mask. As Bonne Bay is connected to the Gulf of St. Lawrence it was necessary to choose a boundary condition at the mouth of the bay that enabled water to flow freely in and out. Further to this, because the problem being examined was one of local forcing only, it was necessary

to have a boundary condition that did not depend on the area outside of the bay, and that would allow energy generated within the system to leave the domain. For these reasons, an Orlanski radiation open boundary condition was applied at the mouth of the bay. Details of the implementation are given in both Orlanski (1976) and Greatbatch and Otterson (1991), but involves using an equation of the form

$$\frac{\partial h}{\partial t} + c\frac{\partial h}{\partial x} = 0 \tag{4.13}$$

to determine the layer thickness ($h_{1,2}$) on the open boundary, where the phase speed c is determined from both previous time steps and from values just inside the boundary.

To validate the model, a test run was done to compare against the analytical results for an impulsive longshore wind stress on a semi-infinite ocean bounded by a single coast, found in Csanady (1984, page 89). The northern wind stress was applied over a rectangular domain of size 1000 km long by 200 km wide, with the coast on the right hand side. Boundary conditions on the 3 other sides were chosen as zero gradient conditions for simplicity. Results from the model agreed with the analytic solutions from Csanady (1984) to within a few percent, for time periods on the order of 1 to 2 days.

4.2.2 Model Results

The model described above was forced with real wind stress from the Rocky Harbour weather station, and the results were compared with data from the ADCP moorings.

Rather than directly comparing velocities from single grid points in the model with ADCP data, the through channel transport was compared. Transport time series were

calculated from the data by interpolating the cross-channel flow in between moorings, and then extrapolating to fill the entire cross section (as discussed in Chapter 2). In order to compensate for the missing two metres of data near the surface (removed because of suspect readings, see Section 2.2), the values in the uppermost bin were extended to the surface.

As it was necessary to compare model results with data for which transport could be calculated (i.e. there were more than two instruments in the water at a time), model runs were limited to the same time periods used in the tidal and subtidal analysis sections, specifically days 251 to 321 2002 and days 301 to 485 2003. Model runs for the upper layer during the periods 251 to 321 2002, 301 to 401 2003, and 400 to 450 2003 are shown in Figures 4.12, 4.13 and 4.14 respectively, and are compared with transport time series calculated from the data. Results from the lower layer were similar, but opposite in sign.

Results from the three models runs in Figures 4.12 through 4.14 show good agreement with the data. There is significant squared coherence ($\sim$0.8) in all cases between at least 0.1 and 0.6 cpd. Coherence squared for the 2003 data is slightly less than that for 2002 ($\sim$0.6), which is consistent with the comparison of EOFs to wind stress in Section 4.1.1, where the effect of ice cover on much of the bay is to reduce the correlation with surface wind stress. Correlation coefficients for the 3 runs are 0.6, 0.44 and 0.4 respectively.

During some strong wind events, the model calculated transports were much higher than those obtained from the data, particularly in the 2003 time period (see days 350, 415 and 437 in Figures 4.13 and 4.14). This discrepancy likely results from the use of interpolated data to calculate the layer transports and that a fixed level

of 8 metres was used for the layer depths. Although there is clearly a mean level at which the boundary between the two layers lies, the layers do change in thickness in response to the wind (see Figures 4.4 and 4.5) and this can have an affect on the calculated transports.

There are time periods when the response of the model appears to be quite different from that of the data. There are exchange events that are either not reflected in the model, or the magnitude of the transport is much higher than predicted. See for example days 258 and 300 in Figure 4.12 as well as days 340 and 366 in Figure 4.13. These discrepancies could be attributed to the quality of wind data obtained from the Rocky Harbour weather station. As was discussed in Section 2.3.2, the mountainous topography around Bonne Bay could greatly influence the local wind field, resulting in some differences between the wind at the Rocky Harbour station, and over the bay itself. In particular, it is possible (and highly likely) that the wind field at any one time over the bay is not uniform, but is topographically steered in different directions in either of the two arms. Considering the highly varied terrain in this region and the different orientations of the two arms, the high correlations between model and data reinforce the dominance of the local wind forced exchange, and the choice of such a simple model. The effect of spatially varying wind will be explored later.

A qualitative comparison of the layer depths between the ADCP data and the model was also performed (see Figure 4.15). Visually the zero contour from the ADCP plot correlates fairly well with the model predicted layer depth, however the scale of the variations is quite different. During an exchange event, the upper layer can change in thickness by 5 to 10 metres (Figure 4.15a), while during the same events in the model the thickness changes by a maximum of 1 metre (Figure 4.15b).

Another difference between the two plots in Figure 4.15 is that of the shallowing of the layer predicted by the model around day 415. This event, characterized by a strong down-inlet wind and subsequent outflow in the surface, shows no movement of the interface in the data. It was believed initially that these discrepancies were attributed to the choice of a large value for the frictional coefficient, however sensitivity tests presented in the following section indicate that it is more likely due to a limitation of the two layer approximation.

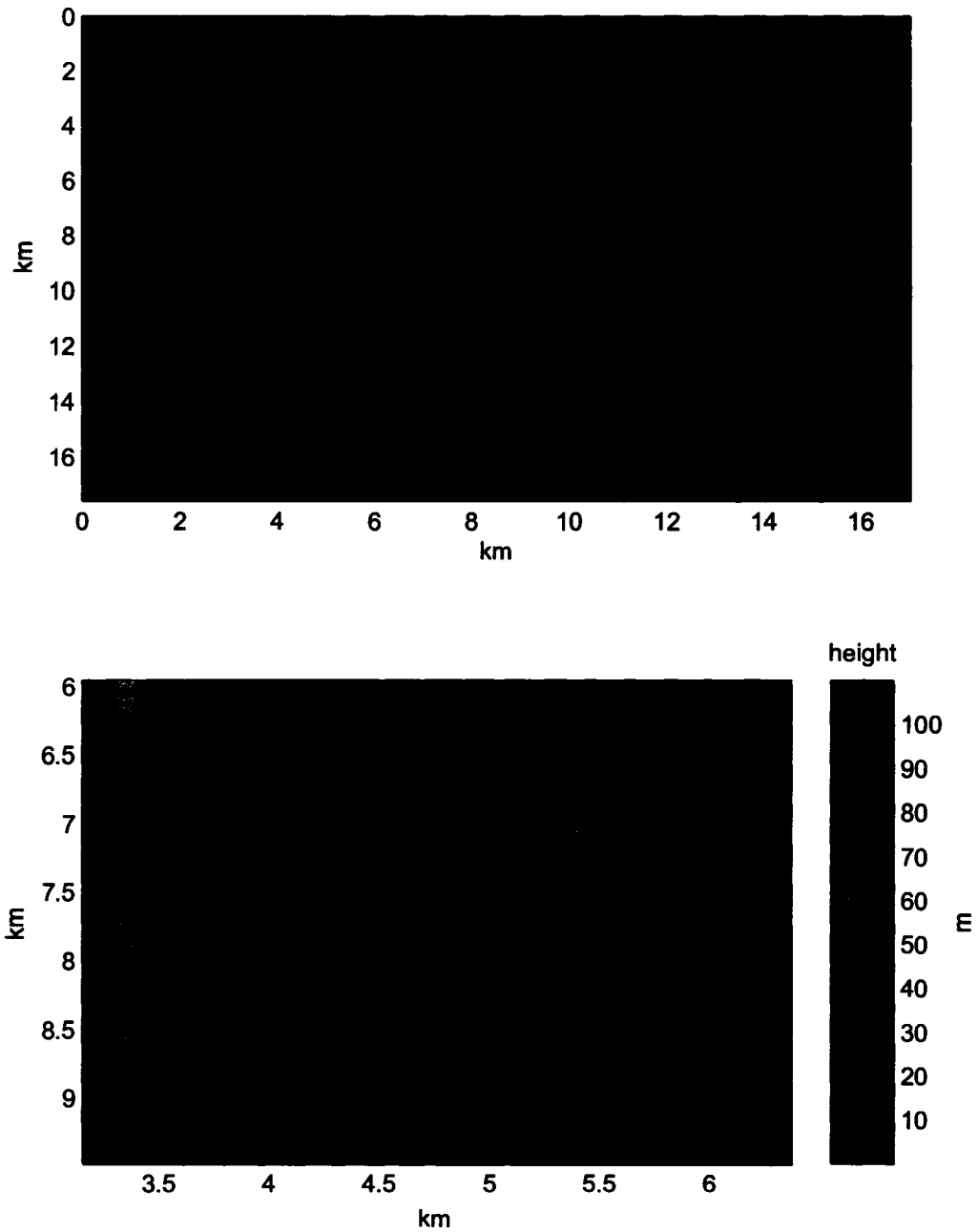

Figure 4.11: Bonne Bay model domain and bottom topography. Contours are at 10 metre intervals. Maximum depth is 100 metres, so the 100 m topography contour is the coastline.

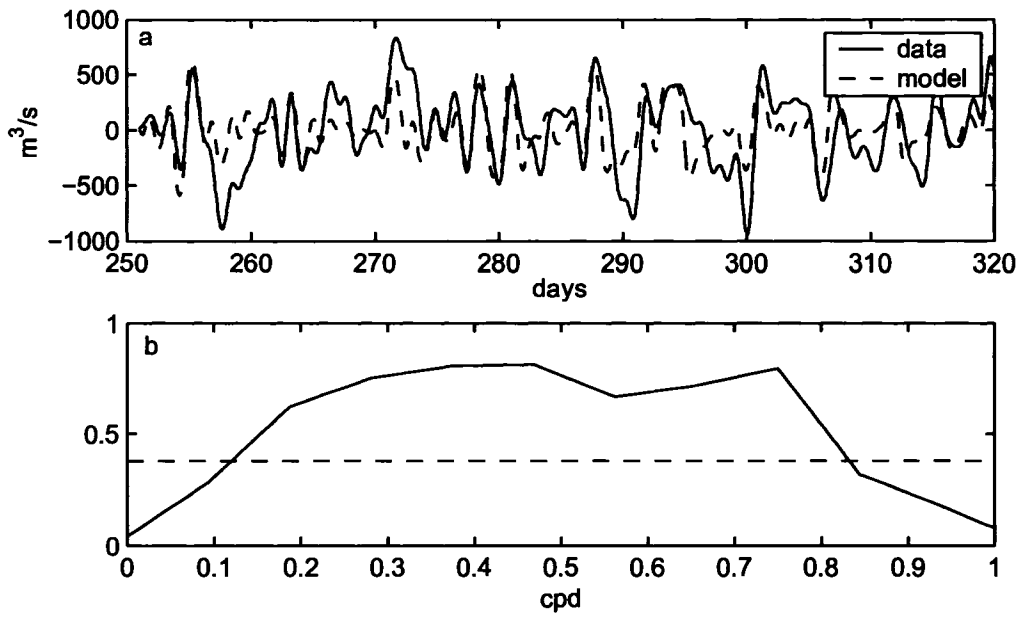

Figure 4.12: a) Time series of through channel transport in the upper layer (solid line) and the transport computed by the model (dashed line) for days 251-321 2002. b) Squared coherence between the two time series in a), with the dashed line indicating the 95% confidence level.

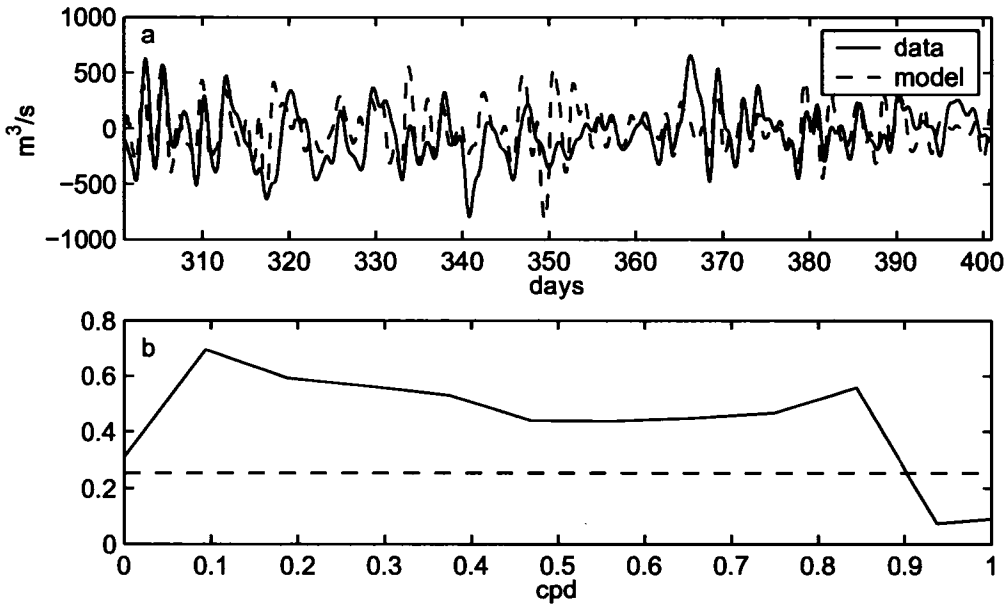

Figure 4.13: a) Time series of through channel transport in the upper layer (solid line) and the transport computed by the model (dashed line) for days 301-401 2003. b) Squared coherence between the two time series in a), with the dashed line indicating the 95% confidence level.

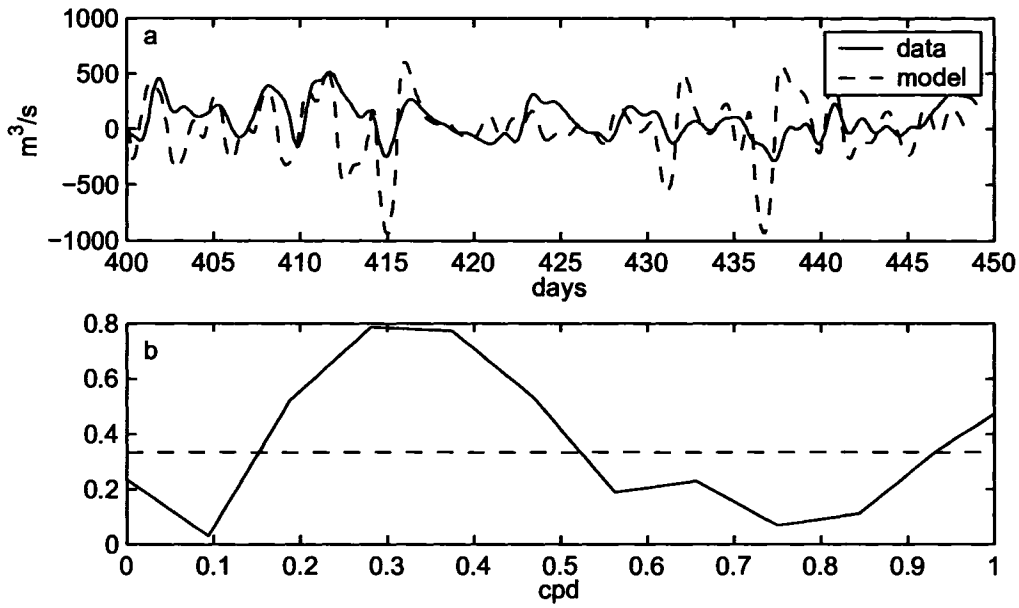

Figure 4.14: a) Time series of through channel transport in the upper layer (solid line) and the transport computed by the model (dashed line) for days 400-450 2003. b) Squared coherence between the two time series in a), with the dashed line indicating the 95% confidence level.

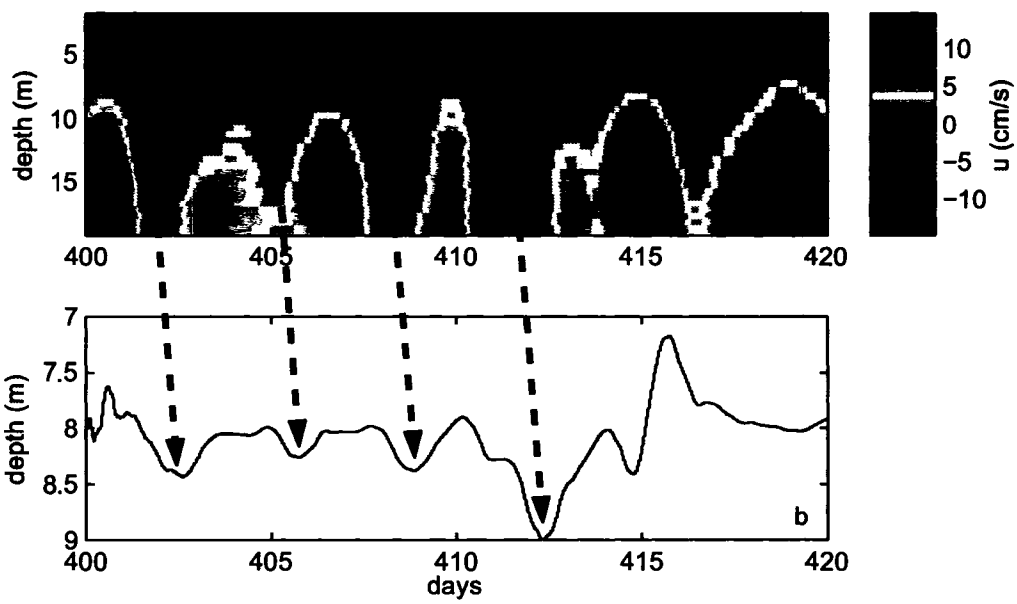

Figure 4.15: Comparison of the interface depth from a) M2-2003 and b) the two layer model. The solid black line shows the zero contour, and correlated events are indicated by the arrows. The lag is approximately 12 hours.

4.2.3 Sensitivity Tests

Aside from the topographic effects on the local wind field, there are several other things that could potentially cause discrepancy between the data and the model predicted transport.

- The model cannot simulate the effects of ice cover on parts of the bay, which would act to reduce the response to wind stress. This should only be a problem during winter months.

- The two layer scheme does not allow for vertical mixing to occur between the layers. This was compensated for by using a large frictional coefficient, but it's possible that this compensation does not accurately reflect the dynamics. In particular, the model cannot predict any deep water renewal events.

- The large value of the frictional coefficient used to account for the lack of vertical mixing could potentially alter the results, especially in the vicinity of the sill, where high velocities and shallow depths would greatly enhance the frictional stresses.

- Changes in stratification throughout the year would change both the layer depths, and and the buoyancy of the two layers. As there were no hydrographic data available for time periods other than June 2004, the value for reduced gravity used in all model runs was estimated from it.

- In order to keep the model stable, the bottom topography had to be simplified somewhat from the real topography. Steep jagged features were smoothed to prevent numerical instabilities, especially in the vicinity of the sill.

As many of the above mentioned drawbacks are inherent either in the choice of a simple model, or the lack of data from the area, it is difficult to directly evaluate directly the effects of different choices. In order to gain some understanding of the sensitivity of the model results to various parameters, some test runs were performed. These runs specifically examined the effect of various values for the frictional coefficient, reduced gravity, and non-uniformity in the wind field.

Friction and Reduced Gravity

Various model runs were performed to examine the effect of different choices for the frictional drag coefficient (c_D) and the value of reduced gravity (g'). In each case the wind stress was sinusoidal with a period of 3 days and a magnitude of 0.1 N/m^2. Naturally the magnitude of the wind stress can have an effect on the magnitude of transport over the sill, so the results presented here are merely an indication of the dependence on the two parameters. Values for c_D ranged from 10^{-3} to 0.5, while values for g' ranged from 0.05 m/s^2 to 0.22 m/s^2.

The transport over the sill in the upper layer shows an asymptotic relationship with c_D for both the maximum value reached and the lag relative to the wind stress (Figure 4.16a,b). The greatest lag between the wind stress and transport is about half a day, for $c_D > 0.25$. For the value of c_D used in the previous model runs (10^{-2}) the lag is close to zero. The value of the maximum layer thickness was seen to vary similarly to the transport (Figure 4.16c), however the timing showed a linear relationship with c_D (Figure 4.16d). The results of this test indicate that the lag of about 12 hours between the movement of the interface in the data and that predicted by the model (see Figure 4.15) is a theoretical lower limit, and has nothing to do with

the value of $c_D = 10^{-2}$ in the model runs being large compared to actual values. It's possible the large lag is a limitation of the two layer model, which may not accurately represent the flow over the sill at all times. However, as the goal of the model was to examine the relationship between wind stress and transport over the sill, this was not considered to be a significant problem.

Model runs examining the effect of different values of g' (and hence density variations in the two layers), show a linear decrease for both the maximum transport and maximum layer thickness (Figure 4.17a - only the variation of maximum transport is shown). The lag between transport and wind stress varied asymptotically (Figure 4.17b), with a maximum lag of about half a day for $g' > 0.2$ m/s^2.

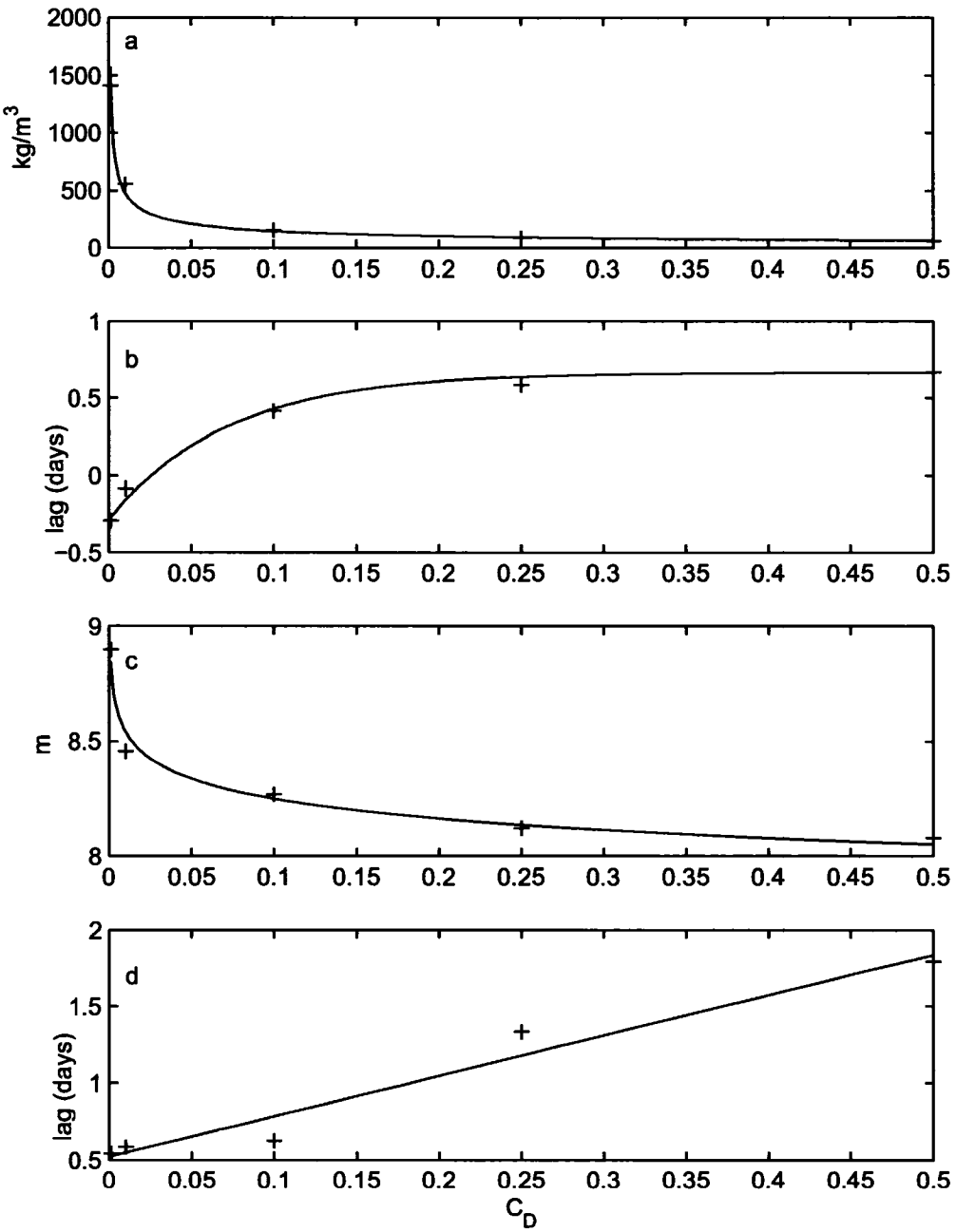

Figure 4.16: Dependence on c_D of a) maximum transport, b) lag of maximum transport with respect to the wind, c) maximum surface layer thickness, and d) lag of maximum surface layer thickness with respect to the wind. Forcing was of the form $\tau = 0.1$ N/m$^2 \sin\left(\frac{2\pi}{T}t\right)$ where $T = 3$ days.

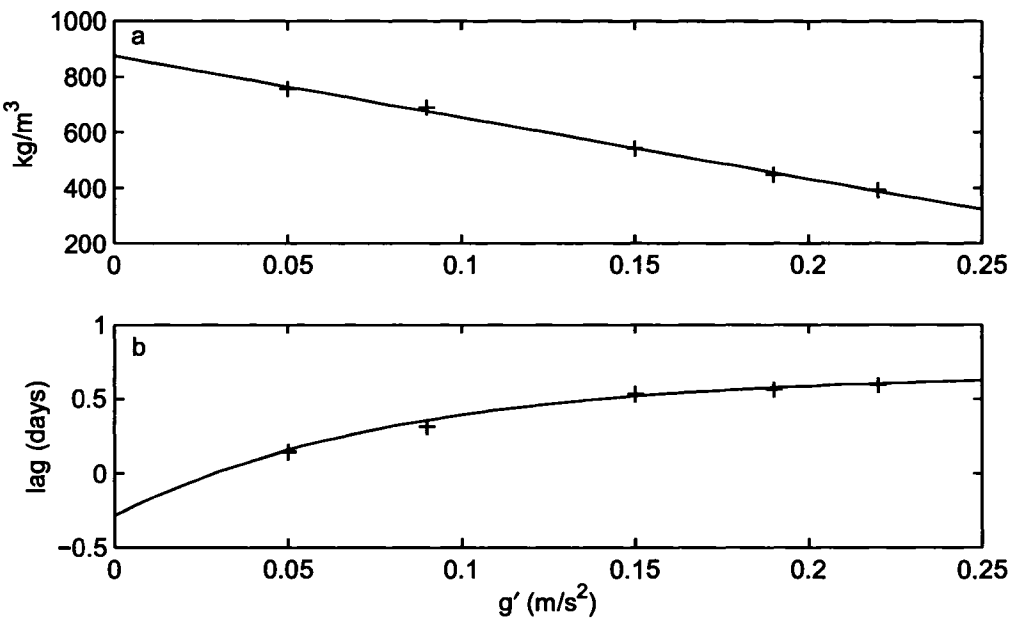

Figure 4.17: Dependence on g' of a) maximum transport, and b) lag of maximum transport with respect to the wind. Forcing was of the form $\tau = 0.1$ N/m$^2 \sin\left(\frac{2\pi}{T}t\right)$ where $T = 3$ days.

Non-Uniform Wind Stress

In the case of the wind data it was possible to modify the code so that wind stress could be applied non-uniformly over the domain, and thus investigate some of the topographic effects. Naturally wind data from areas other than the Rocky Harbour weather station were not available for these time periods, so it was decided to use a sinusoidal wind stress, applied in different areas of the domain.

The first tests performed examined the effect of a sinusoidal wind stress in each of the Arms separately, with no forcing on the other side. Forcing for the South Arm case was from the southwest (and northeast) as indicated in Figure 4.18a, and in all cases the forcing period was 3 days and the amplitude was 0.1 N/m^2. Forcing for the the East Arm case was similar, but from the southeast and northwest (Figure 4.20a). The area in the vicinity of the sill, between the west and east halves of the domain, contained wind stress that varied linearly so that no discontinuities existed between the two regions. In each case, a comparison run was done with the wind stress uniform over the entire domain.

For both of the runs, there was a noticeable difference in response between the spatially uniform wind stress, and that applied to each arm. In each case, the transport over the sill was higher with the uniform wind field, but there were also some variations of the timing of the maximum transport with respect to the wind stress.

In the South Arm case (Figure 4.18b), the maximum transport over the sill in the upper layer occurs approximately 7 hours before the maximum wind stress, as compared to the uniform wind run, where the maximum transport occurs about 5 hours before the maximum wind stress. Though it appears as though the two transports are *leading* the wind forcing, in fact what is occurring is that frictional

resistance to the flow is causing it to peak *before* the wind stress has a chance to turn around.

This was further examined by doing a model run with the South Arm configuration, but with a steadily increasing northeastward wind stress, rather than a sinusoidal one (Figure 4.19). The wind stress was increased from 0 to 0.1 N/m^2 using a hyperbolic tangent function, with the period of maximum change occurring over a time comparable to that from the sinusoidal runs. Aside from the reduced transport, it can be seen that the transport from the single arm forcing run peaks before that from the uniform wind. The time difference between the two maxima is approximately 3.5 hours.

These results indicate that in cases where the wind field is topographically modified so that the wind blows along the northeast/southwest in the South Arm, and not in the East Arm at all, the model predicted transport from a uniform wind field will lag the modelled transport by 2 to 3 hours. Also the model predicted transports will be too large by about 55%.

For the East Arm case, (Figure 4.20b), the maximum transport over the sill occurs approximately 1.5 hours before the maximum wind stress. In this case there is no lag between the uniformly forced transport and the wind. The difference in maximum transport between the East Arm and uniform runs is about 250 m^3/s. These results indicate that in cases where the wind field is topographically modified so that it blows along channel in the East Arm, but is zero elsewhere, the uniform model predicted transports will be too large by approximately 50%, and will lag the modelled transport by about 1.5 hours.

In addition to the single South and East Arm runs, two bi-modal runs were per-

formed to examine the effect of topographic steering of the wind in the two arms of the bay. Because of the mountainous terrain to the north and south of the East Arm (see Figure 1.2), it is likely that the wind will often be along-channel, and thus in or out of the Arm. Two cases were examined, one with a north/south wind outside the East Arm (Figure 4.21a), the other with an east/west wind (Figure 4.22a), and both with along-channel wind in the East Arm. Each case was compared with a uniform north/south or east/west wind stress.

Results of the model runs (Figures 4.21b and 4.22b) show that steering in the East Arm does have an effect on the transport over the sill, at least for certain wind directions. Steering into and out of the Arm in the north/south configuration increased the maximum exchange over the sill by more than 20%. In the east/west configuration however, steering the wind along the channel had little effect on the transport. Based on these runs it can be concluded that the effect of steering in the East Arm is more significant for north/south winds than for east/west ones.

An example of the effect described above can possibly be seen in the comparison of model and calculated transports for day 301 to 309 2003 (Figure 4.23). Two distinct wind events, the first southward (day 303) and the second eastward (day 305) have caused inflow in the upper layer. The transport predicted by the model for the day 305 event (eastward) is quite close to that calculated from the data, however the model underestimated the transport for the day 303 event (southward) by approximately 33%.

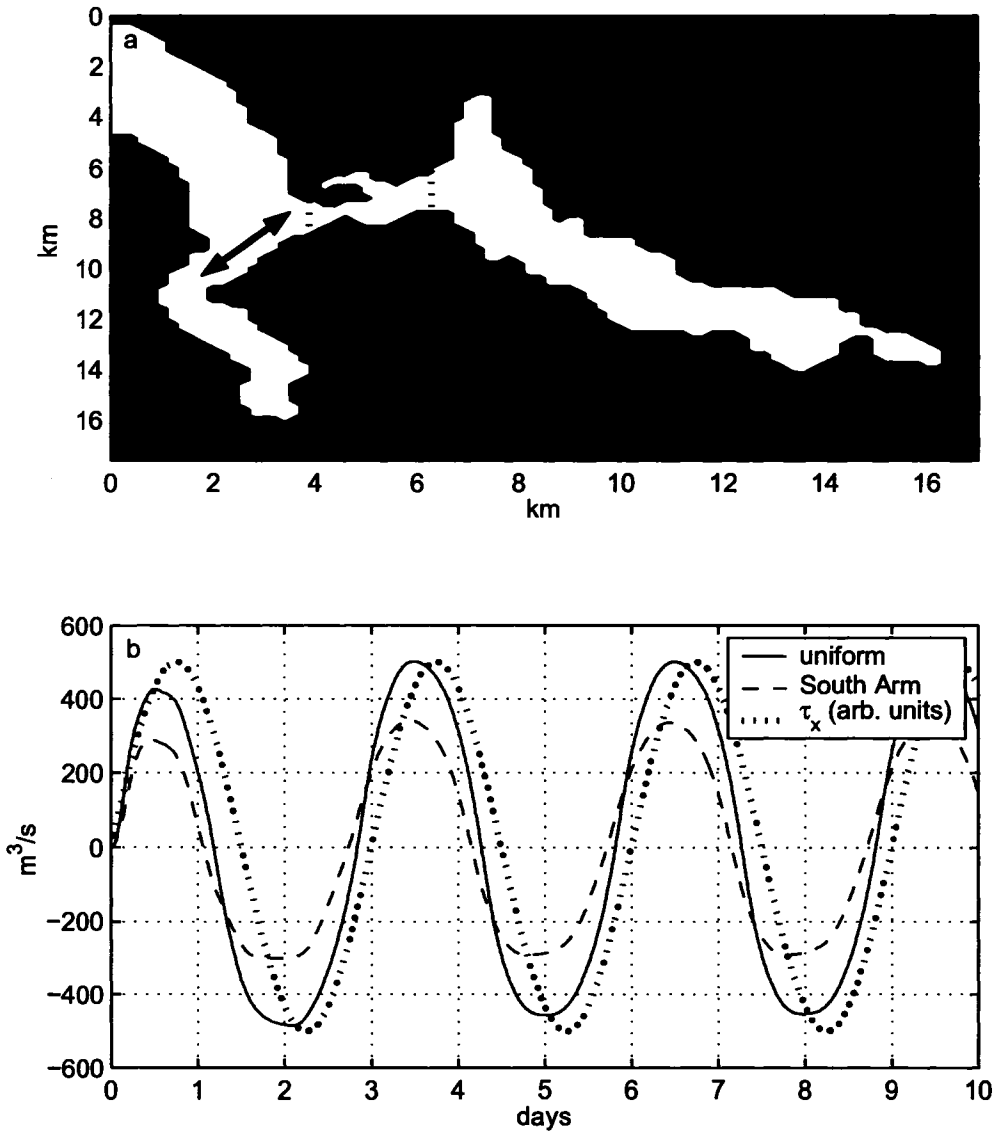

Figure 4.18: a) Model setup, and b) model predicted transports of the upper layer for the single South Arm forcing scheme. Wind is sinusoidal on the west side of the domain in the direction of the arrow, and zero on the east side. Wind stress in the area between the dotted lines is ramped linearly between the two regions. Units for stress have been scaled for comparison with transport time series.

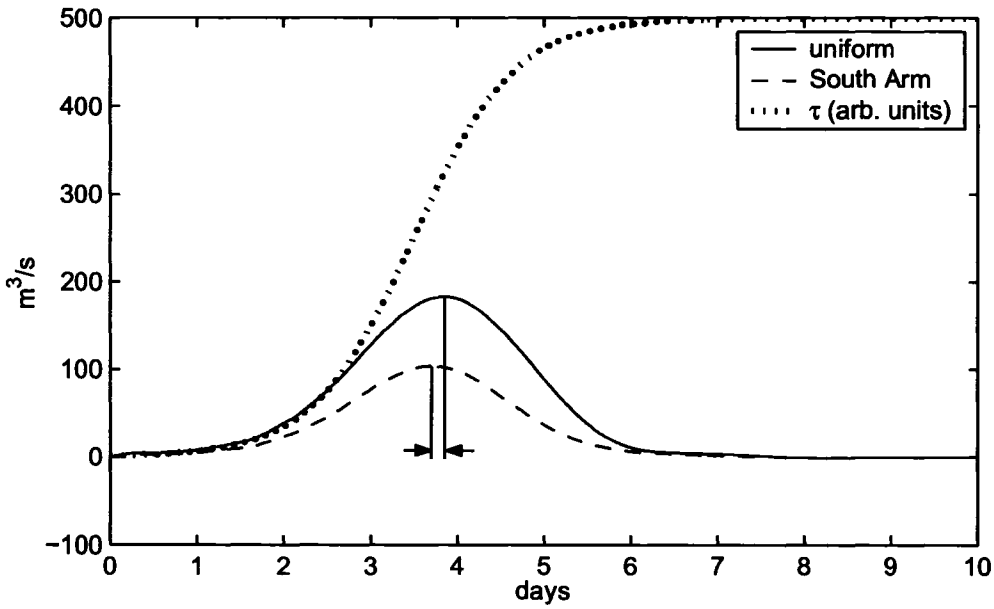

Figure 4.19: Results for upper layer transport from the use of the South Arm configuration (4.18a) but with a steadily increasing northeastern wind stress. The vertical lines show the lag between the maxima of the two transports, equal to 3.5 hours.

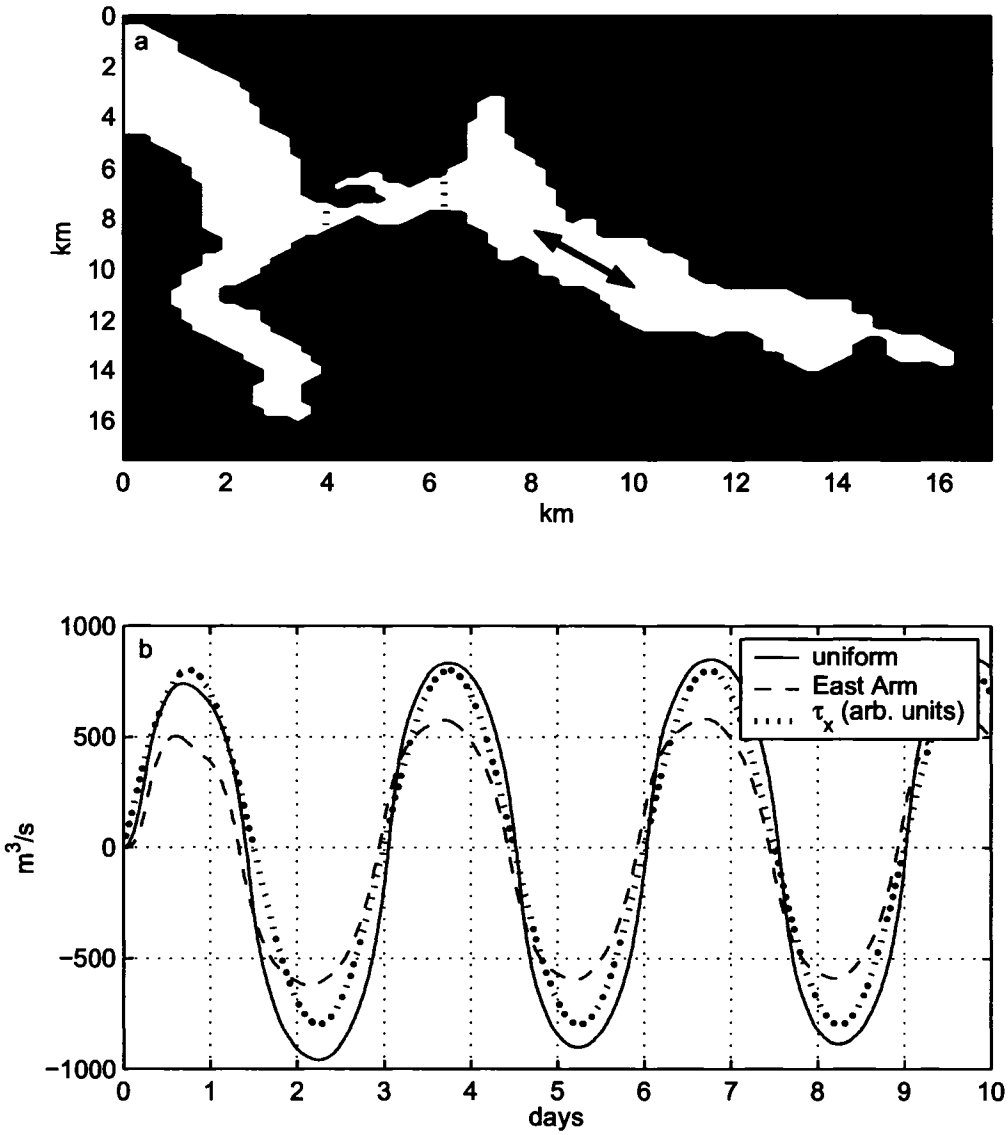

Figure 4.20: a) Model setup, and b) model predicted transports of the upper layer for the single East Arm forcing scheme. Wind is sinusoidal on the east side of the domain in the direction of the arrow, and zero on the west side. Wind stress in the area between the dotted lines is ramped linearly between the two regions. Units for stress have been scaled for comparison with transport time series.

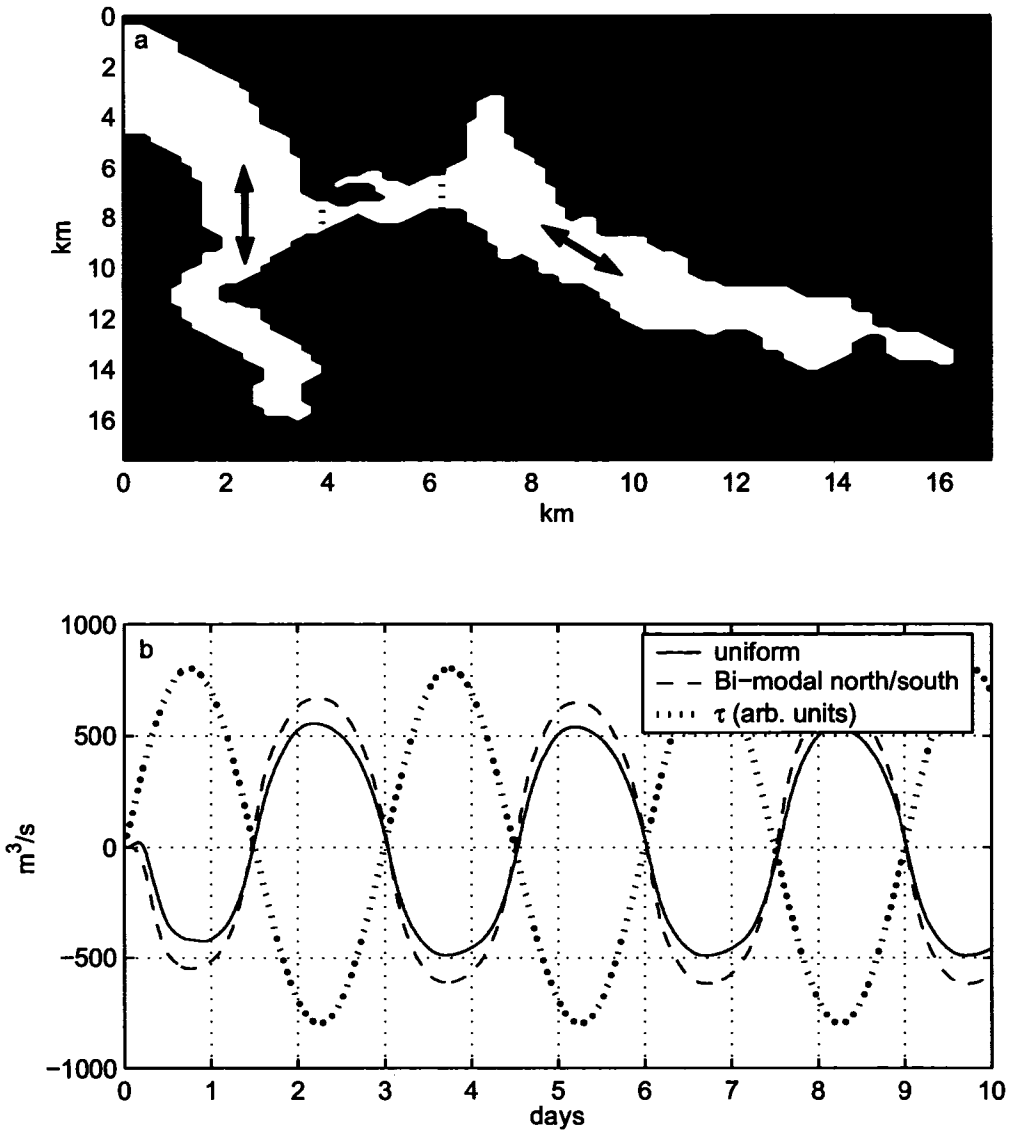

Figure 4.21: a) Model setup, and b) model predicted transports of the upper layer for the bi-modal north/south forcing scheme. Wind is sinusoidal on both sides of the domain, but oriented in the direction of the arrows. Wind stress in the area between the dotted lines is ramped linearly between the two regions. Units for stress have been scaled for comparison with transport time series, and the stress shown is the north/south wind stress on the left side of the domain.

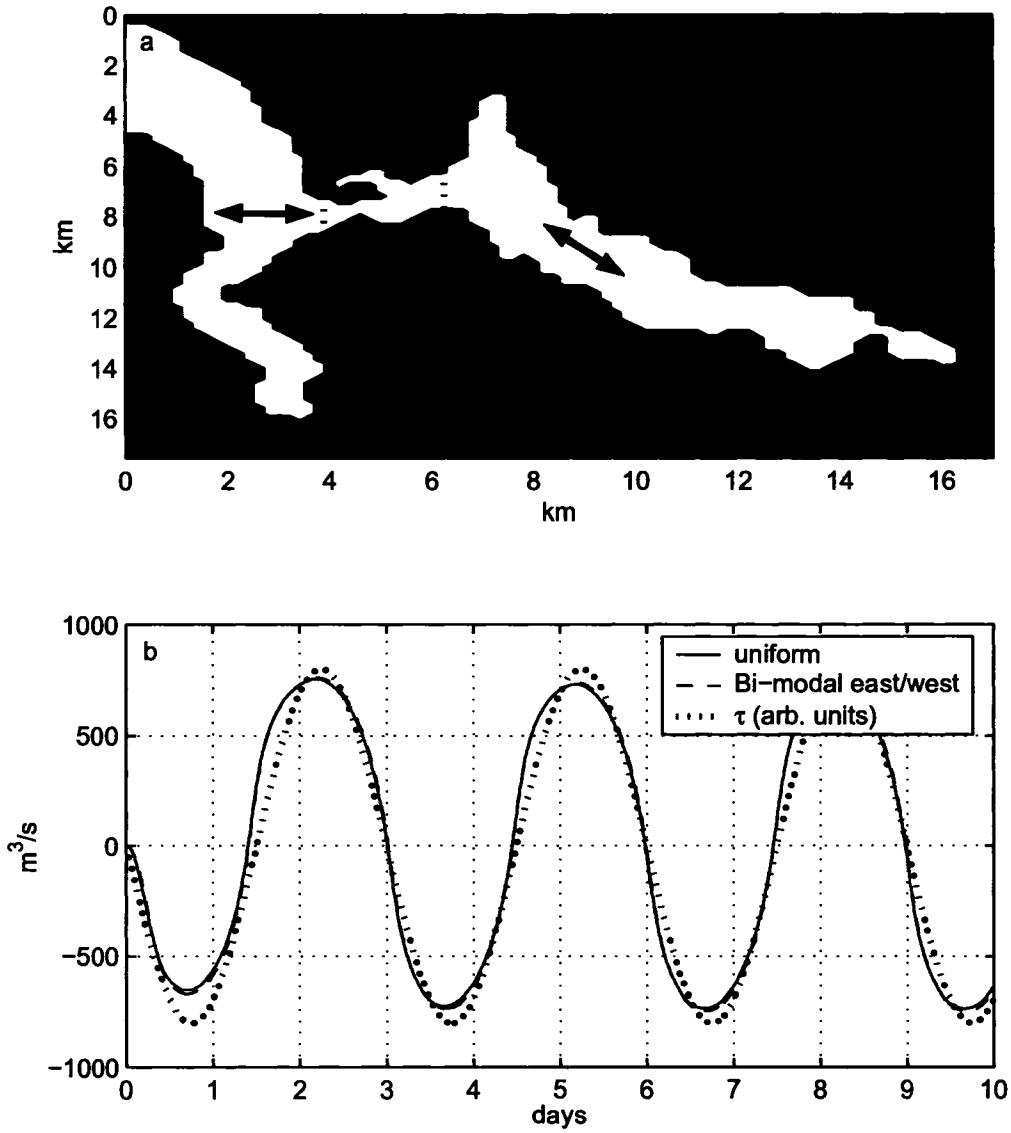

Figure 4.22: a) Model setup, and b) model predicted transports of the upper layer for the bi-modal east/west forcing scheme. Wind is sinusoidal on both sides of the domain, but oriented in the direction of the arrows. Wind stress in the area between the dotted lines is ramped linearly between the two regions. Units for stress have been scaled for comparison with transport time series, and that shown is the north/south wind stress on the left side of the domain.

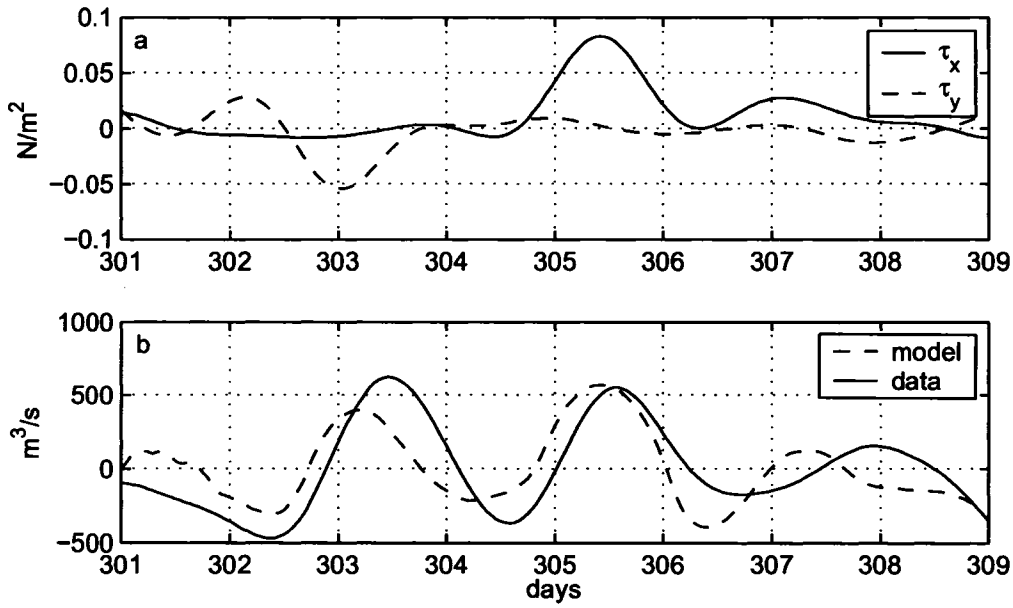

Figure 4.23: a) Wind stress b) calculated and model predicted upper layer transports for day 301 to 309 2003 illustrating the discrepancy between north/south and east/west wind events because of topographic steering in the East Arm.

Chapter 5

Conclusions

5.1 Key Results

The exchange dynamics of Bonne Bay were studied over two years, with particular emphasis on several different timescales, using ADCP data collected on the sill. Subtidal, tidal, and high frequency flow (periods less than 5 hours) were examined using tidal harmonic analysis, Empirical Orthogonal Function analysis, and a two layer numerical model.

Tidal flow over the sill is dominated by the M_2 tidal constituent in the semidiurnal band, and by the K_1 constituent in the diurnal band. The amplitudes of the constituents decrease with depth, with values near the bottom typically about 30 to 50% of those near the surface due to frictional drag. The result of this vertical asymmetry is that the average flow during flood tides, while everywhere into the bay, is enhanced at depth due to the background estuarine circulation. Average ebb flow is strong at the surface, but reverses close to the bottom, where the decreased tidal

amplitude is overcome by the estuarine inflow. EOF analysis of the raw data confirms the dominance of the M_2 constituent, and yields an across channel structure similar to that obtained from the tidal analysis.

Internal tides were detected at the sill, using the temperature data from the ADCPs. Tidal analysis of the temperature records showed that internal tides were present only at certain times of the year. In particular, decreased stratification during the winter months rendered the water column unable to support internal motions, and thus there was no detectable internal tide. For periods where stratification was higher, (or when the depth of the mixed layer was nearer to the instrument depth), oscillations in temperature were dominated by the M_2 tide, with a marked fortnightly modulation.

High frequency flow was attributed to internal wave motion in the vicinity of the sill, and it was found that there was correlation with tidal flow. Squared coherence between the low pass filtered high frequency kinetic energy and the fortnightly modulation of M_2 was seen to depend on both season and depth. Analysis of the coherence between the two time series showed highest coherence at a depth of 8 metres in fall 2002, no significant coherence at any depth for winter 2003, significant coherence at a depth of 15 metres in spring 2003, and a similar pattern to the fall 2002 structure during summer 2003. The areas of significant coherence correspond to the approximate position of the pycnocline, as this is the depth at which internal motion is most intense. The stratification was seen to decrease during the winter months, due to low freshwater runoff, and the mixed layer depth in the spring was greater than during fall and summer.

The subtidal flow over the sill was found through EOF analysis to be primarily

a two layer exchange (containing 74 to 84% of the variance). Coherence analysis with the results from the first mode of the EOF calculation show that the subtidal exchange is primarily forced by local wind stress, particularly for frequencies between 0.2 and 0.8 cpd (periods of 1.5 to 5 days). Coherence between through channel wind and currents was higher for the 2002 data set (day 251 to 321 2002) than the 2003 data set (day 301 to 485 2003) probably due to ice cover on the bay during winter months. Approximate dates for ice cover on Bonne Bay for winter 2004 are from January 8th to May 3rd (corresponding to days 372 to 488 2003). Coherence analysis between the through channel current and precipitation showed significant coherence for frequencies less than 0.1 cpd (periods longer than 10 days) except during the winter.

Results of a two layer numerical model support the analysis, in that the flow is primarily forced by local wind stress. Comparison of model predicted transport for the upper layer and that calculated from the data is in good agreement for the 3 time periods for which the model was run. Coherence between the two time series is significant for frequencies between about 0.1 and 0.6 cpd. Some discrepancies are explained by the assumption for a fixed depth for the interface in the transport calculations from data, and by the non-uniformity of the wind field due to topographic steering.

The possibility of spatial variability of the wind stress was examined with the model for several different cases. Runs comparing the upper layer transport over the sill when the wind forcing was along channel in either the South or East Arms, revealed that model predicted transports using a uniform wind stress may be too large in both cases. Bi-modal runs examining the effect of topographic steering in the

East Arm revealed that in the case of a north/south wind stress, the model predicted transport is smaller than when the wind is steered along channel in the Arm. For an east/west wind stress, the steered and uniform transports are comparable.

5.2 Future Work

While the work conducted so far in Bonne Bay has characterized many different aspects of the flow over the sill, there are still a number of things that can be examined in more detail. This necessitates a more extensive data collection program, which will be facilitated by the recent deployment of the Bonne Bay Ocean Observatory[1] (de Young *et al.*, 2005).

In particular, the observatory will permit year round hydrographic sampling at the sill, along with a similar deployment of ADCPs, and various other instruments such as echo sounders and a video plankton recorder. ADCP and CTD sampling should potentially be extended into the arms of the bay to detect the propagation of deepwater intrusions. Flow monitoring of the main sources of freshwater should be conducted to better characterize the estuarine circulation.

The recent installation of a weather station at the Bonne Bay Marine Station in Norris Point (see Figure 1.2) will yield wind stress data that is more appropriate than that obtained from the Rocky Harbour station, due to its proximity to the sill. Wind data collection should be extended throughout the two arms of the bay however, to try and resolve the issues associated with topographic effects.

Due to the high tidal energy and distinct topography near the sill, Bonne Bay is

[1] www.bonnebay.ca

a prime candidate for the study of internal wave dynamics. In particular, a study of the mixing processes occurring near the sill is relevant not just to the physical aspects of the system, but to biological ones as well.

Continued development of the numerical model as a tool for investigating the response of the bay to forcing is also worthwhile. Despite the success of the simple two layer model, a multilayer or three dimensional model that incorporates vertical mixing schemes would aid in understanding some of the more complex dynamics of the system. This could also potentially be coupled with biological models to study the influence of the physical environment on the various ecosystems found in the bay.

Bibliography

Baines, P. G. (1986). Internal tides, internal waves, and near-intertial motions. In Mooers, C. N., editor, *Baroclinic processes on continental shelves*, volume 3 of *American Geophysical Union Coastal and Estuarine Sciences Series*, chapter 2, pages 19–31. American Geophysical Union, Washington.

Björnsson, H. and Venegas, S. A. (1997). *A manual for EOF and SVD analyses of climatic data.* Department of Atmospheric and Oceanic Sciences and Centre for Climate and Global Change Research, McGill University.

Black, W. A. (1972). Sea-ice as an environmental factor. In *Coastal Zone, Seminar Proceedings*, volume 1, pages 3–18, Dartmouth, N.S. Bedford Inst. Oceanogr.

Bretschneider, D. E., Cannon, G. A., Holbrook, J. R., and Pashinski, D. J. (1985). Variability of subtidal current structure in a fjord estuary: Puget Sound, Washington. *J. Geophys. Res.*, 90(C6):11949–11958.

Cameron, W. M. and Pritchard, D. W. (1963). Estuaries. In Hill, M. N., editor, *The sea*, volume 2, pages 306–324. Wiley, New York.

Csanady, G. T. (1984). *Circulation in the Coastal Ocean.* Environmental Fluid Mechanics. D. Reidel Publishing Company.

de Young, B., Brown, K. M., Adams, R. S., and McLean, S. D. (2005). Design and deployment of the Bonne Bay observatory (B2O). *Oceans 2005*, page 6 pp.

de Young, B. and Pond, S. (1988). The deepwater exchange cycle in Indian Arm, British Columbia. *Estuarine Coastal Shelf Sci.*, 26:285–308.

Deines, K. L. (1999). Backscatter estimation using broadband acoustic Doppler current profilers. In *Proc. of IEEE 6th working conference on current measurement*, pages 249–253, San Diego, CA.

Dyer, K. R. (1997). *Estuaries: a physical introduction.* John Wiley & Sons Ltd, Chichester, 2nd edition.

Emery, W. J. and Thomson, R. E. (1998). *Data analysis methods in physical oceanography.* Elsevier Science Ltd., 1st edition.

Farmer, D. M. (1976). The influence of wind on the surface layer of a stratified inlet: part II. analysis. *J. Phys. Oceanogr.*, 6:941–952.

Farmer, D. M. and Freeland, H. J. (1983). The physical oceanography of fjords. *Progr. Oceanogr.*, 12:147–220.

Farmer, D. M. and Osborn, T. R. (1976). The influence of wind on the surface layer of a stratified inlet: part I. observations. *J. Phys. Oceanogr.*, 6:931–940.

Garrett, C. and Petrie, B. (1981). Dynamical aspects of the flow through the Strait of Belle Isle. *J. Phys. Oceanogr.*, 11:376–393.

Garrett, C. and Toulany, B. (1981). Variability of the flow through the Strait of Belle-Isle. *J. Mar. Res.*, 39:163–189.

Garvine, R. W. (1985). A simple model of estuarine subtidal fluctuations forced by local and remote wind stress. *J. Geophys. Res.*, 90(C6):11945–11948.

Gilbert, D. and Pettigrew, B. (1993). Current-meter data from Bonne Bay, Newfoundland, during the summer of 1991. Canadian Data Report of Hydrography and Ocean Sciences 122, Ministère des Pêches et des Océans, Division Physique du milieu marin, Institut Maurice-Lamontagne.

Gill, A. E. (1982). *Atmosphere-ocean dynamics*, volume 30 of *International geophysics series.* Academic Press, New York.

Gillibrand, P. A., Turrell, W. R., and Elliot, A. J. (1995). Deep water renewal in the upper basin of Loch Sunart, a Scottish fjord. *J. Phys. Oceanogr.*, 25:1488–1503.

Godin, G. (1980). Cotidal charts for Canada. Manuscript Report Series 55, Marine Sciences and Information Directorate, Department of Fisheries and Oceans.

Greatbatch, R. J. and Otterson, T. (1991). On the formulation of open boundary conditions at the mouth of a bay. *J. Geophys. Res.*, 96(C10):18431–18445.

Hansen, D. V. and Rattray, M. J. (1966). New dimensions in estuary classification. *Limnol. Oceanogr.*, 11:319–326.

Helle, H. B. (1978). Summer replacement of deep water in Byfjord, western Norway: mass exchange across the sill induced by coastal upwelling. In Nihoul, J. C. J., editor, *Hydrodynamics of Estuaries and Fjords*, number 23 in Elsevier

Oceanography Series, pages 441–464. Elsevier Scientific Publishing Company, Amsterdam.

Holbrook, J. R., Muench, R. D., and Cannon, G. A. (1980). Seasonal observations of low frequency atmospheric forcing in the Strait of Juan de Fuca. In Freeland, H. J., Farmer, D. M., and Levings, C. D., editors, *Fjord Oceanography*, pages 305–318. Plenum, New York.

Klinck, J. M., O'Brien, J. J., and Svendsen, H. (1981). A simple model of fjord and coastal circulation interaction. *J. Phys. Oceanogr.*, 11(12):1612–1626.

Koutitonsky, V. G. and Bugden, G. L. (1991). The physical oceanography of the Gulf of St. Lawrence: a review with emphasis on the synoptic variability of the motion. In Therriault, J. C., editor, *The Gulf of St. Lawrence: small ocean or big estuary?*, pages 57–89. Can. Spec. Publ. Fish. Aquat. Sci. 113.

Kowalik, Z. and Murty, T. S. (1993). *Numerical modeling of ocean dynamics*, volume 5 of *Advanced Series on Ocean Engineering*. World Scientific.

Large, W. G. and Pond, S. (1981). Open ocean momentum flux measurements in moderate to strong winds. *J. Phys. Oceanogr.*, 11:324–336.

Matsuura, H. (1995). An application of two-layer model to wind driven sub-tidal currents in Puget Sound. *Journal of Oceanography*, 51:571–584.

Matsuura, H. and Cannon, G. A. (1997). Wind effects on sub-tidal currents in Puget Sound. *Journal of Oceanography*, 53:53–66.

O'Brien, J. J. and Hurlburt, H. E. (1972). A numerical model of coastal upwelling. *J. Phys. Oceanogr.*, 2:14–26.

Orlanski, I. (1976). A simple boundary condition for unbounded hyperbolic flows. *J. Comput. Phys.*, 21(3):251–269.

Pawlowicz, R., Beardsley, B., and Lentz, S. (2002). Classical tidal harmonic analysis including error estimates in MATLAB using T_TIDE. *Computers and Geosciences*, 28:929–937.

Pickard, G. L. (1961). Oceanographic features of inlets in the British Columbia mainland coast. *J. Fish. Res. Board Can.*, 18(6):907–999.

Pickard, G. L. and Emery, W. J. (1990). *Descriptive physical oceanography*. Butterworth-Heinemann, 5th edition.

Pond, S. and Pickard, G. L. (1983). *Introductory dynamical oceanography.* Butterworth-Heinemann, 2nd edition.

RD Instruments (1996). *Acoustic Doppler current profiler principles of operation: a practical primer.* RD Instruments, San Diego, CA.

Richards, C. and de Young, B. (2004). Analysis of physical oceanographic data from Bonne Bay, September 2002 - September 2004. Physics and Physical Oceanography Data Report 2004-1, Department of Physics and Physical Oceanography Memorial University of Newfoundland.

Saunders, P. M. (1977). Wind stress on the ocean over the eastern continental shelf of North America. *J. Phys. Oceanogr.*, 7:555–566.

Stigebrandt, A. (1980). Some aspects of tidal interaction with fjord constrictions. *Estuarine Coastal Mar. Sci.*, 11:151–166.

Stigebrandt, A. (1981). A mechanism governing the estuarine circulation in deep, strongly stratified fjords. *Estuarine Coastal Mar. Sci.*, 13:197–211.

Svendsen, H. and Thomson, R. O. R. Y. (1978). Wind-driven circulation in a fjord. *J. Phys. Oceanogr.*, 8:703–712.

Tittensor, D., de Young, B., and Foley, J. (2002). Analysis of physical oceanographic data from Trinity Bay, May - August 2002. Physics and Physical Oceanography Data Report 2002-2, Department of Physics and Physical Oceanography Memorial University of Newfoundland.

Winters, K. B. and Seim, H. E. (2000). The role of dissipation and mixing in exchange flow through a contracting channel. *J. Fluid Mech.*, 407:265–290.